

T-3511

Petrochemical Evolution and Physical
Construction of an Andean Arc:
Evidence from the southern
Patagonian batholith
at 53°S

by
Robert M. Bruce

ARTHUR LAKES LIBRARY
COLORADO SCHOOL of MINES
GOLDEN, COLORADO 80401

ProQuest Number: 10796359

All rights reserved

INFORMATION TO ALL USERS

The quality of this reproduction is dependent upon the quality of the copy submitted.

In the unlikely event that the author did not send a complete manuscript and there are missing pages, these will be noted. Also, if material had to be removed, a note will indicate the deletion.



ProQuest 10796359

Published by ProQuest LLC (2019). Copyright of the Dissertation is held by the Author.

All rights reserved.

This work is protected against unauthorized copying under Title 17, United States Code
Microform Edition © ProQuest LLC.

ProQuest LLC.
789 East Eisenhower Parkway
P.O. Box 1346
Ann Arbor, MI 48106 – 1346

T-3511

A thesis submitted to the Faculty and the Board of Trustees of the Colorado School of Mines in partial fulfillment of the requirements for the degree of Doctor of Philosophy (Geology).

Golden, Colorado

Date 3-16-88

Signed: Robert M. Bruce
Robert M. Bruce

Approved: Eric Nelson
Dr. Eric P. Nelson
Thesis Advisor

Golden, Colorado

Date 3/17/88

Samuel S. Adams
Dr. Samuel S. Adams
Professor and Head,
Department of Geology and
Geological Engineering

ABSTRACT

The construction of an Andean-type magmatic arc involves the transportation and differentiation of material from the mantle, resulting in new continental crust, as well as recycling of pre-existing crust. This study of the southern Patagonian batholith at 53°S (Xaultegua area) identifies the spectrum of plutonic rocks that extend from relatively old (126-80 Ma) gabbro to younger (50-20 Ma) granite with the volumetrically dominant lithology being intermediate age biotite-hornblende tonalite. Low Sr(i) ratios indicate that plutons of the Xaultegua area incorporated only minor old crustal components, in contrast to portions of the batholith containing older plutons. Individual parental magma types and fractionation sequences have resulted in four distinct rock series. The two volumetrically-dominant rock series, calcic and calc-alkaline, formed from two mantle-derived magma types with significantly different K₂O-contents. Two minor rock series, trondhjemite and mixed, are temporally and spatially restricted. The trondhjemite rock series formed by melting of early plutonic rocks during the Andean orogeny. The mixed rock series appears to have formed from contamination of granodioritic magma with trondhjemitic host rocks.

Crustal thickening due to arc plutonism results from the migration of mantle-derived magma into pre-existing continental crust. Relationships between age, lithology, and depth of emplacement for plutons in the Xaultegua area indicate that mafic magma crystallizes at greater depth than felsic magma. Variations in crystallization ages between adjacent areas within a magmatic arc

may not be the result of diachronous plutonic activity, but rather to variations in regional uplift histories. The span of crystallization ages within an area is controlled by the rate of crustal uplift. Continual crustal thickening results in continual uplift. Under these conditions, inflation dynamics and erosion dictate that upper crustal plutons shallow, while lower crustal rocks deepen. Thus, lower crustal rocks will not be exposed until arc magmatism is terminated.

TABLE OF CONTENTS

| | <u>Page</u> |
|--|-------------|
| ABSTRACT | iii |
| LIST OF FIGURES | vii |
| LIST OF TABLES | viii |
| ACKNOWLEDGMENTS | ix |
| Chapter | |
| 1. PREFACE | 1 |
| 2. PETROGENETIC DEVELOPMENT OF THE SOUTHERN PATAGONIAN BATHOLITH: EVIDENCE FROM $^{53}\text{O}_S$ | |
| Introduction | 3 |
| Field Observations | 8 |
| Geochronology | 10 |
| Sr Isotope Geochemistry | 12 |
| Petrologic Rock Series | 14 |
| Two Principal Rock Series | 17 |
| Aerial and Temporal Distribution | 30 |
| Minor Rock Series | 32 |
| Trondhjemite Rock Series | 33 |
| Mixed Rock Series | 37 |
| Conclusion | 40 |
| 3. EFFECTS OF SYNCHRONOUS UPLIFT AND INTRUSION DURING MAGMATIC ARC CONSTRUCTION | |
| Introduction | 43 |
| Geologic and Tectonic Setting | 45 |
| Lithologies of the SPB | 46 |
| Age-Lithology-Crystallization Depth Relationship | 47 |
| Arc Construction Model | 48 |

| | |
|--|-----|
| Geochronology and Sr Isotope Data .. | 51 |
| Effects of Varying Uplift Rates | 55 |
| Crustal Kinematics in Magmatic Arcs . | 59 |
| Application of the Arc Construction Model | 63 |
| Conclusion | 66 |
| REFERENCES CITED | 68 |
| APPENDIXES | |
| A. ANALYTIC METHODS | 73 |
| B. STATION TO SAMPLE NUMBER CORRELATION TABLE | 78 |
| C. MAJOR ELEMENT DATA | 79 |
| D. TRACE ELEMENT DATA | 82 |
| E. MINERAL MODES | 85 |
| F. AR/AR ISOTOPIC DATA..... | 88 |
| G. GPP PROGRAM ADDITIONS AND MODIFICATIONS . | 103 |
| H. PUBLISHED ABSTRACTS | 110 |

LIST OF FIGURES

| <u>Figure</u> | <u>Page</u> |
|---|-------------|
| 2.1 Study Area Location Map | 4 |
| 2.2 Station Location and Plutonic Age Map | 6 |
| 2.3 Age-Sr(i) | 13 |
| 2.4 AFM | 15 |
| 2.5 Ne-O1-Qtz | 16 |
| 2.6 Alkali-Lime Index | 18 |
| 2.7 Modal Classification | 19 |
| 2.8 Chemical Variation Diagrams | |
| a. Al_2O_3 , FeO^* , TiO_2 , MgO | 20 |
| b. K_2O , CaO , Na_2O , P_2O_5 | 21 |
| c. MnO , Rb , Ba , Sr | 22 |
| d. Cu , Nb , Ni , Nd | 23 |
| e. Y , V , Zr | 24 |
| 2.9 K_2O - SiO_2 Variation Diagram | 27 |
| 2.10 Rock Series Map | 31 |
| 2.11 Age Histogram | 36 |
| 2.12 CaO - Na_2O - K_2O Variation Diagram | 39 |

| | | |
|-----|--|----|
| 3.1 | Basic Arc-Construction Model | 50 |
| 3.2 | Age-Lithology-Area Diagram | 53 |
| 3.3 | Multiple Uplift Rates | 56 |
| 3.4 | Synthetic Age-Lithology Histograms | 57 |
| 3.5 | Nodal Plane Dynamics | 61 |

LIST OF TABLES

| <u>Table</u> | | <u>Page</u> |
|--------------|--|-------------|
| 2.1 | Isotopic Ages from Xaultegua | 11 |
| 2.2 | Residual K ₂ O | 26 |
| 3.1 | Isotopic Ages southern Patagonian batholith .. | 52 |

ACKNOWLEDGMENTS

I have benefitted greatly from the time, energy, and experience of many more people than I can individually acknowledge here. My research program at CSM included trips to Chile, Scotland, Ireland, and would not have been possible without financial support. The department and the graduate school have provided funds in support of meeting related travel. NSF funds (EAR 83-07604) supported a seemingly endless array of research expenses and my TA stipend helped keep the monthly bills paid.

My thanks go to Carl Erickson for work on the CSM x-ray machine, Stan Mertzman (Franklin and Marshall Collage) for major element analyses, Steve Weaver for Rb/Sr and Sm/Nd work, Dan Lux for tolerating this slow learner in his argon lab, and Sam Goldich for his iron titration technique. Steve Laudeman, Aksel Quitus-Bosz, and Sue Sobchek made the years of sample prep survivable. I clearly would not have succeeded without their assistance.

Several important people have taken the time to teach and provide guidance during my studies. Bill Romey and Bill Elberty (St. Lawrence University) can be blamed for bringing the science of geology to life and starting me on this quest. Ed Larson and Jim Munos (CU Boulder) patiently allowed me to explore the breadth of geology and cheered my return to igneous petrology and tectonics. Craig Simmons has graciously clouded my mind forever with the tenants of geochemistry, Greg Holden has bolstered my petrologic training as well as my spirit. Richard Yeatts has patiently provided encouragement. Finally without Eric Nelson's insightful analysis of my character and abilities, I may never have had a

chance to work in Chile. Our research program has been a most rewarding one.

Last and certainly not least is the human element of this experience. My new friends at CSM come from the faculty, the staff, my lab assignments, and my graduate student peers. I thank you all for helping get the job done and making it fun. To Bruce and Kate Johnson, who have taught me most of what I know about computers and the English language, I am glad I have a long time to repay my debt. To my parents, I owe much for helping me get to the point where I could dream of and work toward a Ph.D. Thank you for being there from the beginning and down the home stretch. Finally none of this would have come to pass if it were not for the unending support from my wife Deb who has earned this degree as much as I.

Chapter 1

PREFACE

A primary objective of this study was to describe and identify the petrologic origins of plutonic rocks found in a portion of the southern Patagonian batholith (Xaultegua area, 53°S). Field work was conducted with logistical support provided by the R/V Hero, a research vessel operated by NSF. The multiple scientific objectives of the cruise and the regional nature of the investigation dictated that only a reconnaissance petrologic sampling program could be undertaken.

Isotopic geochronology and petrographic studies confirmed and quantified field observations indicating a progression in time from mafic to felsic plutonism. This behavior was also observed in other areas of the batholith. An initial interpretation of these data in terms of synchronous uplift-intrusion mechanics was presented by Bruce et al. (1986a).

Major- and trace-element data provided a more complete characterization of the plutonic rocks in the Xaultegua area. Two volumetrically dominant chemical-petrologic rock series that originated from separate and distinct mantle-derived parental magma types were recognized. Two minor rock series appear to have a crustal origin. These interpretations were presented by Bruce et al. (1987a).

In the field, it was recognized that older plutons in the Xaultegua area crystallized at mesozonal depths, while some of the youngest plutons crystallized

at epizonal depths. This relationship between composition, crystallization depth, and age was later quantified and is interpreted to reflect synchronous intrusion and uplift during magmatic arc construction. The exposed plutons were assembled within a particular crustal horizon during its uplift toward the surface of the earth. The consistent age-Sr(i) relationship of plutons from throughout the batholith demonstrate the regional uniformity of arc magmatic process. The different isotopic age spectra in separate areas can be explained by variations in local uplift histories. This concept was presented by Bruce et al. (1986b).

An effort was made to describe and identify the processes responsible for the observed patterns. This resulted in the creation of a rigorous geometric model of pluton intrusion and uplift that provided the tool necessary to study the effects of changing uplift rate on the age and duration of preserved plutonism. The geometric model demonstrated several difficulties in interpreting regional age-lithology data. This refined model was presented by Bruce et al. (1987b).

The current model incorporates the concept of crustal inflation due to magmatic additions. During crustal thickening which triggers isostatic uplift, not all crustal horizons approach the surface of the earth. A nodal plane separates crustal horizons that are shallowing from those that are deepening. This concept introduces a reference frame needed to identify crustal levels that will not reach the surface under current conditions. All three major components have been included in a manuscript submitted to Tectonophysics in December 1987. Chapter Three is taken from this manuscript with only minor changes to accommodate the C.S.M. thesis format. Copies of the published abstracts appear in appendix H.

Chapter 2

PETROGENETIC DEVELOPMENT OF THE
SOUTHERN PATAGONIAN BATHOLITH:
EVIDENCE FROM 53°SIntroduction

The southern Patagonian batholith (SPB) is one of the large Mesozoic-Cenozoic batholiths that form major portions of western South America. It forms the southernmost segment of a semi-continuous chain of subduction-related, magmatic arc plutons exposed from Venezuela to Cape Horn. The SPB is exposed in the Andes of southern Chile forming a nearly continuous 1200 km-long, 50-100 km wide, curvilinear belt between 46°S and 56°S (Fig. 2.1). At Cape Horn it projects offshore into the Scotia Sea where it has apparently been truncated by Cenozoic rifting (Barker and Griffiths, 1972). The batholith is exposed in a region that varies from the high (4000m), ice-capped peaks of the continental divide along the eastern margin of the batholith, to an insular and peninsular region of fjords and canals along the rugged western coast. Because this region is extremely remote and almost entirely unpopulated, few regional or detailed geologic studies have been undertaken. This contribution reports geochronologic, geochemical and petrologic findings from a study of the Golfo Xaultegua region at 53°S in Chile. No known reconnaissance or detailed

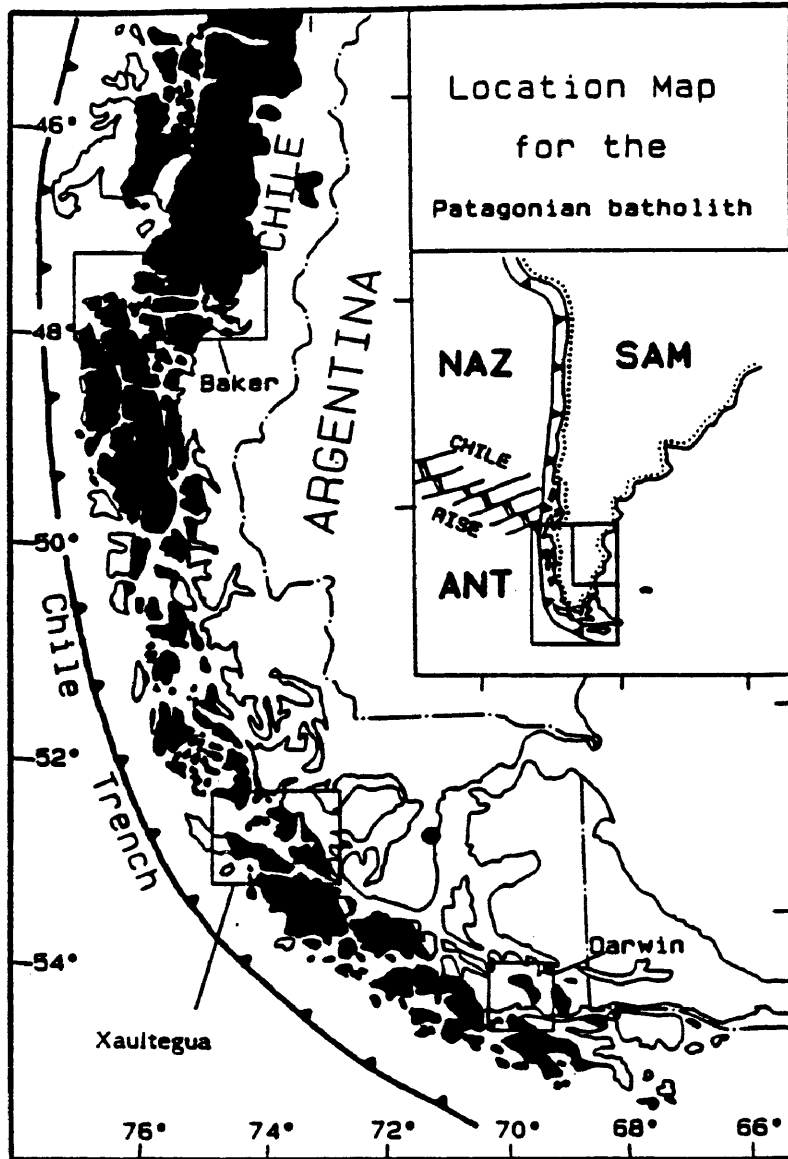


Fig. 2.1 Study Area Location Map

Plutonic outcrops shown in black. NAZ= Nazca plate, SAM= South American plate, ANT= Antarctic plate.

petrologic studies have been published for this region. A review of the early studies of the SPB as well as a general description of the field petrology for the batholith can be found in Nelson et al. (in press).

The study area encompasses approximately 9000 km² centered around the Golfo Xaultegua and the Straits of Magellan at 53°S (Fig. 2.1 and 2.2). Field logistics prevented traditional detailed geologic mapping during this reconnaissance study with observations restricted to sea level exposures and an average station spacing of two nautical miles (Fig. 2.2). Because of the lack of continuous geologic mapping, spatial and temporal relations between individual samples cannot be defined. Therefore, this study focused on the regional, time-integrated petrologic evolution of the batholith, from which systematic changes within and between coherent petrologic rock series can be demonstrated. In most cases, the source and sequence of events responsible for distinct rock series can be interpreted from the data. These new observations provide insights into the magmatic processes and products of mature arcs hosted in relatively thin, young continental crust.

The SPB is situated along the active continental margin of southernmost South America where the Antarctic plate is being subducted beneath the South American plate (Fig. 2.1). The Chile Margin triple junction, at 46°S., marks the northern boundary of the SPB as defined here. North of the triple junction subduction rates are 9 cm/a whereas south of the triple junction they are 2 cm/a (Forsyth, 1975). Holocene volcanic activity is minimal south of the triple junction compared to north of it (Stern et al., 1976). Plutons of the SPB intruded a forearc region of tectono-stratigraphic terrains accreted along the

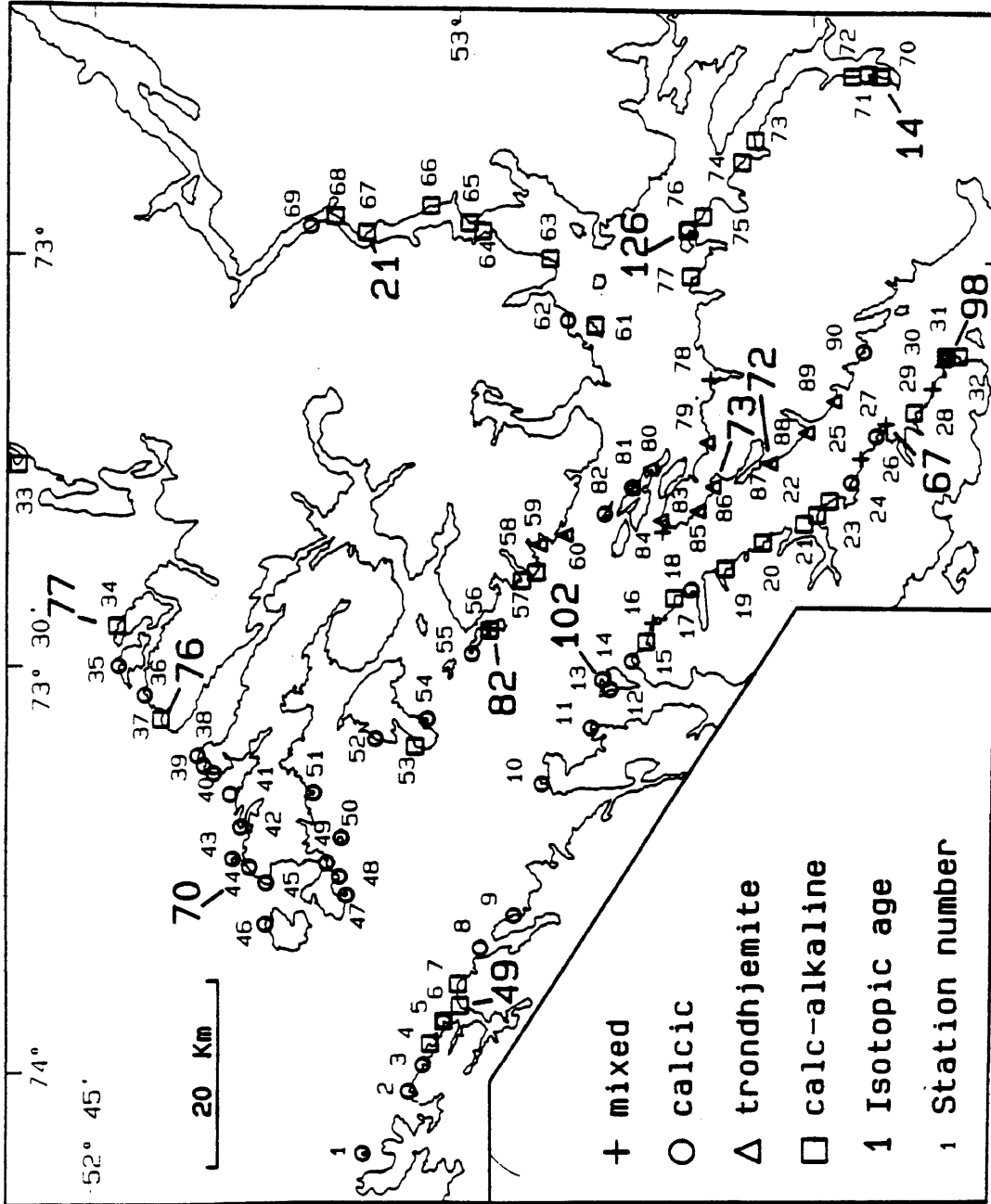


Fig. 2.2 Station Location and Plutonic Age Map

Pacific margin of Gondwanaland, which has been an active continental margin at least since the late Paleozoic (Dalziel, 1981; Forsythe, 1982). The country rocks to the batholith consist of various lithologic elements including 1) volcanoclastic flysch, 2) radiolarian chert, 3) reef limestone, 4) pillow basalt, 5) ultramafic rocks, and 6) quartz-veined phyllite (Mpodozis and Forsythe, 1983) in addition to volcanic rocks of the Late Jurassic Tobifera Formation, early Cretaceous ophiolitic rocks, and early Cretaceous marginal basin infill. Mafic to felsic volcanic rocks of unknown age are also present in isolated exposures within the batholith.

Most of the plutons of the Xaultegua area, comprising two major rock series, are net additions to the continental crust. They were derived principally from the mantle and young mantle derived crustal components, having incorporated relatively minor amounts of old continental material. Geochemical evidence suggests that two distinct parental magma types produced the major rock series. These magma types differed in their large ion lithophile element (LILE) contents and degree of hydration. Two minor rock series originated from crustal melting and contamination processes involving older plutons. The small proportion of host rock within the batholith suggests the batholith grew outward by inflation.

Field Observations

Plutonic rocks of the Xaultegua region contain felsic to mafic lithologies typical of the entire SPB (Bruce et al., 1986a; Nelson et al., in press) as well as two minor felsic peraluminous rock series. Mafic rocks include gabbro, diorite, quartz monzodiorite and mafic quartz diorite which are generally coarse to medium grained with no flow or deformational fabric. Some mafic rocks have clear cumulate textures and cumulate layering. Mafic rocks with a CI between 75 and 40 are relatively rare, comprising only 10 to 20 percent of the outcrop area. Younger, medium-grained, intermediate composition plutons, which include felsic quartz diorite, quartz monzodiorite, and tonalite, comprise the bulk of the batholith in the Xaultegua area and the entire SPB. Some samples have a weak foliation, but lack significant protoclasic or subsequent deformation. The youngest rocks include felsic tonalite, granodiorite, and granite with a CI less than 10 and often less than 5. Compared to the older, more mafic rocks, these felsic rocks tend to be finer grained and have suffered more, though still minor, deuteritic alteration. Mirolitic cavities typify some of the youngest intrusive rocks. Like mafic rocks, felsic rocks are a subordinate component (10 to 20 percent) of this primarily intermediate batholith.

A consistent mafic to felsic lithologic progression exists in the Xaultegua area and the SPB as a whole (Bruce et al., 1986a). Mafic dikes and the two minor rock series are the only exceptions to this behavior.

Contacts between plutons, where observed, are sharp, usually showing signs

of brittle fracture resulting in angular xenoliths of older mafic plutons being rafted into felsic magma. Considerable deformation and recrystallization was observed within mafic xenoliths, but little or no reaction was observed along pluton boundaries. Contacts between older plutons and country rock are generally zones of moderate post-magmatic deformation while younger plutons are bounded by passive stoped contacts. Dikes are common in mafic and intermediate composition plutons, but rare in more felsic plutons. Most plutons contain both syn-plutonic and post-plutonic mafic dikes, suggesting multiple emplacement events. Felsic, pegmatitic, granophyric, and aplitic dikes are rare.

Geochronology

Isotopic ages confirm and quantify the plutonic history inferred from field relations. The period of recorded magmatism in the Xaultegua area ranges from 126 to 11 Ma (Table 2.1). A general lack of deformed plutons and agreement between ages determined with different isotopic dating methods (Table 2.1) indicates that the ages reported are close to the actual crystallization ages. Ages plotted in Fig. 2.2 are ages from Table 2.1 or an average when more than one age was available for an individual sample. These data indicate that progressive changes in pluton composition did not occur in short repetitive cycles as reported in Peru (Pitcher et al., 1985), but that the mafic to felsic progression in Xaultegua reflects some long term process(es). The 115 My-long magmatic history in the area and the 48 My gap between emplacement of the youngest gabbro and the oldest granite precludes these rocks from being the product of a single differentiation event. This long term change in composition may be the product of changing intrusion depth with time in a continually uplifting magmatic arc, as suggested by Bruce et al. (in press).

Table 2.1 Isotopic Ages from Xaultegua

| Map # | Sample | Rock Series | Rock Name | Material | Method | Age (Ma) | |
|-------|--------|-------------|-----------|----------|--------|----------|-----------|
| 44 | BB-2A | K | QD | Horn | Ar/Ar | 71.9 | ± 3.8 |
| | | | | Bio | Ar/Ar | 68.8 | ± 0.5 |
| 37 | BB-6A | K | QMD | Zircon | U/Pb | 76.2 | ± 0.4 |
| 6 | MA-21 | K | TO | Horn | Ar/Ar | 49.2 | ± 2.9 |
| | | | | Bio | Ar/Ar | 49.5 | ± 1.2 |
| 76 | GX-9A | C | QD | Horn | Ar/Ar | 125.9 | ± 2.6 |
| 70 | GX-19 | K | GR | WR | Ar/Ar | 14.0 | ± 1.1 |
| 67 | GX-27 | K | GR | Bio | Ar/Ar | 21.4 | ± 0.5 |
| 13 | MA-28 | C | MTO | Zircon | U/Pb | 102.0 | ± 0.8 |
| 27 | MA-37 | M | GR | Bio | Ar/Ar | 66.5 | ± 1.6 |
| 31 | MA-39C | K | DI | Horn | Ar/Ar | 98.4 | ± 6.0 |
| 56 | MA-66A | K | DI | Horn | Ar/Ar | 81.9 | ± 4.5 |
| 86 | MA-70A | T | TO | Bio | Ar/Ar | 72.6 | ± 5.0 |
| 87 | MA-71B | T | TO | Bio | Ar/Ar | 70.5 | ± 0.9 |
| | | | | Musc | Ar/Ar | 72.8 | ± 0.7 |
| 34 | 3G-210 | K | MTO | Bio | Ar/Ar | 77.3 | ± 1.1 |

Grouped data represent samples from the same pluton.

Rock Series: C=calcic, K=calc-alkaline, M=mixed, and T=trondhjemites.

Rock Names: DI=diorite, GR=granite, MTO=mafic tonalite, TO=tonalite, QD=quartz diorite, QMD=quartz monzodiorite

Material: Bio=biotite, Horn=hornblende, Musc=muscovite
WR=whole rock powder

Sr Isotope Geochemistry

Plutons of the Xaultegua area have low initial Sr ratios, $Sr(i)$, indicating that they were derived principally from mantle or young continental sources and that only minor contamination from old continental crust has occurred (Fig. 2.3). The trend of decreasing $Sr(i)$ observed for the SPB as a whole (Fig. 2.3) indicates that the involvement of an older crustal component was significant, early in the history of the batholith, but decreased over time. Weaver et al., (1986b) and Nelson et al., (1987) using bulk mixing, partial melt mixing, and AFC calculations demonstrated that early SPB plutons could have incorporated 30 to 40 percent of a crustal component equal to the exposed host rocks. Nd and Sr isotopic compositions for rocks from the Xaultegua area along with more extensive Sr and Nd data from the SPB at 48°S (Weaver et al., in press), support the contention that the involvement of continental crust in arc magmatism decreased with time. Significant fractionation may have occurred at crustal levels, but little assimilation of old preexisting crustal material occurred during genesis of the relatively young plutons of the SPB. The Xaultegua area plutons will therefore be considered as primarily products of mantle and young mantle derived crustal components and not the product of recycled older continental crust.

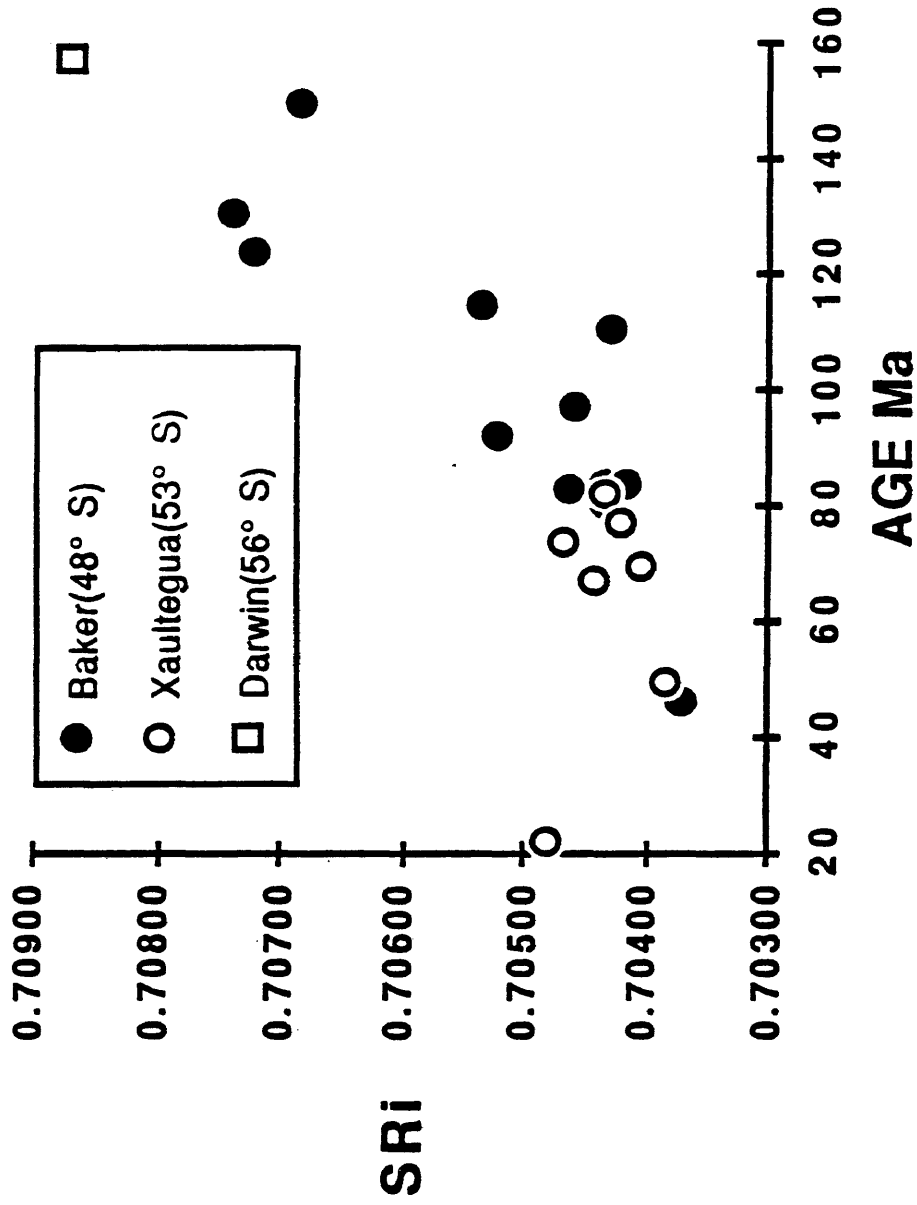


Fig. 2.3 Age-Sr(i)

Data from three study areas within the SPB (Baker: filled circles, Xaultegua: open circles, and Darwin: open square).

Petrologic Rock Series

The plutonic rocks of the Xaultegua region are calc-alkaline according to the AFM criterion (Fig. 2.4), and subalkaline according to the Ne-OI-Q criterion (Fig. 2.5) of Irvine and Baragar (1971). Phaneritic plutonic rocks such as those of the SPB may not represent parental liquid compositions, but mixtures of a diverse phenocryst assemblage and residual interstitial liquid in which some fractionation processes may have occurred. Therefore the exact compositions of liquids from which these rocks formed are uncertain.

Four plutonic rock series have been identified in the Xaultegua area by an iterative multiple cross-correlation of chemical and petrologic data. The four rock series, are here called calc-alkaline, calcic, trondhjemite, and mixed rock series. No single criterion adequately distinguishes all four rock series, but by examining a number of criteria unique populations are recognized.

The mineralogies of plutonic rocks dominate their chemistry and potentially mask compositional differences between parental magma types. The range in parental magma compositions may not be accurately reflected in whole-rock data. An interpretation inherent in this analysis is that three (calcic, calc-alkaline, and trondhjemite) rock series result from unique parental magma types and fractionation histories.

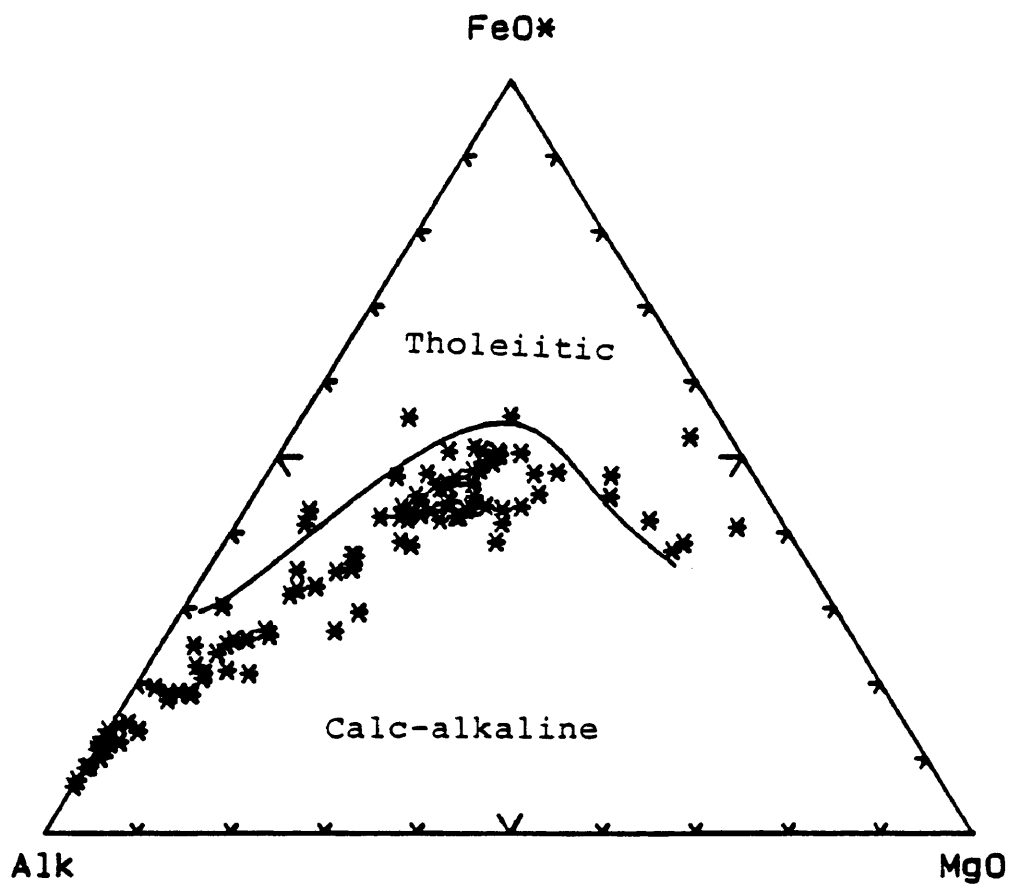


Fig. 2.4 AFM

Major element data from the Xaultegua area plotted using the classification method of Irvine and Baragar (1971).

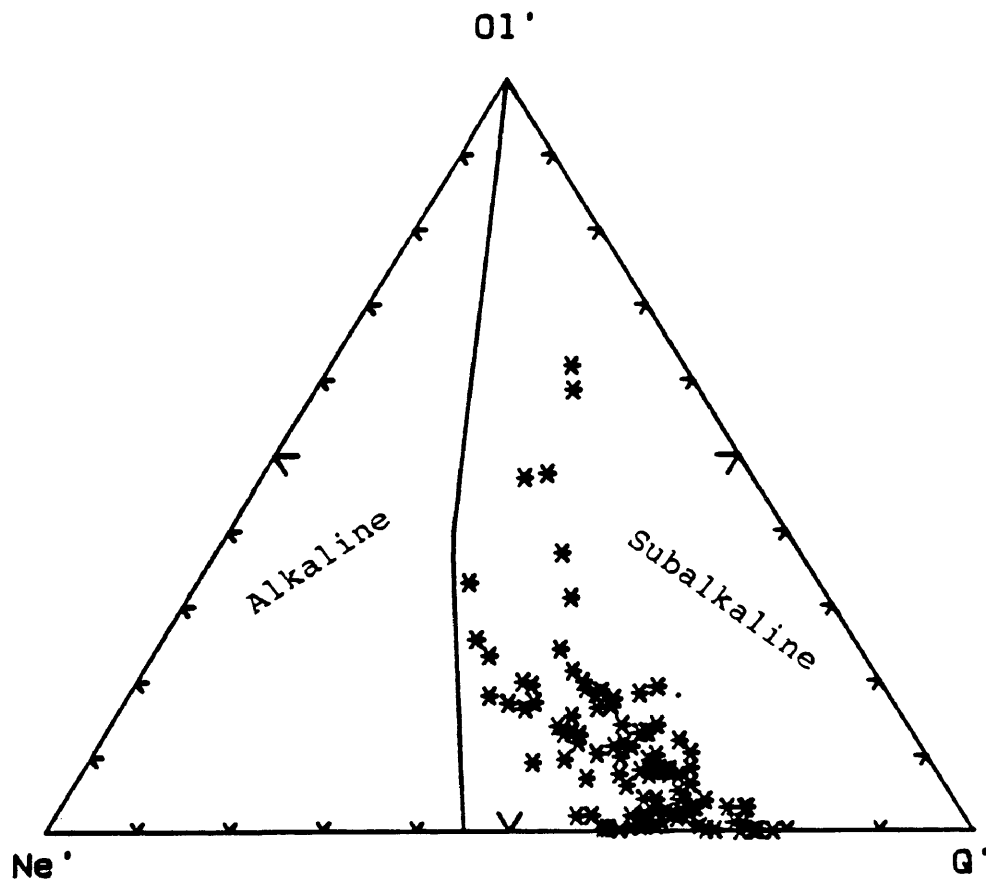


Fig. 2.5 Ne-OI-Qtz

Normative data plotted using the classification method of Irvine and Baragar (1971). Calculated minerals: Ol' =olivine, Ne' =nepheline, Q' =quartz.

Two Principal Rock Series

The calcic and calc-alkaline rock series comprise most of the plutonic rocks exposed in the Xaultegua area (Fig. 2.2). The calcic and calc-alkaline designations are based on their distinction using the alkali-lime index of Peacock (1931), later modified by Brown (1979; Fig. 2.6). Quartz and feldspar modes (Fig. 2.7), demonstrate the wide range in felsic mineral proportions within and between each rock series. The rock series range from mafic diorite and gabbro to felsic tonalite and granite. Calcic series rocks contain little or no alkali feldspar; this is true for mafic diorite and gabbro right through the series to felsic tonalite. In contrast, calc-alkaline series rocks contain notable alkali feldspar; mafic rocks contain minor, late-stage intergranular orthoclase and more felsic rocks contain a much larger percentage of early crystallizing alkali feldspar. The difference in mineralogy is interpreted to result from a significant difference in the K_2O content between the two parental magmas types.

The difference in mineralogical composition and the distinct evolutionary paths followed by these two rock series are also reflected in marked chemical differences (Fig. 2.8). Although parental magma compositions cannot accurately be defined for each series, a significant difference in K_2O content can be demonstrated by comparing mineral modes and whole rock chemical data for samples at equivalent points in their evolution, as reflected by SiO_2 content. Four samples have been chosen for this analysis, two from each rock series with approximately the same silica content. SiO_2 , K_2O , and mineral modes for these samples are listed in Table 2.2. At 49% SiO_2 the K_2O content between the two

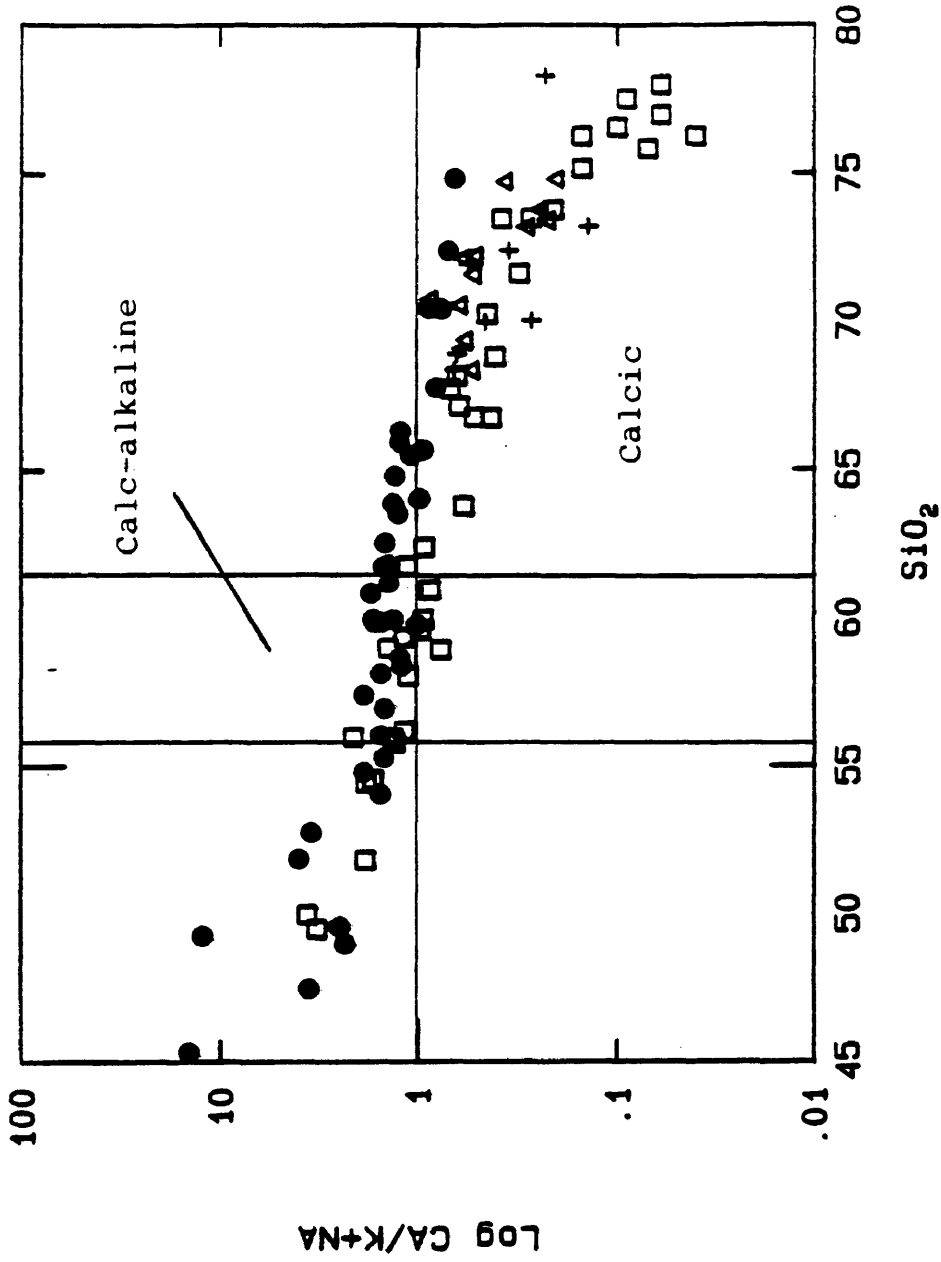


Fig. 2.6 Alkali-Lime Index
Elemental data plotted using classification of Peacock (1931) modified by Brown (1981). (Calc-alkaline: open squares, Calcic: filled circles, Trondhjemite: open triangles, Mixed: plus symbol)

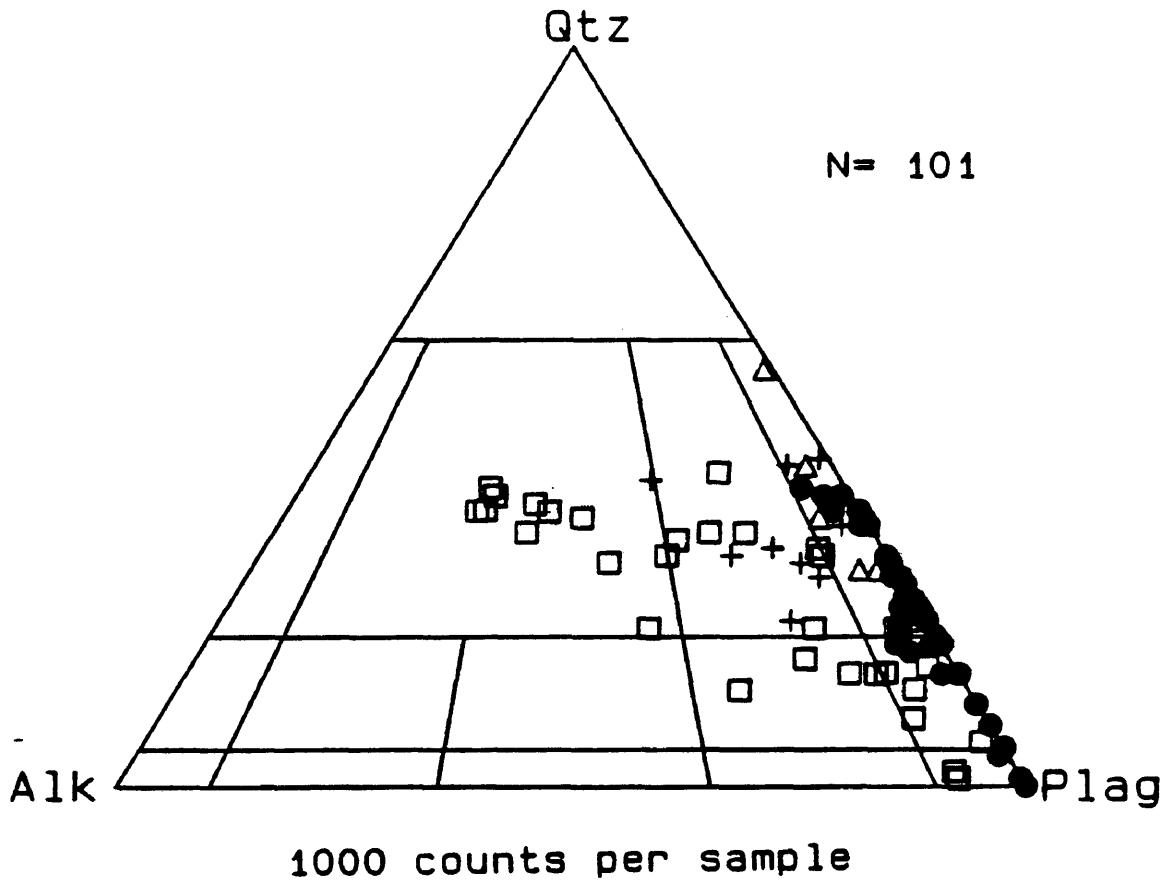


Fig. 2.7 Modal Classification

Mineral data from the Xaultegua area plotted according to the method of Streckeisen (1976), (Calc-alkaline: open squares, Calcic: filled circles, Trondhjemite: open triangles, Mixed: plus symbol).

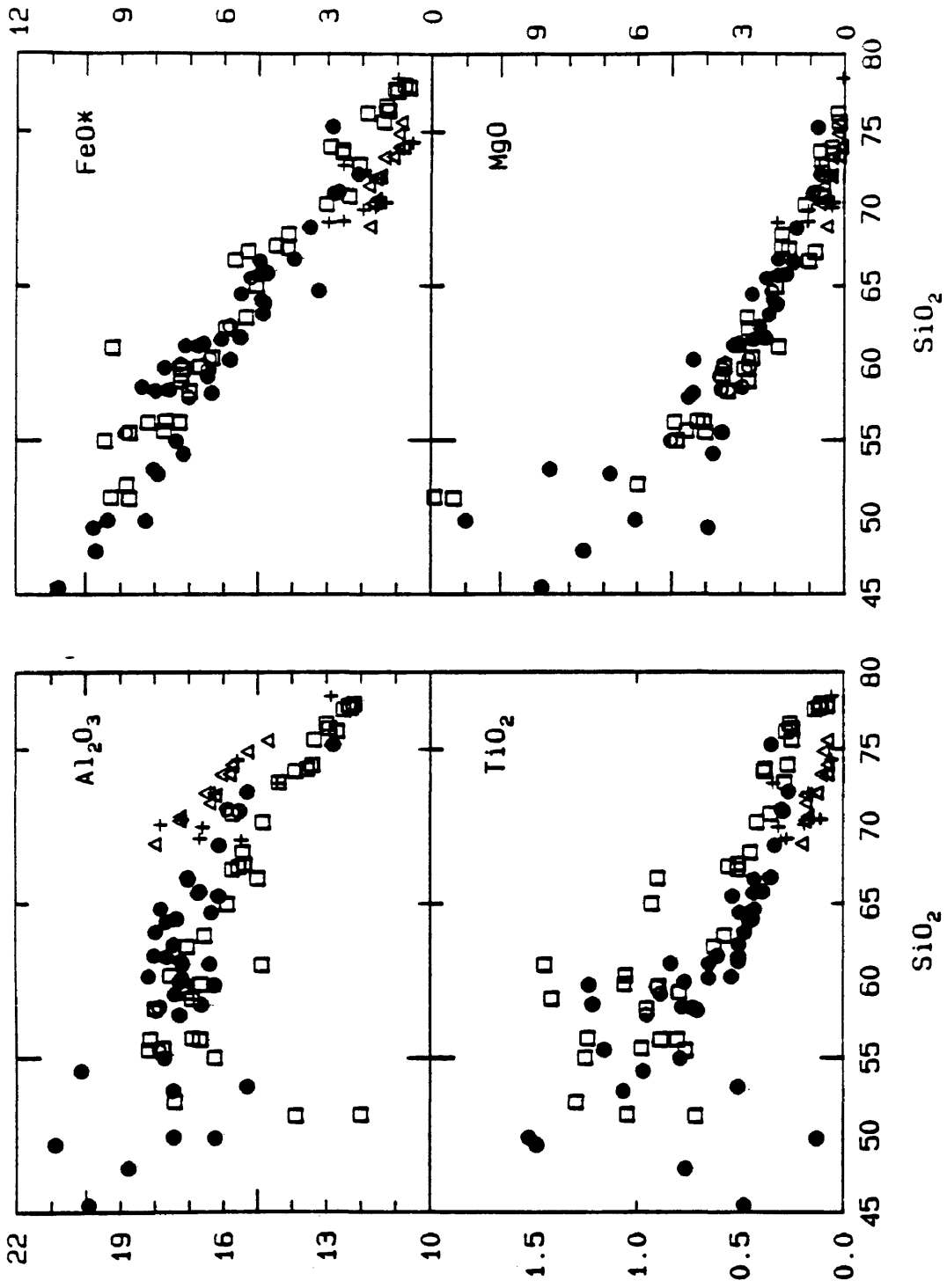


Fig. 2.8 a Chemical Variation Diagrams
Elemental data from the Xaultegua area, (Calc-alkaline: open squares, Calcic: filled circles, Trondhjemite: open triangles, Mixed: plus symbol)

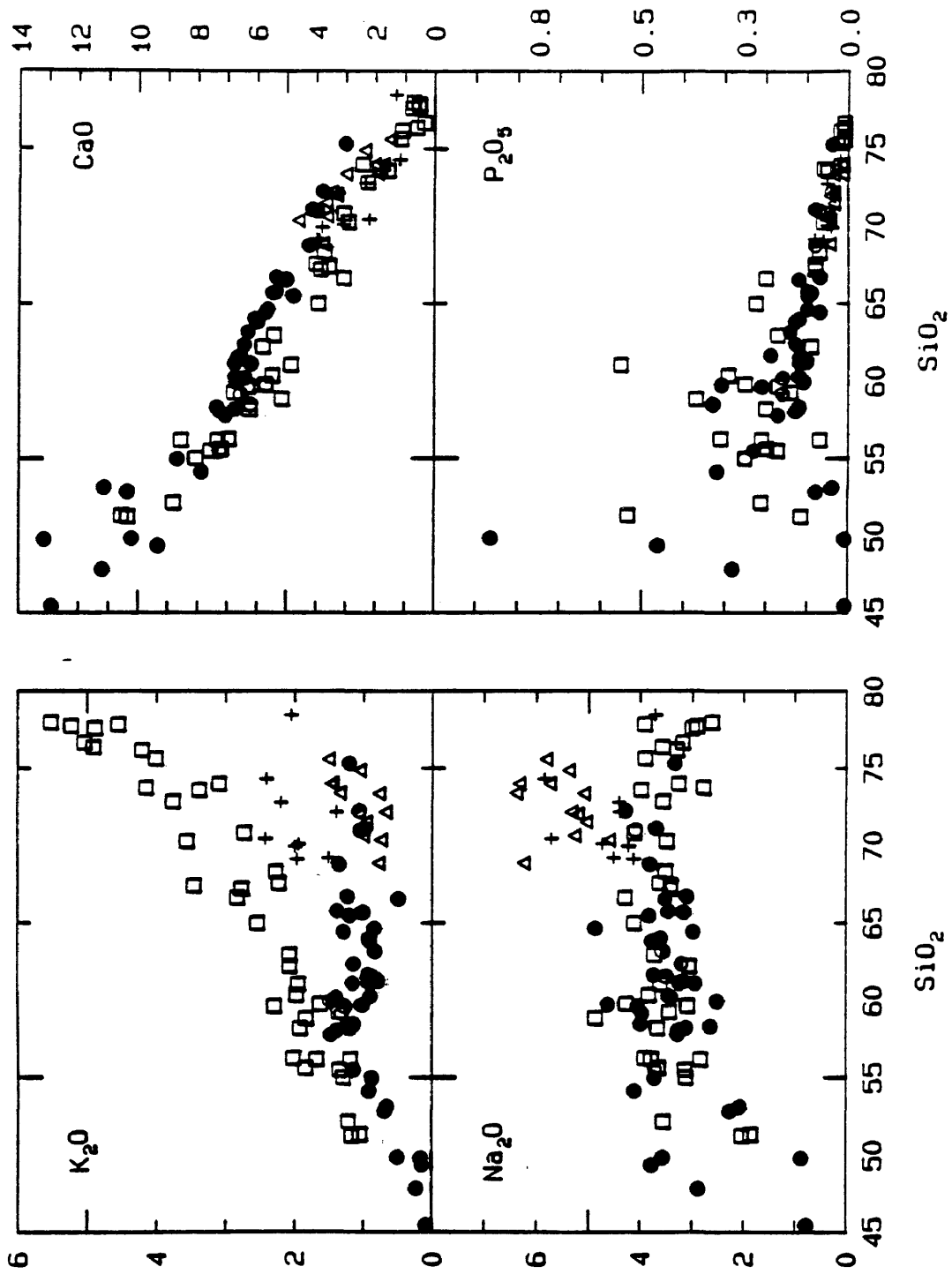


Fig. 2.8 b Chemical Variation Diagrams
Elemental data from the Xaultegua area, (Calc-alkaline: open squares, Calcic: filled circles, Trondhjemite: open triangles, Mixed: plus symbol)

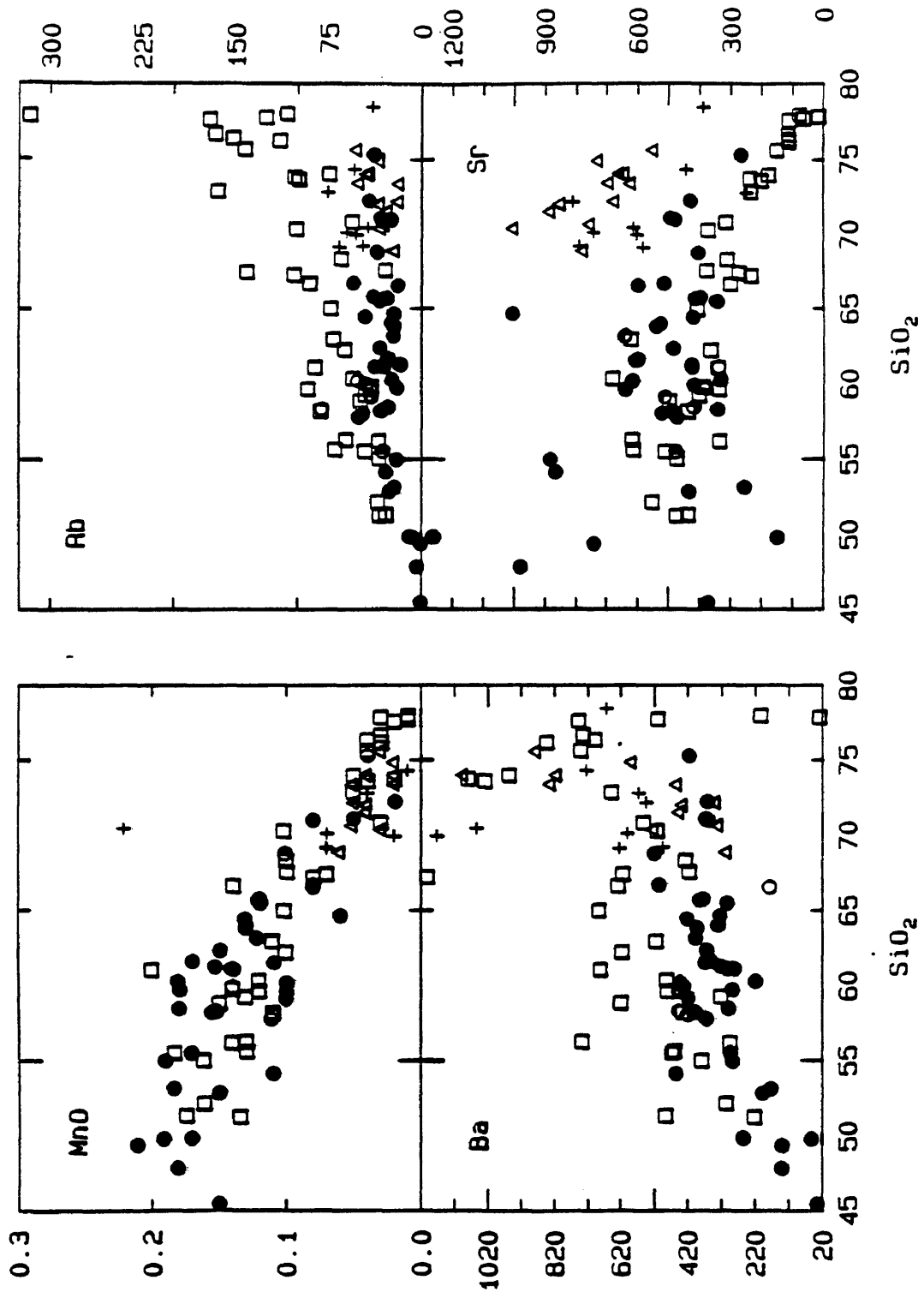


Fig. 2.8 c Chemical Variation Diagrams

Elemental data from the Xaultegua area, (Calc-alkaline: open squares, Alkaline: filled circles, Trondhjemite: open triangles, Mixed: plus symbol)

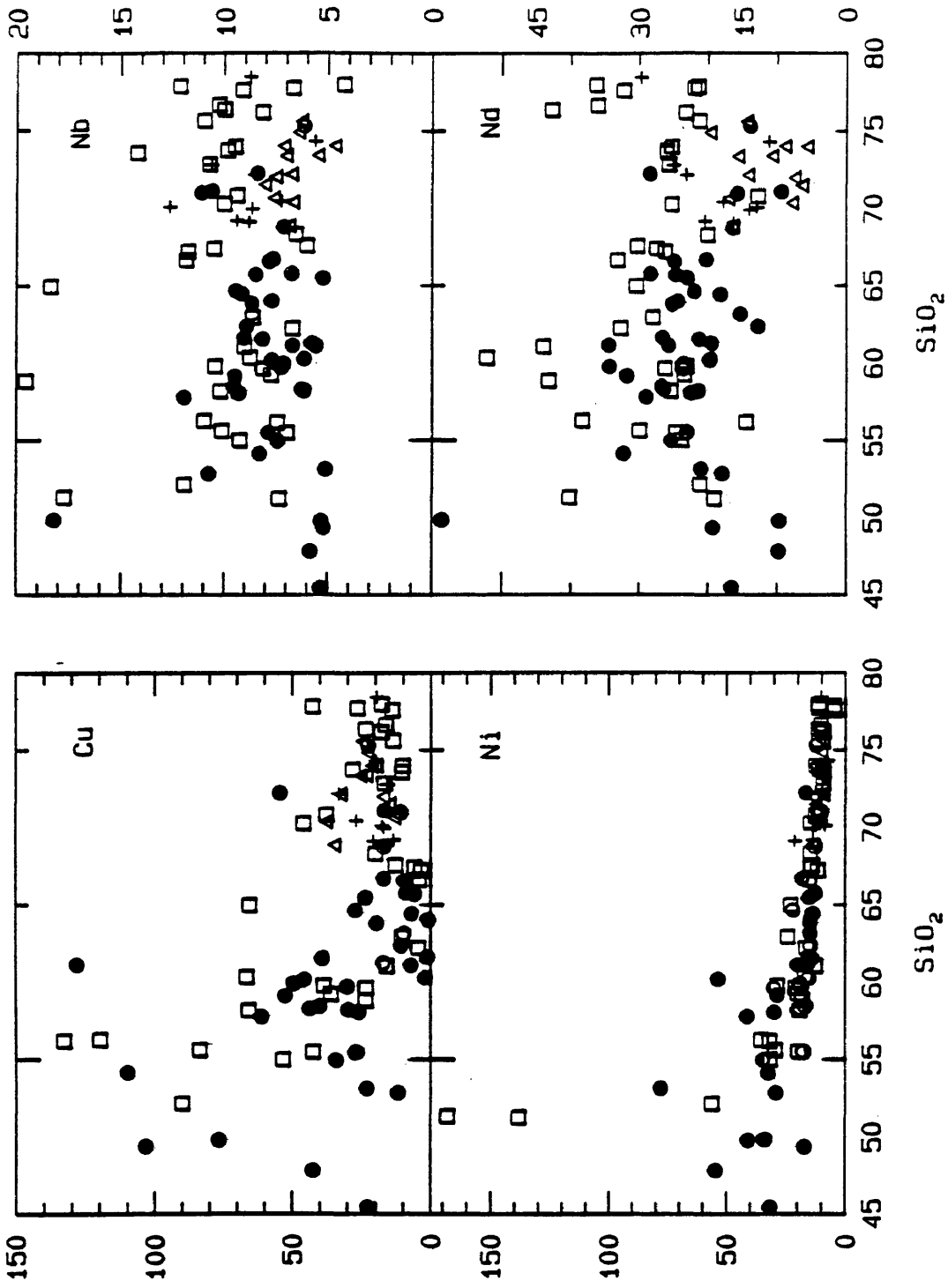


Fig. 2.8 d Chemical Variation Diagrams

Elemental data from the Xaultegua area, (Calc-alkaline: open squares, Calcic: filled circles, Trondhjemite: open triangles, Mixed: plus symbol)

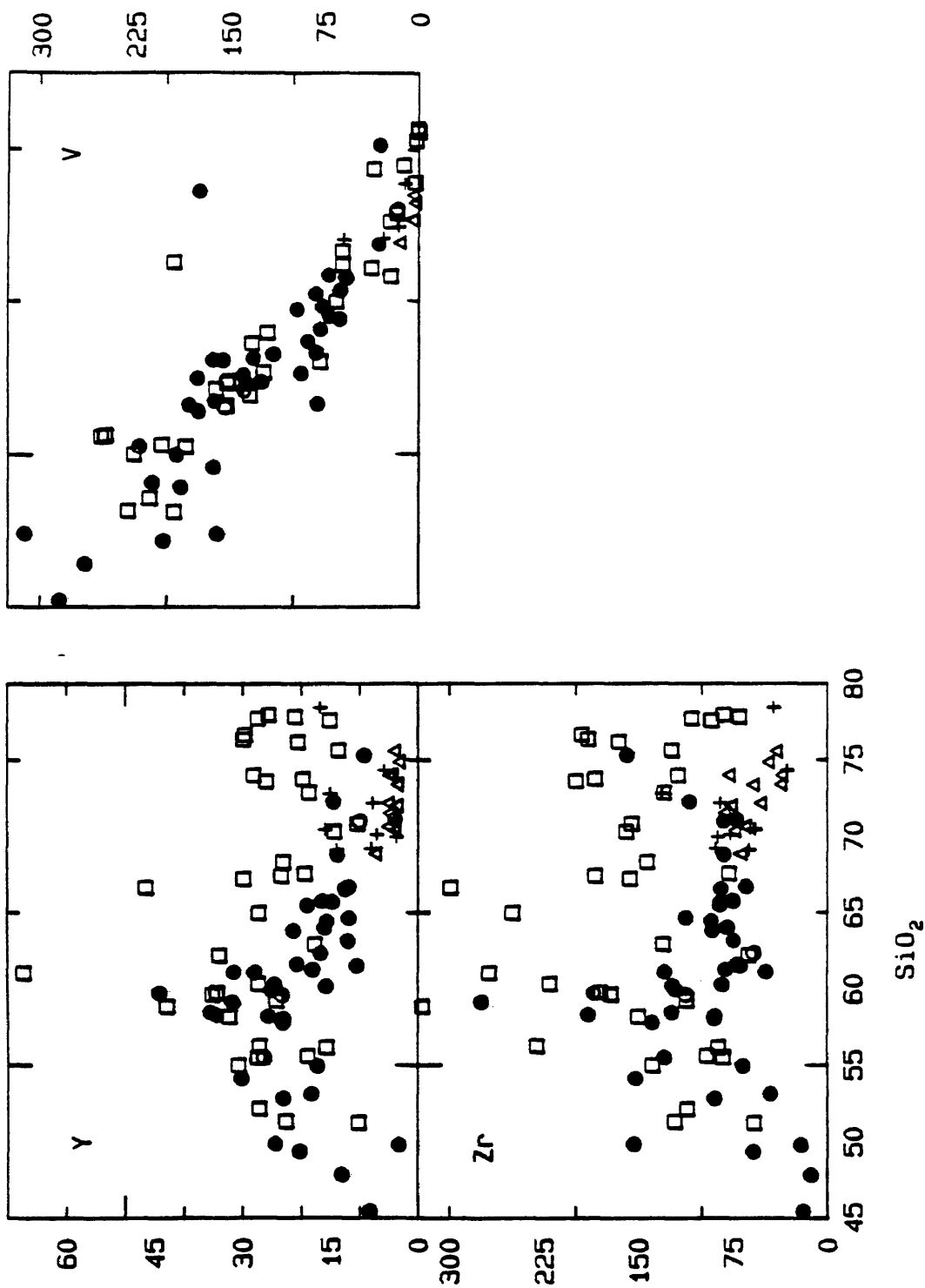


Fig. 2.8 e Chemical Variation Diagrams
Elemental data from the Xaultegua area, (Calc-alkaline: open squares, Calcic: filled circles, Trondhjemite: open triangles, Mixed: plus symbol)

rock series differs by an order of magnitude. It could be argued that these rocks are cumulates and that the difference is due to the notable difference in their modal mineralogies. To test this hypothesis, stoichiometric K_2O in biotite and alkali feldspar (K_2O -rich cumulate phases) was subtracted from their whole rock values (Table 2.2). The remaining K_2O must reside in plagioclase and hornblende in amounts proportional to the activity of K_2O in the magma from which they crystallized. The residual K_2O in the calc-alkaline rocks is much greater than in the calcic rocks suggesting that, though the rocks sampled may be cumulates, the analysis still indicates that potassium content was higher in the calc-alkaline magma. This analysis supports the conclusion derived from petrographic observations that the two rock series originated from separate magma types; a higher K_2O calc-alkaline parent and a lower K_2O calcic parent.

Although both rock series contain hydrous mafic minerals, magmas of the calcic series appear to have been less hydrous than those of the calc-alkaline rock series. Hornblende and biotite are the dominate mafic minerals of intermediate and mafic rocks of both rock series, but orthopyroxene and clinopyroxene are common (Fig. 2.9), usually present as irregular shaped cores in reaction relation with rims of hornblende and biotite. Pyroxene cores appear to have reacted with the liquid as fH_2O increased with increasing crystallization. A few samples from the calcic series contain more pyroxene than the sum of biotite and hornblende. In general pyroxene-bearing calcic rocks have less extensive reaction rims than pyroxene-bearing calc-alkaline rocks, though biotite is common in both rock series. In calc-alkaline rocks, biotite is present in the outer portion of reaction rims, as in calcic rocks, and also as detached euhedral

Table 2.2 Residual K₂O

| | Sample | Whole Rock | | Residual K ₂ O |
|------------------------|--------|------------------|------------------|------------------------------|
| | | SiO ₂ | K ₂ O | |
| Calc-alkaline Rocks | MA-66A | 49.47 | 1.13 | 0.62 |
| | MA-39C | 49.95 | 1.02 | 0.45 |
| Calcic Rocks | MA-20B | 48.96 | 0.16 | 0.03 |
| | MA-25B | 49.25 | 0.17 | 0.06 |

| Sample | Qtz | Plag | Modal Mineralogies | | | | Px | Opq |
|--------|-----|------|--------------------|-----|------|------|-----|-----|
| | | | K-spar | Bio | Horn | | | |
| MA-66A | 1.2 | 32.3 | 3.1 | 0.3 | 65.8 | 0.0 | 0.1 | |
| MA-39C | 0.3 | 22.4 | 1.4 | 3.6 | 72.7 | 0.0 | 0.2 | |
| MA-20B | 0.9 | 77.2 | 0.0 | 1.4 | 10.4 | 3.1 | 5.7 | |
| MA-25B | 0.3 | 54.5 | 0.0 | 1.2 | 19.7 | 25.8 | 0.6 | |

Calculation of residual K₂O after stoichiometric K₂O in K-bearing phases is removed.

crystals. Some mafic calc-alkaline rocks contain no recognizable pyroxene cores and contain euhedral hornblende and biotite, suggesting that pyroxene never existed or was completely resorbed. These observations suggest that magmas parental to the calcic series rocks had lower fH₂O than magmas parental to the calc-alkaline series rocks, or may be another manifestation of the difference in their LIL contents.

Interpretation of petrographic data and the variations of K₂O with SiO₂ (Fig. 2.9) indicate that not only did the two rock series have different parental magma compositions, but that their differentiation produced divergent evolutionary paths. Calc-alkaline rocks exhibit an exponential increase of K₂O

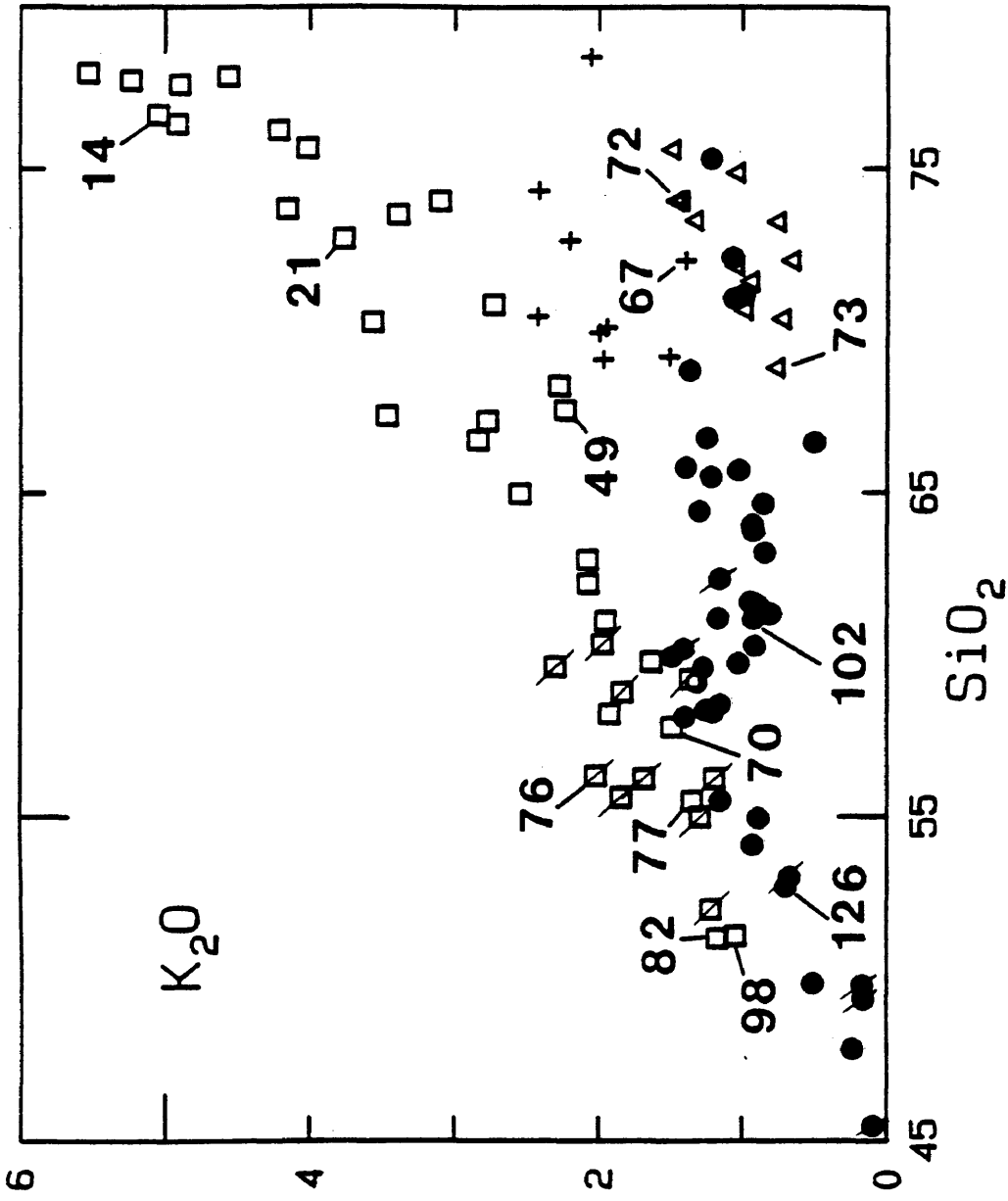


Fig. 2.9 K₂O-SiO₂ Variation Diagram

Numbers indicate isotopic age, diagonal lines note samples containing pyroxene, (Calc-alkaline: open squares, Calcic: filled circles, Trondhjemite: open triangles, Mixed: plus symbol)

with SiO_2 , analogous to the behavior of incompatible trace elements during fractional crystallization. Potassium is not a trace element and therefore is not an incompatible element in the traditional sense, but its exponential increase with increasing SiO_2 is still indicative of a crystallization process that concentrates K_2O in the melt. The progressive increase in K_2O is correlated with an exchange of biotite for hornblende as the dominant mafic mineral and a progressive increase in alkali feldspar content.

Variations of K_2O with increasing SiO_2 in the calcic rock series suggests a more complicated history. The mafic end of the series is similar to that of the calc-alkaline trend, but the increase in K_2O ceases at about 58% SiO_2 and K_2O remains constant throughout the more felsic portion of the rock series (Fig. 2.9). Variations along the mafic portion of the curve can be ascribed to fractional crystallization as in the case of the calc-alkaline rocks. The invariant portion of the curve could be interpreted to result from magma mixing, although no known low potassium, high silica mixing component has been identified. The marked change in curvature for the K_2O vs SiO_2 data from calcic rocks at 58% silica suggests that K_2O was buffered in the intermediate and felsic members and coincides with the change from hornblende-dominant to biotite-dominant mafic mineral assemblages within the calcic rock series. A precise explanation for the change in slope can not be defined, though the general parameters of the system can be identified. In a low K_2O parental magma, the change to K_2O saturated phases in the crystallizing assemblage could moderate K_2O in the resulting rocks. A crystallizing assemblage that incorporates K_2O at or above the concentration level of the liquid, will produce a stable or decreasing potassium content in the

magma and prevent potassium contents from rising in subsequent rocks. As the rocks become more silicic, the CaO content falls (Fig. 2.8) and the increasingly albitic plagioclase is better able to incorporate potassium. The increasing compatibility for potassium developed by plagioclase plus the growing proportion of biotite would enable the evolving crystallizing assemblage to more effectively incorporate potassium and stabilize its content in resulting rocks. This is opposite of what is observed in calc-alkaline rocks where potassium was incorporated into the crystallizing assemblage at a concentration lower than in the parental liquid. The increasing concentration of K_2O in the evolving magma resulted in higher concentrations of K_2O in successive rocks. This again suggests that the K_2O content of calc-alkaline magmas were substantially greater than that of calcic magmas.

Aerial and Temporal Distribution. Exposures of the calcic and calc-alkaline series rocks overlap geographically, but each type dominates a separate portion of the study area (Fig. 2.10). Most of the calcic series rocks are located in the western, seaward side, of the study area, while most of the calc-alkaline series rocks are located in the eastern, continental side. Calcic rocks in the east are relatively old isolated diorite and mafic tonalite plutons. Calc-alkaline rocks in the west consist of a young granite-granodiorite complex and isolated mafic tonalite and quartz monzodiorite plutons. Calcic plutons become more mafic to the north and east whereas calc-alkaline plutons become more felsic to the east.

A west to east migration of magmatic activity has been reported in northern Chile (Farrar et al., 1970). This is not characteristic of the SPB as a whole (Bruce et al., 1986a; Nelson et al., in press), and Weaver et al. (1986) have shown that magmatism is progressively younger toward the center of the SPB at 48°S. At 53°S the primary criterion for determining the nature of magmatic migration is field data and the erratic and inconsistent distribution of isotopic ages. Magmatism did not uniformly or linearly migrate with time. The central locus of magmatism moved from west to east, but old plutons exist in the east and plutons were continually emplaced throughout the lateral extent of the SPB. The discontinuous nature of the field data, and the limited number of isotopic dates do not allow for a rigorous definition of the spatial magmatic history.

Isotopic ages (Table 2.1, Fig. 2.9) suggest that the calcic rock series may be older than the calc-alkaline rock series. Dated mafic and intermediate calcic series rocks are older than any dated calc-alkaline series rocks. The lack of isotopic ages for felsic calcic series rocks, makes it impossible to determine if

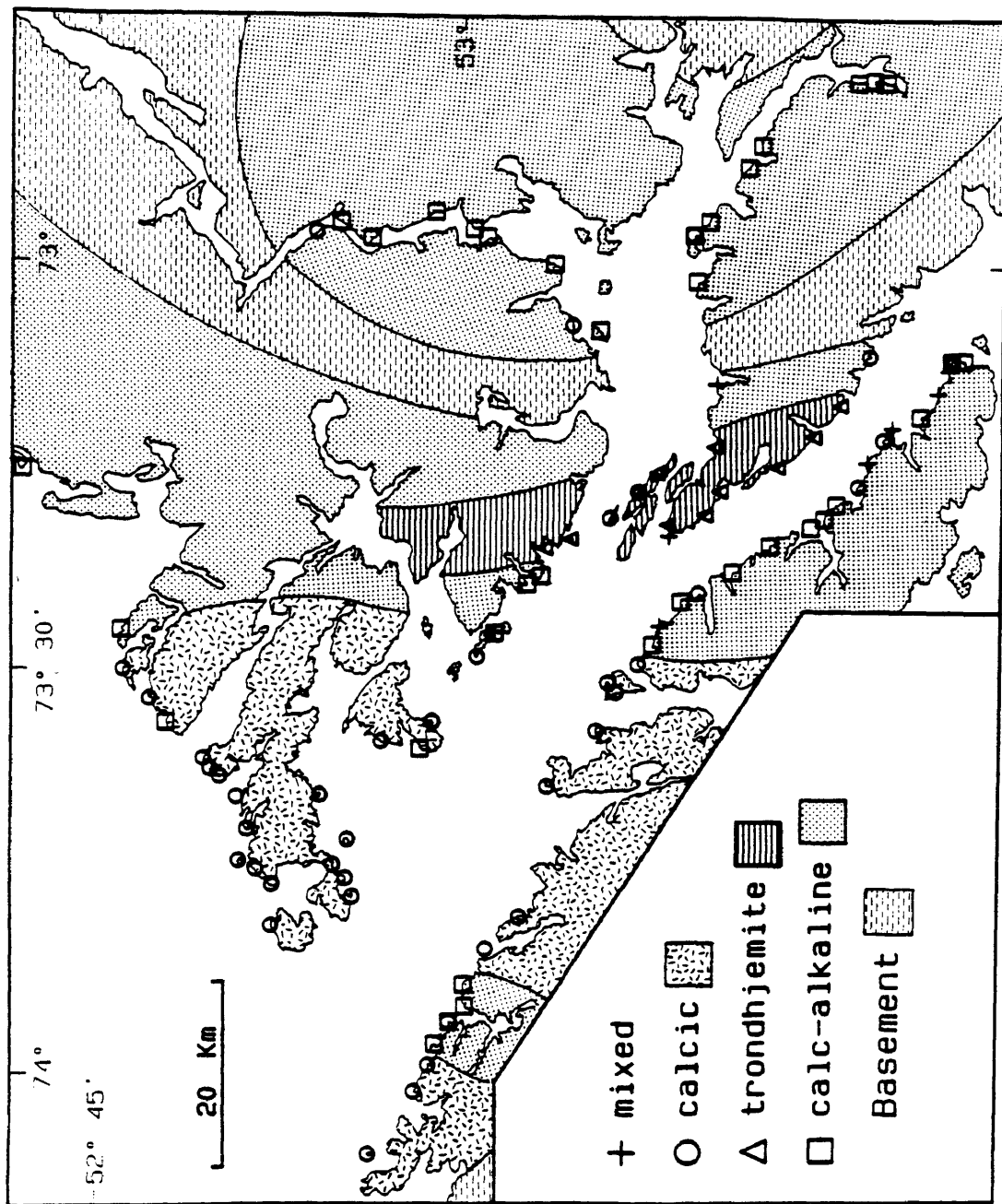


Fig. 2.10 Rock Series Map

Note how mixed rocks, marked by a +, are located within and adjacent to the trondhjemite dominated region.

the two rock series are coeval. The small gap in time between the youngest calcic age and the oldest calc-alkaline age suggest that some overlap may exist. Because of the geographic distribution of these two rock series, their apparent age difference further supports the idea that the center of magmatic activity migrated from west to east.

Minor Rock Series

Two volumetrically minor rock series, exposed in the Xaultegua study area, are atypical of plutonic lithologies found in the SPB. Plutons of these rock series are geographically and temporally restricted, and consist of a suite of trondhjemites and a suite of tonalites and granodiorites. Both suites are strongly peraluminous and might be considered to result from crustal melting of sedimentary rocks. However, they have relatively low Sri ratios (0.70443 and 0.70469) and because the basement has an average Sri of 0.7125 Weaver et al. (in press), it is concluded that these two rock series have incorporated little of the sedimentary basement assemblage. Their age and chemistry suggest they were generated from, or significantly contaminated by, older plutons of the SPB.

Trondhjemite Rock Series. Rocks of the trondhjemite series are felsic with a maximum sum of biotite, muscovite, garnet and opaque minerals of 10 percent. Biotite and muscovite vary greatly in their relative proportions. Garnet and the opaque minerals, dominated by magnetite, are only locally present. The rocks are medium grained with a marked foliation defined by aligned micas and partially recrystallized ribbon quartz. With a CI less than 10 and oligoclase as the plagioclase feldspar, these rocks are trondhjemites as defined by Barker (1979). Plagioclase is relatively free of sericitic alteration and biotite, muscovite and magnetite grains are unaltered. The unaltered nature of the minerals suggests the original plutonic composition of the rocks is relatively unchanged.

The trondhjemite series is compositionally similar to other trondhjemite suites, (Barker et al. 1976; Barker and Millard, 1979; Barker et al. 1979). These rocks have an Al_2O_3 content greater than 15 percent at 70 percent SiO_2 (Fig. 2.8) and are classified as high alumina trondhjemites (Barker, 1979). The high alumina content is characteristic of trondhjemites hosted in continental settings (Arth, 1979).

Hanson and Goldich (1972) and Arth and Hanson (1972) proposed that trondhjemitic liquids could form from basaltic sources, and the mafic members of the calcic rock series in the Xaultegua area would be a reasonable source composition of trondhjemite magma. Partial Melting of hydrous hornblende-plagioclase-rich rocks, such as those presented in Table 2.2, could yield trondhjemitic melts (Barker, 1979).

It is assumed that crustal melting within active magmatic arcs occurs under hydrous conditions, because all plutons in the Xaultegua area contain primary

hydrous minerals and the assumed presence of volatiles derived from the subducting oceanic crust. Higher a_{H_2O} increases hornblende stability, but also depolymerizes silicate melts and lowers the stability of framework silicates such as plagioclase. Thus, at middle to lower crustal pressures (5 to 25 kb) plagioclase will melt before hornblende as temperature increases (Wyllie, 1971). Preferential melting of plagioclase over hornblende produces an identifiable chemical signature in the resulting magma.

The low potassium content of the trondhjemites (0.65 to 1.47 percent K_2O) indicates they were derived from a low potassium source such as the mafic calcic series rocks (Fig. 2.8 and Table 2.2). The small and inconsistent percentage of potassium phases in the mafic calcic series rocks and varying degrees of partial melting could explain the range of Ba values. The high Ba contents suggest that whatever potassium phases originally existed in the source melted early.

Chemical evidence suggests that the trondhjemites were produced by preferential melting of plagioclase in the presence of a hornblende residuum, a proposed host similar to mafic calcic series rocks. Most calcic and calc-alkaline series rocks contain between 3 and 4 percent Na_2O , whereas the trondhjemites contain between 4.59 and 6.39 percent Na_2O (Fig. 2.8). The higher Na_2O content can be explained by melting of plagioclase in the source, which produces a sodic melt (Bowen, 1913). Hornblende would not buffer Na_2O resulting in a melt with a higher concentration of Na_2O than its source. Another indication that plagioclase melted in the presence of hornblende is the decoupling of CaO and Sr (Fig. 2.8). CaO is significantly lower in the trondhjemites than in the mafic calcic rocks as would be expected from melting of plagioclase. The trace

element Sr generally behaves like CaO and is compatible in plagioclase, but is incompatible in hornblende (Arth, 1976). Sr is higher in the trondhjemites than in many of the mafic calcic rocks, indicating that as plagioclase melted, CaO was incorporated in the residual assemblage of increasingly calcic plagioclase and hornblende while Sr was not. Effectively, hornblende incorporated CaO released during melting while the Sr accumulated in the melt. Further evidence of residual hornblende can be seen in the Y data (Fig. 2.8). All trondhjemite samples have Y concentrations less than 10 ppm, suggesting that a mineral such as hornblende (in which the HREE elements are highly compatible) remained in the residuum during partial melting. Again these data suggest that plagioclase was the primary phase melted and that hornblende remained in the residuum. The low TiO₂ content of the trondhjemites (Fig. 2.8) indicates that melting did not proceed to the point of involving significant amounts of iron-titanium oxides.

The age and location of the trondhjemites suggests that they were a product of the Andean orogeny. The two dated samples (73 and 72 Ma) crystallized after the peak of metamorphism associated with this orogeny, estimated at 100 to 85 Ma in the Cordillera Darwin area at 55°S (Fig. 2.1; Nelson, 1981; Herve et al., 1981), and after the peak of maximum recorded magmatism in the SPB as a whole (Fig. 2.11). The coincidence of a crustal thickening event (Andean orogeny) and high heat flow associated with a peak in magmatic activity would create conditions appropriate for melting of mafic plutonic rocks. If the trondhjemites represent crustal melting, their confinement to a narrow belt along the center of the batholith (Fig. 2.2 and 2.10) suggests that only in the center of the magmatic arc did the temperature rise sufficiently

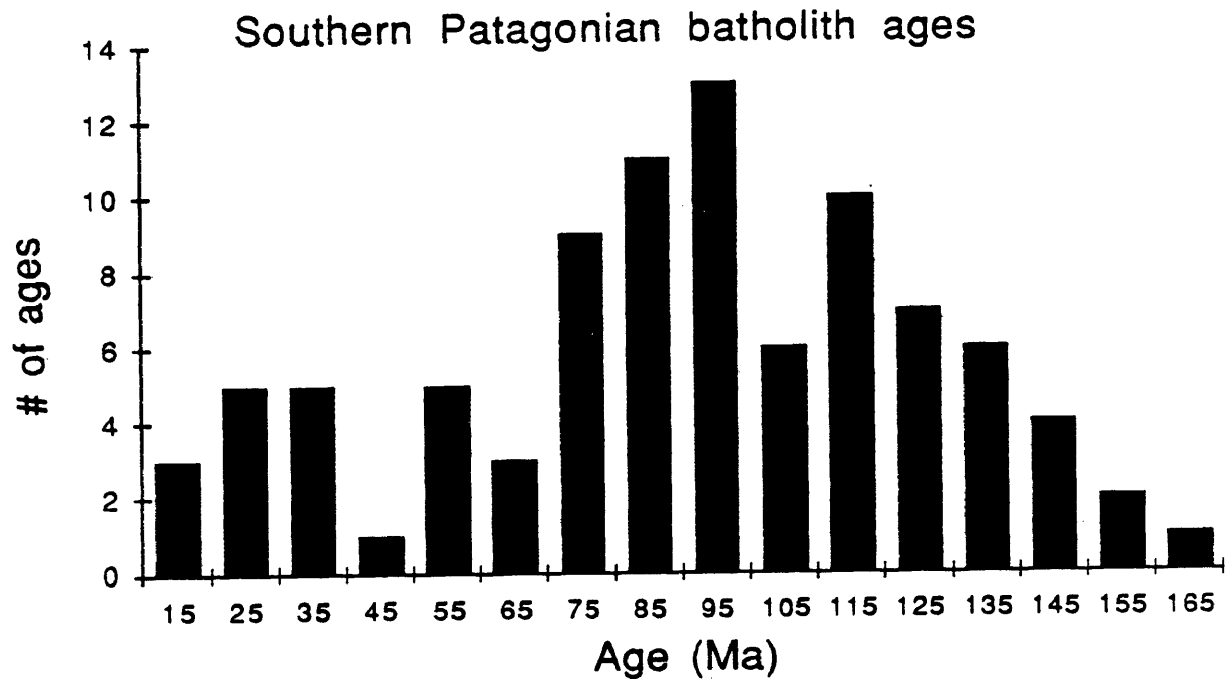


Fig. 2.11 Age Histogram

Data from plutonic rocks from the southern Patagonian batholith, 48°-55° S. compiled from: Halpern, 1973; Herve et al., 1981; Herve et al., 1984; Bruce et al., 1986a; Bruce unpublished; Suarez et al., 1986.

to induce melting of mafic plutonic rocks.

In the Xaultegua area, trondjemites have a deformation fabric whereas older and younger plutonic rocks do not. This suggests that, at the emplacement level exposed today, deformation was not very intense and that only rocks intruded during or shortly before the deformation were thermally weakened enough to be affected. The age and intensity of deformation are less than to the south in Cordillera Darwin, and it appears likely that the northward migration and decrease in intensity of deformation recognized in the foreland (Winslow, 1982) also occurred in the magmatic arc portion of the orogen.

Mixed Rock Series . The mixed rock series consists of medium-grained tonalites and granodiorites (Fig. 2.7) that border (Fig. 2.2), and postdate the trondhjemites (Fig. 2.9). These rocks are locally deformed, though significantly less so than the trondhjemites. Euhedral plagioclase grains show significant sericite alteration that may have affected the original igneous composition of these rocks. Biotite (1 to 10%) is present in every sample and trace amounts of muscovite and garnet are present in most samples. The alteration, aluminous mafic minerals, composition, and variable deformation are characteristics intermediate between the trondhjemites and felsic calc-alkaline rocks.

In addition to the age, location, and petrographic data, chemical evidence supports the hypothesis of a mixed origin for this rock series. Fig. 2.8 demonstrates the variable affinity these rocks have for the other rock series.

The criterion that best displays the potential mixed origin of these rocks is the plot of CaO-K₂O-Na₂O (Fig. 2.12). With the data displayed in this manner, it is clear that samples of the mixed rock series lie between the trondhjemite series and the intermediate and felsic members of the calc-alkaline series.

Rocks of the mixed series have only been recognized in exposures adjacent to the trondhjemite belt. They are younger than the trondhjemites as determined from intrusive relationships and isotopic dating (Figs. 2.2 and 2.9). Rocks in the border zone of the trondhjemite belt that are not members of the mixed rock series are all older, more mafic plutons of the calcic and calc-alkaline rock series.

The available data are consistent with the mixed rock series having formed as a result of interactions between rocks of the trondhjemite series and younger felsic calc-alkaline magma. Plutons of the mixed rock series are younger than, and peripheral to, the trondhjemites. They have chemical, mineralogical, and textural characteristics intermediate between the trondhjemite series and the felsic members of the calc-alkaline rock series. Their geographic restriction suggests a relationship between the mixed and trondhjemite rock series. The temporal relationship suggests that the mixed rock series represents a younger magmatic event than the trondhjemite rock series. Only the mixed and felsic calc-alkaline plutons are younger than the trondhjemites.

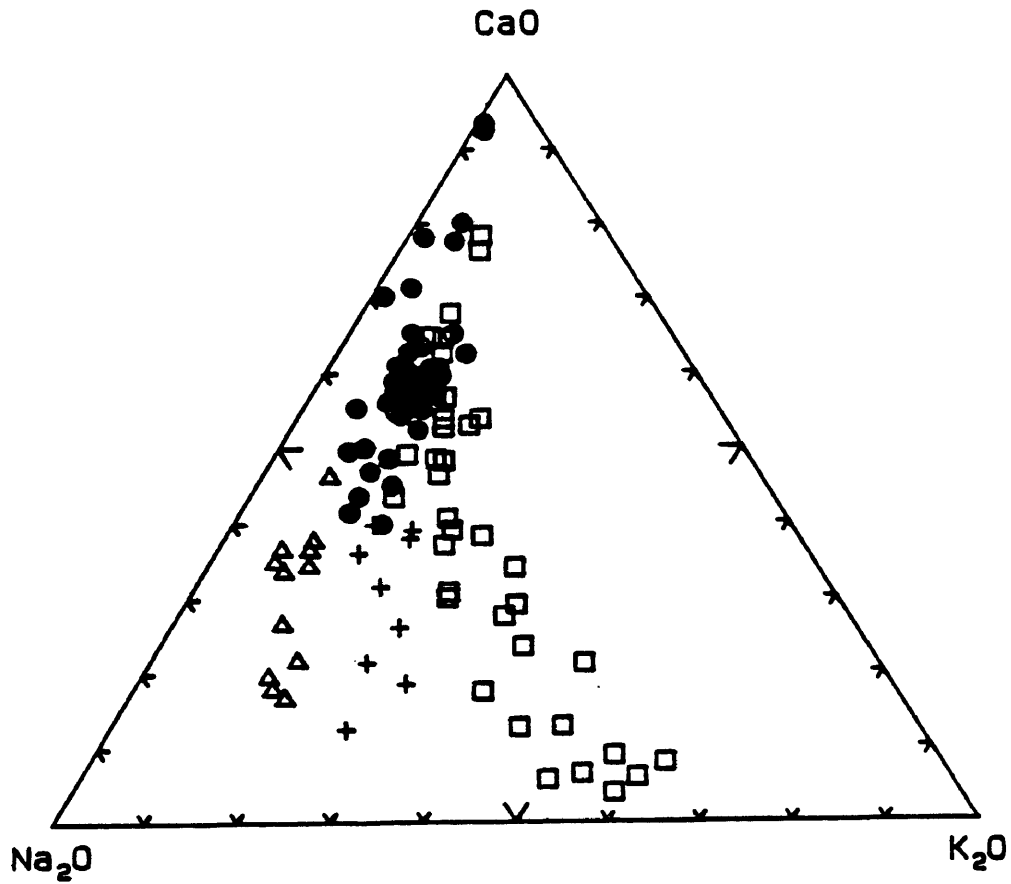


Fig. 2.12 CaO-Na₂O-K₂O Variation Diagram

Major element data from the Xaultegua area, (Calc-alkaline: open squares, Calcic: filled circles, Trondhjemite: open triangles, Mixed: plus symbol)

Conclusion

Sr(i) data suggest that plutons of the Xaultegua area were principally derived from mantle- and young mantle- derived sources without significant involvement of old continental components. The broad compositional range and divergent lithological trends indicate that complex and varied fractionation and mixing processes were involved. Magma evolution processes, that originated in the mantle, continued within the crust. The lack of recognized short, repeated, magmatic evolutionary cycles indicates that the petrogenetic processes involved are not analogous to those studied in Peru.

Based on available data, the large range of isotopic crystallization ages and the slow lithologic progression precludes a simple model involving all plutons crystallizing from a single magmatic event. Because of the large distance and time separating samples within the calcic and calc-alkaline rocks series they can not be cogenetic in the sense of originating from a single batch of magma. The fact that the two trends maintain their integrity over such large distances and long time intervals suggest the petrogenetic processes involved in magmatic arc plutonism are extremely stable and long lived. The two rock series are the product of distinct parental starting magma types and fractionation systematics which were repeatedly followed by individual batches of magma over a long period of time. The progressive change in lithology representing ever more evolved portions of these sequences reflects gradual changes in the chemical and physical parameters of the arc environment.

The Xaultegua area is volumetrically dominated by rocks of the calcic and

calc-alkaline series. Field observations from throughout the SPB and findings from the Xaultegua area indicate that the SPB is dominated by plutons from these two rock series. The age and spatial distinction between the two rock series indicates that their development was physically, temporally, and chemically independent. These differences signify evolving crustal and mantle processes and conditions during magmatic arc evolution.

The distinctive character of the trondhjemite rock series appears related to crustal melting of mantle-derived, hornblende-bearing mafic plutons, such as the early mafic calcic series rocks. This interpretation suggests that other felsic plutonic rocks in the Xaultegua area may also be the product of crustal melting that did not result in as distinctive and identifiable a lithology. Very little true granite is produced by fractional crystallization of a primitive parental magma. Because granite is present in greater abundance (10 to 20% in the Xaultegua area and throughout the SPB), some of these granites may have resulted from partial melts of intermediate and mafic members of the calc-alkaline rock series.

Rocks of the mixed series appear to have resulted from contamination of evolved calc-alkaline magmas by their aluminous trondhjemite host rocks. It is thus likely that other crustal contamination events have occurred, but the resultant hybrid rocks may not be sufficiently distinctive to be recognized in this reconnaissance study. The compositional overlap between the mafic and intermediate members of the calcic and calc-alkaline rock series may result from crustal magma mixing processes.

The fact that the oldest and youngest plutons occur along the eastern margin of the batholith suggests that most of the magmatic activity occurred

within the original confines of the early plutons. Subsequent intrusions effectively pushed older plutons outward as appears evident at 48°S, (Weaver et al., 1986) which suggests that arc plutonism may have occurred under extensional conditions. The batholith appears to have grown from within as the margins moved outward. This may explain why few supracrustal rocks exist within the batholith and why crustal contamination decreases with time.

Chapter 3

EFFECTS OF SYNCHRONOUS UPLIFT AND INTRUSION DURING MAGMATIC ARC CONSTRUCTION

Introduction

The relationship between composition, age, and crystallization depth, of plutonic rocks in the southern Patagonian batholith (SPB), suggests that uplift and plutonism, operating synchronously, strongly influence the evolving structure and composition of magmatic arcs. Plutonic records from individual areas within the batholith show a consistent mafic to felsic intrusion history. In addition, field and geobarometric evidence suggests that mafic plutons generally crystallized at greater depths than felsic plutons. Also, plutonic records from different areas have unique and overlapping age ranges, suggesting diachronous magmatism. However, all plutonic samples, regardless of lithology or field location, fit on a trend of decreasing initial Sr (Sr_i) with decreasing age. This indicates a progressive decrease in crustal involvement throughout the arc, and suggests that magmatism was not diachronous, but occurred in all areas during the same protracted period of arc construction. We present an arc construction (AC) model involving synchronous and continual plutonism and uplift to explain the observed relationship between plutonic age, composition, and crystallization depth.

The AC model is useful in comparing the uplift histories of individual areas within an arc. Variations in the age of the oldest pluton and the length of the plutonic record indicate differences in the rate and amount of uplift. In addition petrologic and temporal differences between the mesozonal environment exposed in the SPB and the epizonal environment exposed in the Coastal batholith (CB) of Peru can be explained using the AC model. The spectrum of exposed plutons is a function of the rate and depth of magmatic additions to the crust, as well as the uplift-erosion history.

The AC model includes assumptions of continual uplift and continual plutonism in magmatic arcs at convergent continental margins. The model focuses on the effect of changing plutonism and uplift rates. Therefore, it cannot be used to interpret age, lithology, and crystallization depth patterns produced during episodic magmatism. Because the AC model pertains to the crust as a whole, intermittent magmatic records exposed at the surface need not invalidate the model.

Previous work in the SPB includes early reconnaissance studies (e.g., Darwin, 1846; Kranck, 1932) that reported general lithologic data from isolated locations, and more recent petrochemical and geochronological studies of specific areas or transects (e.g., Halpern, 1973; Stern and Stroup, 1982; Suarez, 1977; Bartholomew and Tarney, 1984; Herve et al., 1984). We have mapped and sampled much of the SPB exposed at sea level in reconnaissance, and have undertaken more detailed geochronology and geochemistry in three areas: Darwin, Xaultegua, Baker (Fig. 2.1) (Nelson et al., 1980; Bruce et al., 1986a; Weaver et al., 1986a).

Geologic and Tectonic Setting

The SPB, exposed in the southern Andes of Chile, is one of the largest Mesozoic-Cenozoic circum-Pacific batholiths (Fig. 2.1). The southern Andes are situated along the active continental margin of southernmost South America where the oceanic Nazca and Antarctic plates are being subducted below the continental South American plate (Fig. 2.1). This region has probably been a convergent margin continually since at least the late Paleozoic (Dalziel, 1981; Forsythe, 1982).

Host rocks of the SPB are predominantly late Paleozoic to early Mesozoic(?) accreted forearc assemblages including 1) volcanoclastic flysch, 2) radiolarian chert, 3) metamorphosed mafic-ultramafic rocks, 4) reef limestone, 5) pillow basalt, and 6) quartz-veined phyllite (Forsythe, 1982). Other host rocks, exposed along the eastern contact and in isolated exposures within the SPB, include late Jurassic silicic volcanic rocks, early Cretaceous ophiolitic rocks, and early Cretaceous shale and volcanoclastic flysch. Isolated Tertiary plutons intrude late Cretaceous foreland basin sedimentary rocks east of the main batholith and are considered by some (e.g., Stern and Stroup, 1982) to be part of the batholith. In addition, mafic to felsic volcanic rocks of unknown age are present in isolated exposures within the SPB. They are generally moderately altered and locally foliated; they may represent syn-plutonic volcanic rocks down-faulted into the batholith, volcanic rocks preserved in intra-arc basins, or pre-batholith volcanic rocks preserved in roof pendants.

Lithologies of the SPB

The SPB consists of a typical spectrum of calc-alkaline and calcic plutonic rocks (Nelson et al., 1985; Bruce et al., 1986a; Weaver et al., 1987). Mafic rocks include gabbro, gabbro and hornblende diorite. Intermediate rocks include hornblende quartz diorite and biotite-hornblende tonalite. These rocks make up a majority of the batholith. Felsic rocks include biotite granodiorite, tonalite and granite, with a minor population of leucocratic granite and hypabyssal microgranite. Mafic xenoliths are common but not ubiquitous, and mafic dikes or irregular aphanitic bodies intrude all but the most felsic plutons. Both syn- and post-plutonic mafic dikes are present; together they make up between 5 and 35 percent of most plutons. Cross-cutting relationships within a given area indicate that, excluding dike rocks, mafic rocks are older than felsic rocks.

I-type rocks predominate, but a small percentage of crustally-derived or contaminated rocks also exist (Nelson et al., in press). These plutons vary in their relative age, whereas the I-type rocks crystallized in a consistent age-lithology pattern. The crustally-derived or contaminated rocks crystallized at different times in the intrusive sequence, usually early in the magmatic history. These lithologies include granite, granodiorite, and high-alumina trondhjemite. Many samples contain the magmatic aluminous phases biotite, muscovite, garnet; some also contain dumortierite.

Age-Lithology-Crystallization Depth Relationship

Field, petrographic, and geobarometric data from plutonic rocks demonstrate a relationship between lithology, crystallization depth and crystallization age. Within the Xaultegua study area (Fig. 2.1) the youngest plutonic rocks are granite and rhyolite; both contain miarolitic cavities indicative of crystallization at shallow depths. Older, more mafic rocks are medium- to coarse-grained granodiorite, tonalite and quartz diorite. The oldest rocks are medium- to coarse-grained diorite and gabbro whose textures suggest that they crystallized at greater depths than the granite.

Some of the oldest rocks contain magmatic epidote in equilibrium with hornblende and biotite, an equilibrium assemblage that constitutes 50% to 70% of the rock. This assemblage is interpreted as resulting from crystallization at pressures between 6 and 8 kb, suggesting emplacement at a depth of 18 to 24 Km (Zen and Hammarstrom, 1984). Geobarometry, using alumina compositions of hornblende, confirms the high pressure crystallization of these old mafic rocks with calculated pressures as high as 10 kb (Hammarstrom per. com. 1987).

The intermediate composition plutons throughout the SPB appear to have crystallized at mesozonal depths. They crystallized deeper than the young epizonal granites and shallower than the old mafic plutons. These observations suggest that there is a decrease in crystallization depth recorded in successively younger and more felsic plutons.

Arc Construction Model

A simple arc construction model explains the available field and laboratory data. The model involves uplift synchronous with plutonism, with magma composition influencing pluton crystallization depth. Construction of a batholith above a steady state subduction zone involves essentially continual magmatic inflation of the arc, resulting in continual uplift and erosion. Thus for simplicity, the model assumes constant rates of plutonic input and uplift for a given area. Following crystallization of the earliest plutons, uplift and erosion will bring these plutons progressively closer to the surface. As older plutons are uplifted to shallower depths, younger, more felsic, plutons intrude and crystallize adjacent to them. The mechanism is analogous to an assembly line, where the crust is a vertical conveyer belt and the plutons of decreasing age and changing composition are parts assembled over a long time period. The end product, seen at the surface today, is a batholith composed of a broad spectrum of lithologies with vastly different ages.

Figure 2.11 is a histogram of plutonic crystallization ages from the SPB screened to remove both model ages with assumed Sr ratios and unduplicated potassium-argon determinations. A simple interpretation of the histogram suggests that plutonism began 160 million years ago and has occurred continually ever since. However the AC model shows that such histograms may not accurately portray the timing and nature of magmatism in an uplifting arc. We will demonstrate how simple analysis of age histograms can result in inaccurate

interpretations of magmatic histories.

The fact that some old plutons crystallized at depths as great as 24 km, whereas some young plutons crystallized only a few kilometers below the surface, suggests that uplift occurred during the period of recorded magmatism. Thus the exposed suite of plutonic rocks represents a collection of plutons, each of which crystallized within the same crustal horizon during its ascent toward the earth's surface. From the persistent relationship between plutonic ages and compositions, we infer that magma composition controlled crystallization depth. Thus, mafic plutons appear to have crystallized at greater depths than felsic plutons.

Our AC model, diagrammed in Fig. 3.1, shows continual crystallization of plutons during continual uplift. Mafic plutons crystallize at greater depths than felsic plutons and both the rate of uplift and the rate of plutonic input are held constant. The suite of plutons that reaches the surface in the model is created by the continual crystallization of magma within an uplifting crust. The resulting plutonic suite matches the pattern of age, composition and crystallization depth observed in the SPB. Note, however, that the suite does not accurately record the age and composition of plutons input into the model. The apparent lithologic progression is an artifact of synchronous uplift and plutonism and the relationship between crystallization depth and magma composition.

If magma composition changes with time, only a limited range of lithologies will be produced at any given time. If this is true, magma composition need not influence crystallization depth. The following geochronologic and Sr isotopic data suggest that magma composition does not change with time and that a relationship does exist between magma composition and emplacement depth.

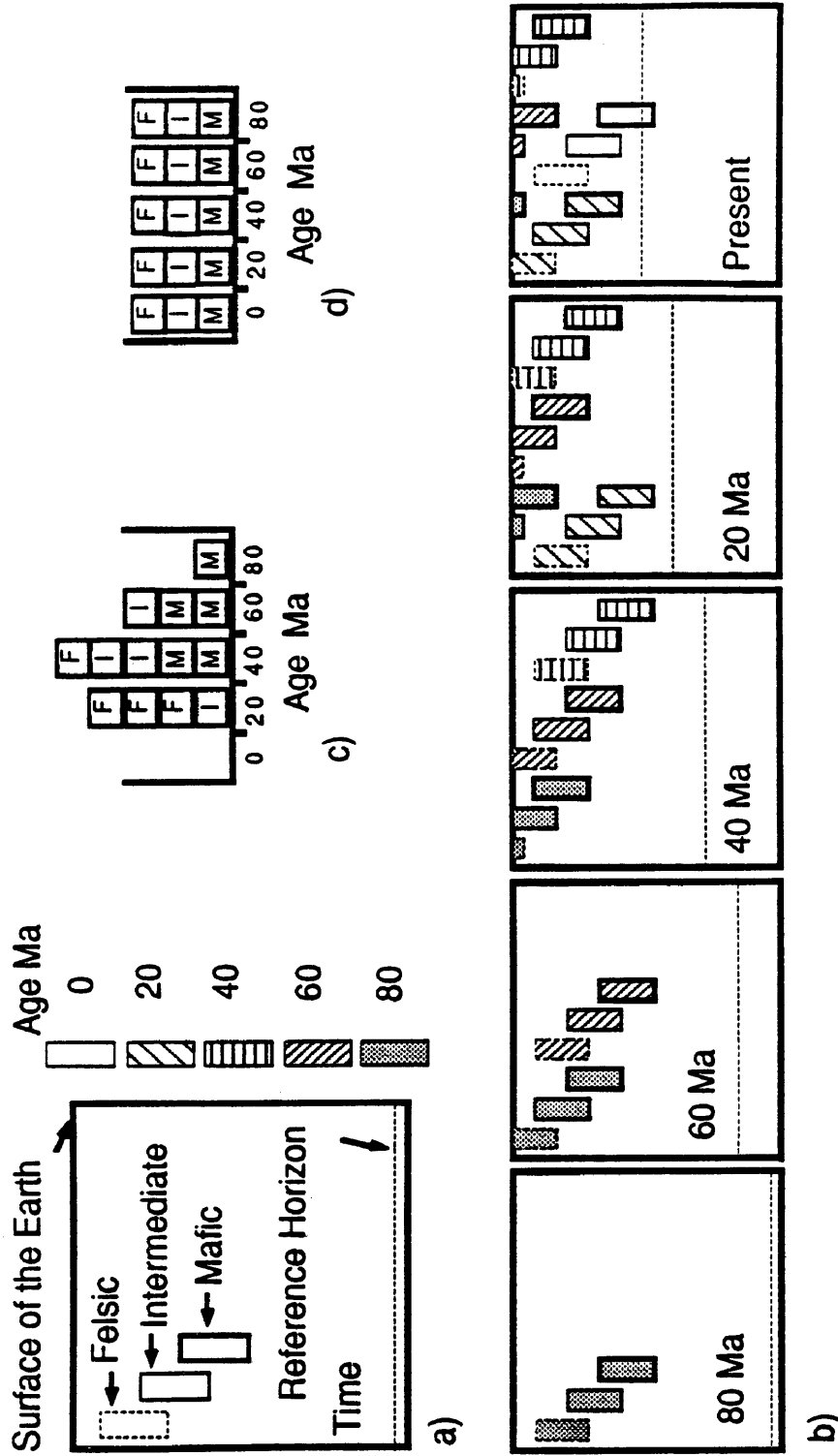


Fig. 3.1 Basic Arc-Construction Model

A) Key to symbols. Large boxes are cross sections of the upper crust (not to scale). Small rectangles represent plutons; pluton lithology is distinguished by bounding lines; age of crystallization is distinguished by fill patterns. The age of each image is noted in the lower left. Age-lithology histograms: C) plutons exposed on erosion surface in last frame (Present) of model. D) all plutons input to the model. Lithologies are identified as F=felsic, I=intermediate, and M=mafic plutons.

Geochronology & Sr isotope data

New isotopic age determinations from plutons in the SPB appear to record the age of crystallization. These data (Table 3.1) demonstrate an age concordance between Ar/Ar mineral ages from the same sample, between Ar/Ar mineral ages and Sr isochron ages from the same sample, and between Ar/Ar mineral ages and U-Pb zircon ages from the same pluton. In addition, most individual Ar/Ar release spectra show good plateaus, suggesting that these isotopic systems were not thermally reset or isotopically-disturbed.

Crystallization ages from the three study areas confirm and quantify the relative ages obtained from the field (Fig. 3.2). The ages also show that the lithologic progression occurs over a period of 50-80 m.y. This is longer than the expected life of a single evolving batch of magma. For example Pitcher et al. (1985) describe mafic to felsic cycles in the Coastal batholith of Peru that are interpreted to have formed as the product of an evolving magma in 5-10 m.y. The long term lithologic progression observed in the SPB must result from long lived processes that existed throughout the arc. Also note that exposures in each individual area record only a portion of the entire period of magmatic activity. These differing records can be explained by variations in uplift rate.

The different ages of the oldest plutons in different areas suggest either that magmatism was diachronous along the arc or that each area had a different uplift history. Diachronous magmatism implies that the arc was segmented into discrete tectonic domains, each with a unique period of active magmatism.

Table 3.1 Isotopic Ages, southern Patagonian batholith

| Sample # | Mineral | $^{40}\text{Ar}/^{39}\text{Ar}$ | Rb/Sr | U/Pb |
|----------|-------------|---------------------------------|------------|-----------------|
| RB-106 | zircon | | | 149.3 \pm 0.8 |
| | biotite | 144 \pm 6 | | |
| OE-5 | zircon | | | 113.1 \pm 0.7 |
| OE-6A | biotite | 109 \pm 1 | | |
| RB-98 | plag-bio-wr | | 92 \pm 6 | |
| | biotite | 90 \pm 1 | | |
| BB-6A | zircon | | | 76.2 \pm 0.4 |
| 3G-210 | biotite | 77.3 \pm 1.1 | | |
| MA-71B | biotite | 70.5 \pm 0.9 | | |
| | muscovite | 72.8 \pm 0.7 | | |
| MA-70A | biotite | 72.6 \pm 5.0 | | |
| BB-2A | hornblende | 71.9 \pm 3.8 | | |
| | biotite | 68.6 \pm 0.5 | | |

Grouped data represent samples from the same pluton

Considering the 160 m.y. magmatic record in the SPB, such an effective and prolonged segmentation of the arc seems unlikely. Studies of the more recent geologic history of northern Chile and Peru have identified segments of the arc with separate tectonic and magmatic histories. The segments are related to the age of subducted ocean crust, subduction geometry, and the location of subducting aseismic ridges (Pilger, 1981; Jordan et al., 1983; Wortel, 1984). However the boundaries of these segments are transitory and would not remain stationary for 160 m.y. In southern Chile no such segmentation has been documented in the sedimentary and deformational history of the foreland basin adjacent to the

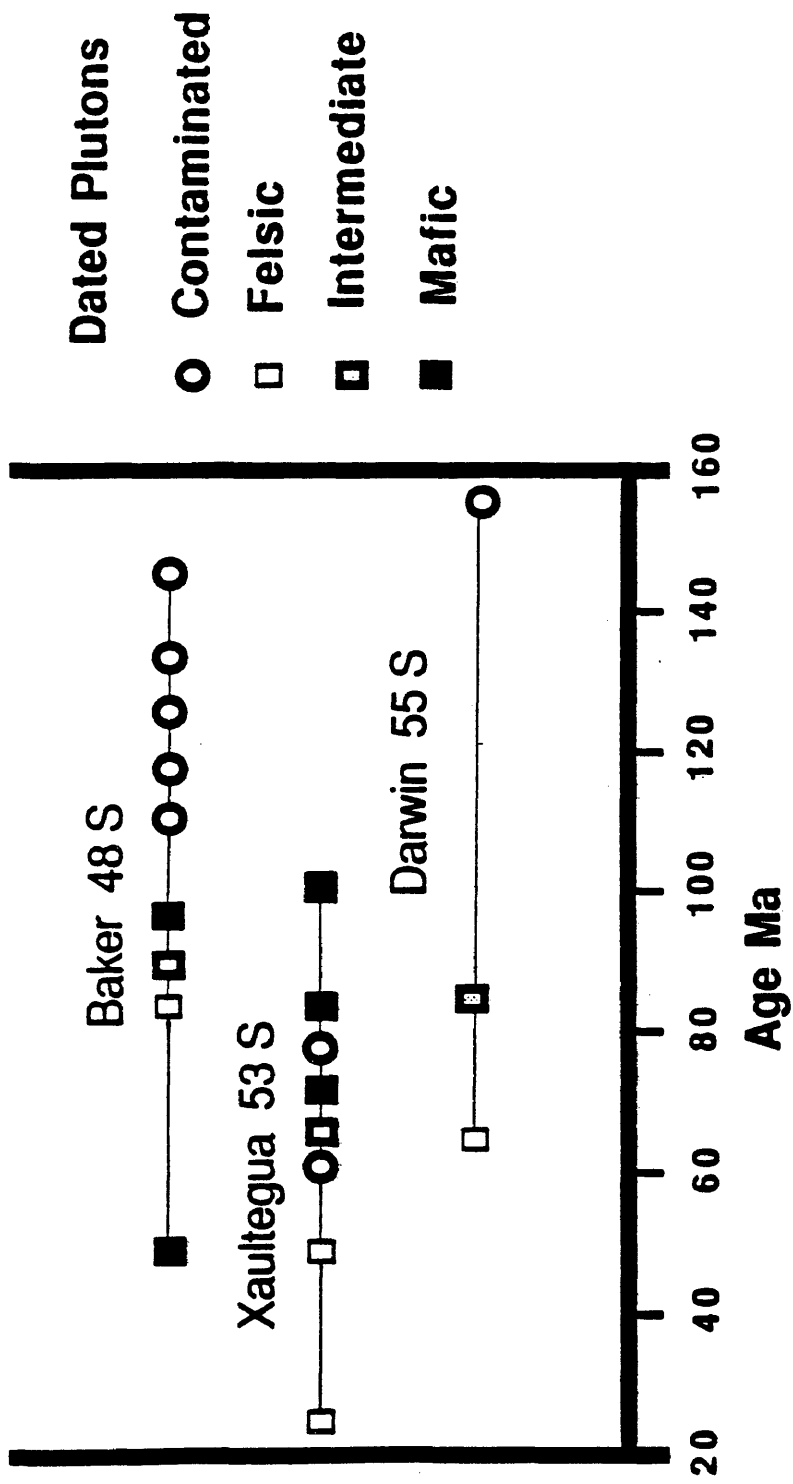


Fig. 3.2 Age-Lithology-Area Diagram

Data for the three study areas within the southern Patagonian batholith.

SPB (Dott et al., 1982; Winslow, 1982). The conclusion that the arc experienced a common magmatic history is also supported by isotopic data.

In plutonic rocks from the three study areas within the SPB (Fig. 2.1), Sri decreases with decreasing age (Fig. 2.5), regardless of sample location or lithology. The regional nature of the Sri trend suggests that the entire SPB shared a unified magmatic history. These data have been interpreted as representing a decrease in crustal contamination of mantle-derived magma with time (Weaver et al., 1986a, 1986b; Nelson et al., 1987). The age-Sri relationship suggests that regions containing only young plutons with low Sri were the site of older magmatism. The older magmatism diluted the accretionary prism sediments and converted them to a more refractory and less reactive assemblage. These older plutons were subsequently uplifted and eroded.

The interpretation that different areas within the batholith experienced a common magmatic history has three significant implications. The first is that lithology is not a time dependent function. Granite and gabbro plutons were crystallized over wide and overlapping time intervals and those that crystallized at the same time have similar Sri values (Figs. 3.2 and 2.3). Thus magmas of a wide range of compositions crystallized throughout the period of recorded magmatism. The second implication is that mafic plutons crystallize at greater depths than felsic plutons. Finally, crustal blocks exposing only young plutons with low Sri were the site of older more radiogenic plutonism.

Effects of varying uplift rates

Plutonic age spectra can yield information about uplift histories in magmatic arcs. Relatively slow uplift requires a longer period of time to bring the old, deeply emplaced plutons to the surface. Slow uplift thus preserves the early magmatic history and leaves long plutonic records. Rapid uplift results in a shorter plutonic record and a younger initiation of recorded magmatism.

Figure 3.3 illustrates how different age distributions are predicted from areas with different uplift rates during plutonism. Synthetic age-lithology histograms (Fig. 3.4a) for the three modeled uplift rates demonstrate the younger and shorter age distributions that are predicted for areas with more rapid uplift. Even though the age range is shortened by rapid uplift, the mafic to felsic lithologic progression remains evident. A composite, synthetic age-lithology histogram (Fig. 3.4b), combines all three histograms from Fig. 3.4a, simulating the effect of tabulating ages from distant locations with different uplift histories. As in the individual synthetic histograms, the observed age-lithology progression is an artifact of the uplift mechanics that exposed the observed plutonic suite. This can be seen by comparing a histogram containing the total magmatic input to the model (Fig. 3.4c) with the preserved record of exposed plutons (Fig. 3.4a and 3.4b). Because a batholith is sampled only at one erosion level, the composite histogram (Fig. 3.4b) is not a true record of arc magmatism.

The influence of uplift rate on the plutonic age distributions illustrated by the model (Fig. 3.4a and 3.4b) suggests that caution should be used in interpreting plutonic age histograms. It is reasonable to conclude that magmatic

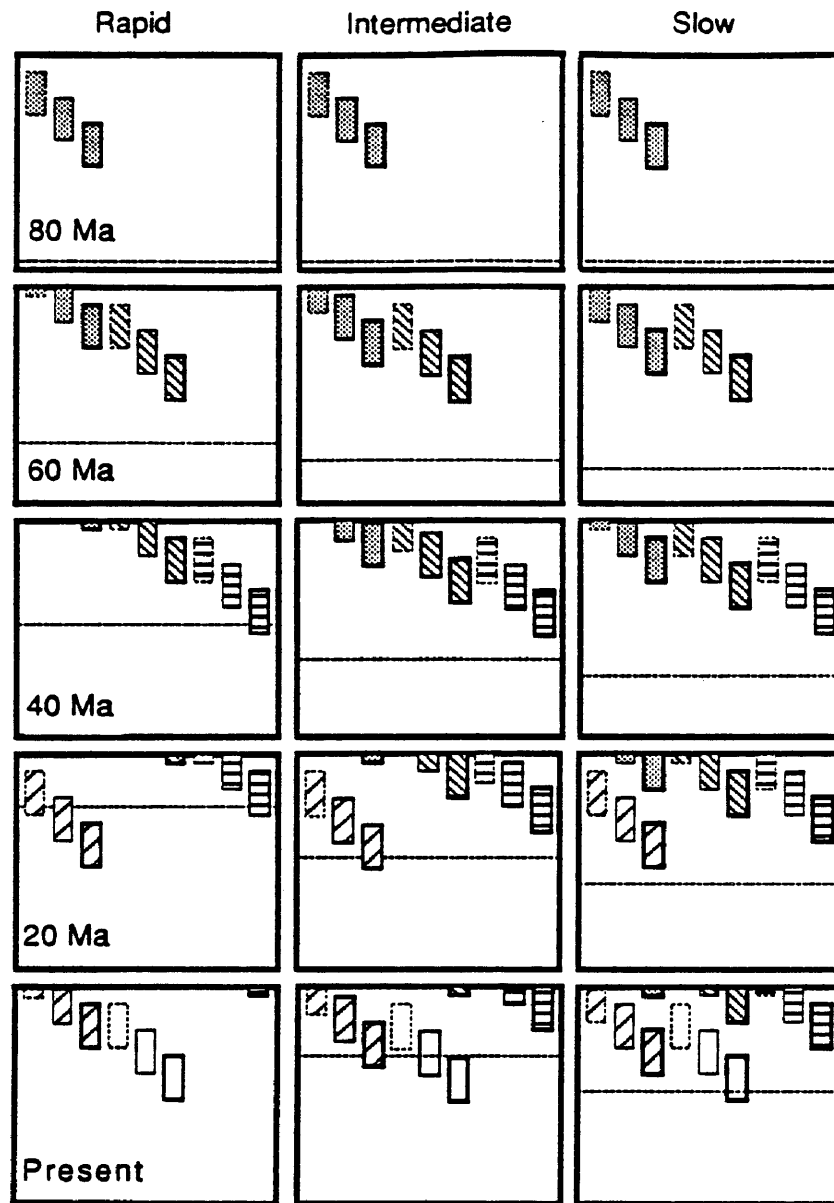


Fig. 3.3 Multiple Uplift Rates

For an explanation of pluton ages and lithologies, see Fig. 3.1. All three models start at the top and proceed downward in 20-my increments. Each uplift rate results in a different suite of exposed plutons.

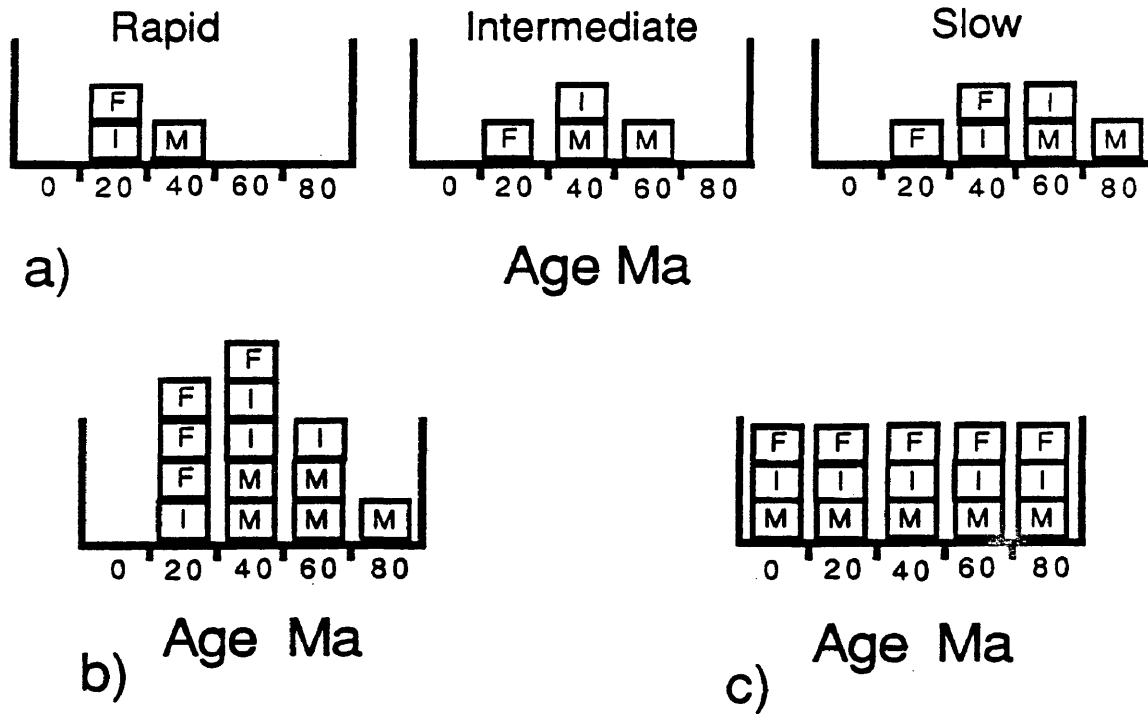


Fig. 3.4 Synthetic Age-Lithology Histograms

Letters signify lithology, M=mafic, I=intermediate, F=felsic rocks. a) results of the three separate rate uplift models in Fig. 2; b) summation of the data from all three histograms in Fig. 3a; c) record of the total plutonic input in the model.

activity may have occurred prior to the oldest dated pluton. The compositional variability and timing of magmatism also may not match the exposed record. Tectonic and petrologic reconstructions must be tempered by the knowledge that the observed plutonic record may not be an accurate reflection of past magmatic events.

A comparison of the plutonic ages in the Baker and Xaultegua areas illustrates the utility of the AC model. In the Baker area plutonic ages range from 149 Ma to 46 Ma, an interval of 103 m.y. In the Xaultegua area, plutonic ages range from 99 Ma to 22 Ma, an interval of 77 m.y. The older initial age and the longer magmatic period in the Baker area suggests this region experienced slower uplift than the Xaultegua area. The older plutonic record in the Baker area also indicates the region experienced less total uplift than the Xaultegua area.

Assuming continual magmatic activity, the magmatic record should continue to the present. However, both regions appear to lack portions of their youngest magmatic record. Few young plutonic rocks and no Holocene volcanic rocks are known in these two areas. Thus, the AC model as described thus far does not fully explain the relatively recent history of these areas. To address this discrepancy and to further explore the relationship between uplift and magmatism, we have expanded the model to account for changes in the rate of magmatism and erosion and changes in the vertical distribution of magmatic additions to the crust.

Crustal Kinematics in Magmatic Arcs

Uplift cannot be measured directly with paleogeobarometers utilizing rock texture, mineral assemblage, or mineral chemistry. These tools can be used to estimate depth relative to the paleo-surface of the earth. This depth measurement is insensitive to the location or motion of the earth's erosion surface relative to some fixed reference. In other words, uplift may occur, but if a pluton does not approach the surface, uplift will not be detected by these methods. Changes in depth are caused by erosion. If the rate of uplift exceeds that of erosion a lag time will occur between uplift and changes in depth recorded by geobarometry. Because of the difference between uplift and changing crustal depth, they must be clearly distinguished in the following discussion. Uplift and subsidence will be used to refer to vertical motion relative to a fixed reference and shallowing and deepening will be used to refer to changes in depth relative to the earth's surface.

The result of these crustal processes is that rocks below a particular depth move away from the erosion surface and may never be exposed. Therefore this depth will have an important affect on the suite of plutons exposed, and must be accounted for in the AC model. In magmatic arcs, crustal thickening, through magmatic inflation combined with isostatic compensation, causes uplift of the upper crust accompanied by subsidence of the base of the crust.

We introduce the concept of a nodal plane to evaluate the vertical motion of rocks at depth induced by changes in crustal thickness. The nodal plane is a theoretical surface within the crust, above which the mass of magmatic additions

equals the mass removed by erosion within a given time interval (Fig. 3.5a). Rocks above the nodal plane will experience shallowing while rocks below the nodal plane will experience deepening. No shallowing is experienced below the nodal plane because the mass removed by erosion is balanced by magmatic additions above the nodal plane. Magmatic additions below the nodal plane are not balanced by erosion and hence contribute to crustal thickening. Thus, rocks below the nodal plane will not reach the surface of the earth until changes in the rate or depth of magmatism, or changes in the rate of erosion, lower the nodal plane. Rocks below the nodal plane may experience both deepening and uplift during crustal thickening. Thus, apparent subsidence observed in time-depth histories can be created during periods of crustal growth and active uplift. The nodal plane thus provides a useful reference in understanding the relationship between uplift and shallowing during crustal growth.

The depth of the nodal plane is not fixed, and is the result of a dynamic balance between the rates of erosion, the rates of magmatic inflation, and the vertical distribution of magmatic additions to the crust. If this balance changes with time, the nodal plane will move. It is likely that the nodal plane will exist at different depths at different locations, resulting in a surface that is not horizontal.

Assuming no change in the vertical distribution of magmatic additions or in the rate of erosion, increased magmatic activity will result in a shallowing of the nodal plane (Fig. 3.5a and 3.5b). Decreased magmatic activity will result in a deepening of the nodal plane. Assuming no change in the rate of magmatism or in the rate of erosion, an increase in the proportion of volcanic and shallow

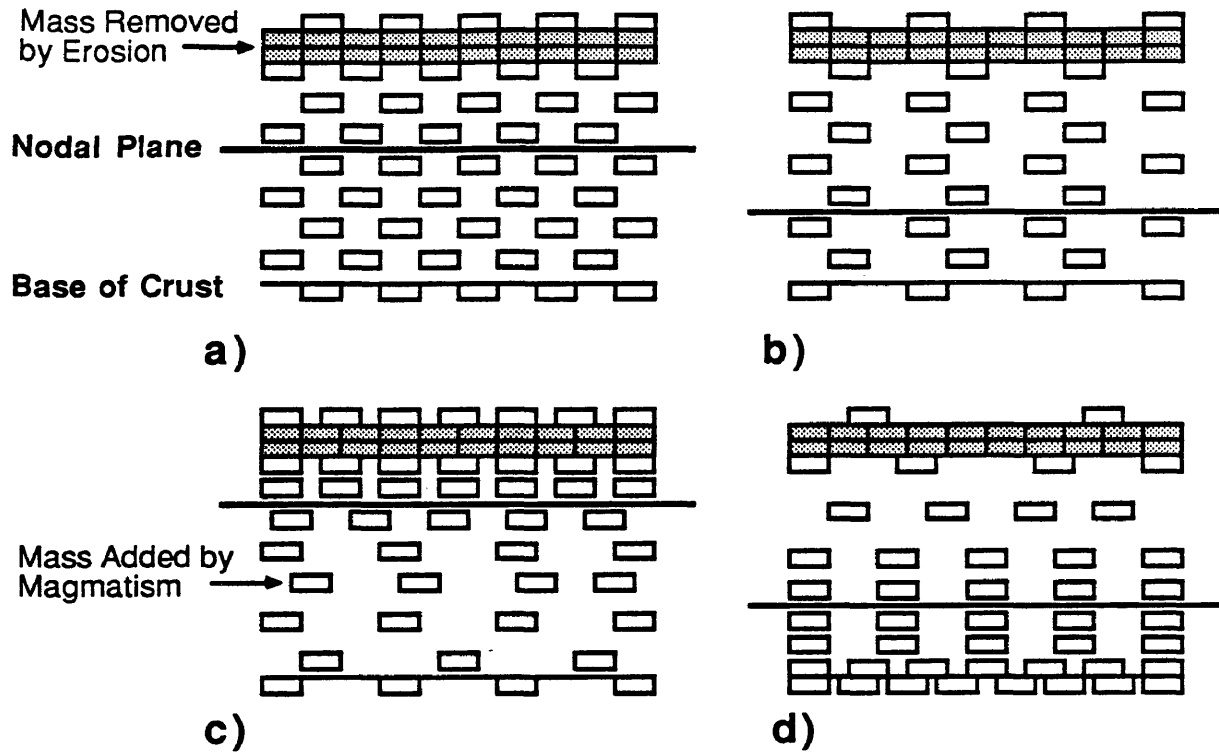


Fig. 3.5 Nodal Plane Dynamics

Depth of nodal plane in crustal sections under situations of varying magmatic additions and erosion rates. The nodal plane is located at a depth above which the mass (here depicted as area) of magmatic additions equals the mass removed by erosion. Cross-hatched boxes represent magmatic additions to crust (those on top are volcanic). Dotted boxes represent material removed by erosion. Erosion is the same in A-D. A and B have an even distribution of magmatic additions but variable mass added. C and D have an uneven distribution of magmatic additions but the same mass added.

plutonic additions will result in shallowing of the nodal plane (Fig. 3.5c). An increase in the proportion of deep plutons will result in deepening of the nodal plane (Fig. 3.5d). Assuming no change in the rate of magmatic inflation or in the vertical distribution of magmatic additions, changes in erosion rate will also affect the depth of the nodal plane. An increase in erosion rate will deepen the nodal plane. This effect is opposite to the effect of increasing the rate of magmatism. Increased magmatism will cause uplift, which in turn causes accelerated erosion. Thus, a buffering relationship exists between magmatism and erosion that tends to stabilize the depth of the nodal plane.

Because only rocks above the nodal plane are brought to the surface through uplift and erosion, the depth of the nodal plane controls the range of crystallization depths and plutonic ages exposed. Relatively deep nodal planes will result in older and longer plutonic age distributions due to the longer crustal transit time of uplifting plutons emplaced at greater depth. Shallow nodal planes will result in young and short age distributions due to a relatively rapid cycling of upper crustal environments.

Areas that do not expose young shallow plutons could result from a cessation of magmatism. With no magmatic replacement for mass removed by erosion, volcanic and shallow crustal environments would be eroded, leaving only mid-crustal levels exposed. Variations in the period of recorded magmatism and the crystallization depth of exposed plutons can be explained by understanding processes that effect the relative motion of the erosion surface, the nodal plane, and the base of the crust.

Nodal plane depth also may be affected by tectonic conditions that

influence crustal thickness and magmatic activity. The plutonic age histogram for the SPB (Fig. 2.10) shows that the apparent period of maximum magmatic activity (100–70 Ma) correlates with a worldwide maximum in seafloor spreading rates (Larson and Pitman, 1972). This suggests that the nodal plane may shallow during periods of accelerated seafloor spreading. However, note that the synthetic age histograms demonstrate that the apparent magmatic maximum may result from continual magmatism and uplift. Other tectonic controls include shallow subduction and underplating of oceanic crust both empirically associated with subduction of young oceanic crust. Shallow subduction in turn results in termination of volcanic activity and assumedly in plutonism (Cross and Pilger, 1982). Underplating and compressional shortening may accompany shallow subduction and will thicken the crust, resulting in uplift and deepening of the nodal plane due to the corresponding increase in erosion. If crustal thickening accompanies a decrease in magmatism, both effects will contribute to a deepening of the nodal plane.

Application of the Arc Construction Model

Comparison of the Coastal batholith (CB) of Peru and the SPB of Chile provides an instructive example of the usefulness of the AC model. Plutons in the CB crystallized in an epizonal environment (Pitcher et al., 1985). Most of the plutons in the SPB crystallized at middle crustal depths (as deep as 24 km).

Epizonal plutons are known in only one location and Quaternary volcanic rocks are restricted to one recognized volcanic center. Published plutonic ages from the CB range from 107 to 37 Ma (Pitcher et al., 1985). Plutonic ages from the SPB range from 166 to 12 Ma (Bruce et al., 1987). A shallow nodal plane results in a short magmatic record, a young initial age, and only plutons from shallow crystallization depths. All these features are found in the CB, suggesting that the nodal plane was never more than a few kilometers below the surface. A deep nodal plane results in a long magmatic record, an old initial age, and plutons ranging from shallow to relatively deep crystallization depths. The record in the SPB thus suggests that the nodal plane was considerably deeper than in the CB.

Assuming equivalent erosion rates, which may not be valid, the AC model predicts two possible scenarios for producing a deeper nodal plane in Chile. Either the rate of magmatic addition was slower or magmas crystallized at greater depths in the SPB than in CB. Similarly, the model predicts that the SPB should contain young epizonal and young volcanic rocks assuming magmatic additions took place at all crustal levels. Their general absence suggests that the difference between the two areas may be related to a recent change in the rate of magmatism or to recent tectonic uplift, rather than to a significant difference in the long term magma production histories of the two magmatic arcs.

The most obvious explanation for the different plutonic histories of the two batholiths is related to differences between the current configuration and kinematics of subduction along the Peru-Chile trench. The convergence rate in

the trench off Peru is 9 cm/a, and the age of the subducting oceanic crust ranges from 40 Ma to 47 Ma (Corvalan, 1981). This convergence rate has persisted in Peru over the past 25 m.y. (Pilger, 1984; Thorpe et al., 1981). The present convergence rate in southern Chile is 2 cm/a and the age of the subducting oceanic crust ranges from 12 Ma to 15 Ma. The SPB is located along a part of the arc below which portions of the Chile rise, an oceanic spreading center, were subducted between 14 Ma and 9 Ma (Herron, 1981). Volcanism essentially ceased in the portion of the arc above the subducted rise. The cessation of magmatism creates a situation in which erosion may not be balanced by addition of magmatic material, thus causing the nodal plane to deepen. In addition, if crustal underplating has occurred in response to ridge collision, the increase in crustal thickness will induce uplift and accelerate erosion, also causing the nodal plane to deepen. Both processes acting together would lead to an exposed plutonic record lacking young plutons that crystallized at shallow depths. Thus, the effects of ridge collision in southern Chile may explain the lack of exposed shallow plutons and the deep crustal levels exposed in the SPB. Although the recent tectonic history may be sufficient to explain differences in the plutonic record between CB and SPB, other differences also exist.

The SPB was emplaced in the accretionary prism of a Paleozoic arc (Forsythe, 1982). The relatively thin Paleozoic crust would prevent extensive lower crustal melting in the arc environment, a conclusion supported by isotopic data (Nelson et al., 1987; Weaver et al., 1986b; Weaver et al., in press). In contrast, the CB is hosted in a very thick continental crust, one that would promote lower crustal melting. Lower crustal melting would redistribute mass

upward in the crust, effectively shallowing the nodal plane and preventing shallowing of the lower crust. This, plus the positive effect a warmer crust may have on magma ascent, suggests that crustal thickness may have played a role in producing differences in the two batholiths.

Climatic differences between the two areas are quite dramatic at present. Peru is dominated by mountainous terrain of significant local relief and a very dry climate. Based on geomorphological and geochronological data, Mortimer (1973) and Baker (1977) concluded that the present arid climate in the central portion of the Andes has persisted for at least the past 20 m.y. Southern Chile is also mountainous, but the climate is very moist and the region has been eroded by alpine glaciation at least since the Pleistocene. Thus the erosion rate in Chile is probably greater than that in Peru. This would tend to deepen the nodal plane in Chile and help explain the observed differences in the exposed plutonic record.

Conclusion

The arc construction model appears to explain the pattern of plutonic age, lithology, and crystallization depth exposed in the SPB. Differences between areas within the SPB can be accounted for by variations in uplift histories. Differences between the CB of Peru and the SPB are in part related to differences in their recent tectonic and climatic history and in part due to

differences in the depth of the nodal plane during protracted arc construction.

Several significant implications result from the AC model. Within the middle crust of magmatic arcs, pluton crystallization depth appears to be controlled by magma composition. Although the plutonic records suggest that magma composition in the SPB changed with time, analysis of isotopic and age-lithology data, plus synthetic histograms, demonstrates that the observed change in composition may be an artifact of crustal uplift kinematics. Finally, the exposed plutonic ages and compositions may not be a true record of the timing or nature of magmatism in a magmatic arc.

Uplift and shallowing of individual crustal horizons depend on their depth, the rates of erosion and magmatic inflation, and the vertical distribution of magmatic additions to the crust. The nodal plane provides a frame of reference useful in distinguishing the difference between uplift and shallowing. It also marks the depth above which rocks will reach the surface and explains why, during active arc magmatism, lower crustal rocks are not brought to the surface and exposed. Rocks emplaced below the nodal plane during periods of crustal thickening will experience deepening even though the crust is in a period of active uplift. Rocks below the nodal plane will not experience shallowing until the nodal plane descends below them. Because of the relationship between the rate of magmatism and the rate of erosion due to uplift, movement of the nodal plane may be buffered.

REFERENCES CITED

- Arth, J.G., and Hanson, G.N., 1972. Quartz diorites derived by partial melting of eclogite or amphibolite at mantle depths. *Contrib. Miner. Pet.*, 37:161-174.
- Arth, J.G., 1976. Behavior of trace elements during magmatic processes- A summary of theoretical models and their applications. *J. Research U.S.G.S.*, v. 4, no.1, p. 41-47.
- Arth, J.G., 1979. Some Trace Elements in trondhjemites- Their Implications to Magma Genesis and Paleotectonic Setting. In: F. Barker (Editor), *Trondhjemites, Dacites, and Related Rocks*. Elsevier, Amsterdam, pp. 123-132.
- Baker, M.C.W., 1977. Geochronology of upper Tertiary volcanic activity in the Andes of Northern Chile. *Geo. Rdsch.*, 66:455-465.
- Barker, P.F., and Griffiths, D.H., 1972. The evolution of the Scotia Ridge and Scotia Sea. *Phil. Trans. R. Soc. London*, A271:151-183.
- Barker, F., Arth, J.G., Peterman, Z.E., and Friedman, I., 1976. The 1.7- to 1.8-b.y. old trondhjemites of southwestern Colorado and northern New Mexico: Geochemistry and depth of genesis. *Geol. Soc. Am. Bull.*, 87:189-198.
- Barker, F., 1979. Trondhjemite: Definition, Environment and Hypothesis of Origin. In: F. Barker (Editor), *Trondhjemites, Dacites, and Related Rocks*. Elsevier, Amsterdam, pp. 1-12.
- Barker, F., and Millard, H.T. Jr., 1979. Geochemistry of the type trondhjemite and three associated rocks, Norway. In: F. Barker (editor), *Trondhjemites, Dacites, and Related Rocks*. Elsevier, Amsterdam, pp. 517-529.
- Barker, F., Arth, J.G., and Millard, H.T. Jr., 1979. Archean Trondhjemites of the southwestern Big Horn Mountains, Wyoming: a Preliminary Report. In: F. Barker (editor), *Trondhjemites, Dacites, and Related Rocks*. Elsevier, Amsterdam, pp. 401-414.
- Bartholomew, D.S. and Tarney, J., 1984. Geochemical characteristics of magmatism in the southern Andes (45° - 46°). In: R.S. Harmon and B.A. Barrieo (Editors), *Andean Magmatism Chemical and Isotopic Constraints*. Shiva Publishing Limited, Nantwich, pp. 220-230.
- Bowen, N.L., 1913. Melting phenomenon of plagioclase feldspar. *Am. J. Sci.*, 35:577-599.
- Brown, G.C., 1981. Space and time in granite plutonism. *Phil. Trans. R. Soc. London*, A301:321-336.

- Bruce, R.M., Nelson, E.P., Weaver, S.G., and Lux, D.R., 1986a. Geochronology and Petrology of the Patagonian batholith: Implications for Magma Genesis and Arc Evolution. American Geophysical Union Abstracts, 67-16:412.
- Bruce, R.M., Nelson, E.P., Weaver, S.G., and Lux, D.R., 1986b, Age-Lithology Relationships in the Patagonian batholith: A Model for Arc-Crustal Growth, American Geophysical Union Abstracts, 67-44:1276.
- Bruce, R.M., Nelson, E.P., Weaver, S.G., 1987a, Magmatic Rock Series of the Patagonian batholith: Evidence for Multiple Parental Magma Types, American Geophysical Union Abstracts, 68-16:442.
- Bruce, R.M., Nelson, E.P., and Weaver, S.G., 1987b, Pluton Emplacement and Magmatic Arc Construction: A Model from the Patagonian Batholith, Workshop on the Growth of Continental Crust, Lunar and Planetary Institute, held in Oxford England, July 1987.
- Bruce, R.M., Nelson, E.P., and Weaver, S.G., 1987c, Changing Contributions of the Crust and Mantle During Andean Arc Construction, Geological Society of America, Abstracts with Programs, Vol. 19, No. 7.
- Bruce, R.M., Nelson, E.P., and Weaver, S.G., in press. Effects of Synchronous Uplift and Intrusion During Magmatic Arc Construction. Tectonophysics.
- Corvalan J., 1981. Plate-Tectonic Map of the Circum-Pacific Region Southeast Quadrant. 1:10,000,000; AAPG.
- Cross, T.A., and Pilger, R.H., 1982. Controls of subduction geometry, location of magmatic arcs, and tectonics of arc and back-arc regions. Geol. Soc. Am. Bull., 93:545-562.
- Dalziel, I.W.D., 1981. Back-arc extension in the southern Andes: a review and critical reappraisal. Phil. Trans. R. Soc. London, A300:319-335.
- Darwin, C., 1846. Geological Notes on South America, London.
- Dott, R.H., Winn, R.D., and Smith, C.H.L., 1982. Relationship of Late Mesozoic and Early Cenozoic Sedimentation to the Tectonic Evolution of the Southernmost Andes and Scotia Arc. In: Craddock C. (Editor), Antarctic Geoscience. University of Wisconsin Press, Madison, pp. 193-202.
- Farrar, E., Clark, A.H., Haynes, S.J., Quirt, G.S., Conn, H., and Zentilli, M., 1970. K-Ar evidence for post-Paleozoic migration of granitic foci in the Andes of northern Chile. Earth Planet. Sci. Lett., 10:60-66.
- Forsyth, D.W., 1975. Fault plane solutions and tectonics of the South Atlantic and Scotia Sea. Journal of Geophysical Research, 80:1429-1443.

- Forsythe, R., 1982. The late Paleozoic to early Mesozoic evolution of southern South America: a plate tectonic interpretation. *Jour. Geol. Soc. London*, 139:671-682.
- Goldick, S.S., 1984. Determination of Ferrous Iron in Silicate Rocks. *Chemical Geology*, 42:343-347.
- Halpern, M., 1973. Regional geochronology of Chile south of 50° latitude. *Geol. Soc. Amer. Bull.*, 84-2401-2422.
- Hanson, G.N., Goldich, S.S., 1972. Early Precambrian rocks in the Saganaga Lake-Northern Light Lake area, Minnesota-Ontario Pt. 2, Petrogenesis. In: B.R. Doe and D.K. Smith (editors), *Studies in mineralogy and Precambrian geology*. *Geol. Soc. Am. Mem.*, 135:179-193.
- Herron, E.M., 1981. An active spreading center collides with a subduction zone; a geophysical survey of the Chile margin triple junction. In: Kulm, L.D. (Editor), *Nazca Plate; crustal formation and Andean convergence*, *Geol. Soc. Amer. Memoir* 154, pp. 683-701.
- Herve, F., Nelson, E., Kawashita, K., and Suarez, M., 1981. New isotopic ages and timing of orogenic events in the Cordillera Darwin, southernmost Chilean Andes. *Earth and Planetary Sci. Let.*, 55:257-265.
- Herve, F., Suarez, M., and Puig, A., 1984. The Patagonian batholith S. of Tierra del Fuego, Chile: timing and tectonic implications. *Jour. Geol. Soc. London*, 141:877-884.
- Irvine, T.N., and Baragar, W.R.A., 1971. A guide to the chemical classification of the common volcanic rocks. *Can. Journal Earth Sci.*, 8:523-548.
- Jordan, T.E., Isacks, B.L., Allmendinger, R.W., Brewer, J.A., Ramos, V.A., and Ando, C.J., 1983. Andean tectonics related to geometry of subducted Nazca plate. *Geol. Soc. Am. Bull.*, 94:341-361.
- Kranck, E.H., 1932. Geological investigation on the Cordillera of Tierra del Fuego. *Acta Geog. Helsingfors*, 4:1-231.
- Larson, R.L., and Pitman, W.C., 1972. World-Wide Correlation of Mesozoic Magnetic Anomalies, and Its Implications. *Geol. Soc. Am. Bull.* 83:3645-3662.
- Mortimer, C., 1973. The Cenozoic history of the southern Atacama Desert, Chile. *Jour. Geol. Soc. London*, 129:505-526.
- Mpodpzis, C.; and Forsythe, R., 1983. Stratigraphy and geochemistry of accreted fragments of the ancestral Pacific floor in southern South America. *Palaeogeography, Palaeoclimatology, Palaeoecology*, 41:103-124.

- Nelson, E., Dalziel, I.W.D., and Milnes, A.G., 1980. Structural geology of the Cordillera Darwin -- collisional style orogenesis in the southernmost Chilean Andes. *Ecologiae Geol. Helv.*, 73:727-751.
- Nelson, E., Bruce, R., Elthon, D., Kammer, D., and Weaver, S., 1985, Regional Petrologic Variations in the Patagonian batholith, *Comunicaciones*, 35:175-176.
- Nelson E.P., Bruce R.M., Weaver S.G., Lux D., and Brueckner H.K., 1987, Variable crystal contamination in the Patagonian batholith, Symposium on Circum-Pacific Phanerozoic Granites, IGCP project 249, Tucuman, Argentina, Sept. 1987.
- Nelson, E.P., Bruce, R.M., Elthon, D., Kammer, D., Weaver, S., in press, Regional Lithological Variations in the Patagonian Batholith, *Jour. of S. Am. Earth Sciences*.
- Peacock, M.A., 1931. Classification of igneous rock series. *Journal of Geology*, 39:54-67.
- Pilger, R.H., 1981. Plate reconstructions, aseismic ridges, and low-angle subduction beneath the Andes. *Geol. Soc. Am. Bull.*, 92:448-456.
- Pilger, R.H., 1984. Cenozoic plate kinematics, subduction and magmatism: South American Andes. *J. Geol. Soc. London*, 141:793-802.
- Pitcher, W.S., Atherton, M.P., Cobbing, E.J., and Beckinsale, R.D., 1985. *Magmatism at a Plate Edge: The Peruvian Andes*. Blackie, London, 328 pp.
- Stern, C.R., Shewes, M.A., and Duran, M., 1976. Volcanismo orogenico in Chile austral. *Congreso Geologica de Chile, Santiago, Chile*, 2:195-212.
- Stern, C.R., and Stroup, J.B., 1982. The petrochemistry of the Patagonian batholith, Ultima Esperanza, Chile. In; C. Craddock (Editor), *Antarctic Geoscience*, University of Wisconsin Press, pp. 135-142.
- Suarez, M., 1977. Notas geoquimicas preliminares del batolito Patagonico al sur de Tierra del Fuego, Chile. *Rev. Geol. Chile*, 4:15-33.
- Suarez M., Puig, A., and Herve, M., 1986. K-Ar dates on granitoids from Archipelago Cabo de Hornos, southernmost Chile. *Geol. Mag.*, 123(5):581-584.
- Thorpe, R.S., Francis, P.W., and Harmon, R.S., 1981. Andean andesites and crustal growth. *Phil. Trans. R. Soc. Lond.*, A301:305-320.
- Weaver, S.G., Nelson, E.P., and Bruce, R.M., 1986a, Sr and Nd Isotope Systematics of the Patagonian Batholith, 48 degrees South, Chile, *American Geophysical Union Abstracts*, 67(16):413.

- Weaver, S.G., Nelson, E.P., Bruce, R.M., LeHuray, A., and Mertzman, S.A., 1986b, Magmatic evolution in the Patagonia batholith: isotopic and trace element constraints, American geophysical union Abstracts, 67(44):1276.
- Weaver S.G., Bruce, R.M., and Nelson E.P., 1987, Plutonism of the Southern Patagonian Batholith: Mantle and crustal sources, The Origin of Granites Symposium, The Royal Society of Edinburgh, Sept. 1987.
- Weaver S.G., Bruce, R.M., and Nelson E.P., in press, Crustal Contamination in the Patagonian Batholith: Implications for the Evolution of Magma-Crust Interactions, GSA Memoir.
- Winslow, M.A., 1982. The Structural Evolution of the Magallanes Basin and Neotectonics in the Southernmost Andes. In: Craddock C. (Editor), Antarctic Geoscience. University of Wisconsin Press, Madison, pp. 193-202.
- Wortel, M.J.R., 1984. Spatial and temporal variations in the Andean subduction zone. J. geol. Soc. London, 141:783-791.
- Wyllie, P.J., 1971. The Dynamic Earth. John Wiley and Sons, New York, 416 pp.
- Zen, E., and Hammarstrom, J.M., 1984. Magmatic epidote and its petologic significance. Geology, 12:515-518.

Appendix A

ANALYTIC METHODS

Chemistry powders were obtained from fresh rock samples starting with an interior slab created during the preparation of thin section chips and mode counting slabs. Slab edges were removed and the interior portion broken to accommodate the jaw crusher. Samples were crushed and split to approximately 50 gram portions, one of which was then pulverized in a tungsten carbide puck mill to finer than 200 mesh. These stock powders were used for all subsequent whole rock analyses.

Major element analysis by X-ray fluorescence

Oven dried (100°C) whole rock powder, 0.5000 grams, was mixed with 4.5000 grams of dry $\text{Li}_2\text{B}_4\text{O}_7$ for several hours in an inclined rotary ball mill. The mixture is placed into a PT crucible (95% Pt and 5% Au) with three drops of a LiI, 0.5N, solution. The crucible is then covered with a PT mold/cover and the sample is fused over a bunsen burner. After all refractory phases melted, the mold is removed and placed upright on a heat resistant surface and the sample is poured into the mold. The resulting glass disk will release from the mold as it shrinks and is labeled after it cools.

The major element glasses were analyzed by Stan Mertzman at Franklin and

Marshall College in Lancaster Pennsylvania. The reported precision and accuracy of their methods, tabulated below, was confirmed by their running of blind standards and our inclusion of duplicate samples.

| Element | \pm wt. % | Element | \pm wt. % |
|--------------------------------|-------------|--------------------------------|-------------|
| SiO ₂ | 0.40 | Al ₂ O ₃ | 0.12 |
| Fe ₂ O ₃ | 0.10 | FeO | 0.04 |
| TiO ₂ | 0.02 | MnO | 0.01 |
| MgO | 0.07 | CaO | 0.03 |
| Na ₂ O | 0.09 | K ₂ O | 0.02 |
| P ₂ O ₅ | 0.02 | | |

Trace element analysis by X-ray fluorescence

Oven dried whole rock powder and microcrystalline cellulose are mixed in a two to one ratio, two parts sample to one part cellulose, for several hours. Sample size is dependent on the size of pellet desired. A backing of additional microcrystalline cellulose and the sample mixture are then pressed into a pellet. The samples must be stored in a desiccator except when they are actually being analyzed.

Trace element samples were run at C.S.M. utilizing the procedures established by Carl Eriksson. Blind standards were included in each run to test the accuracy and precision of this method. Data covering a six month period demonstrates the high precision of the technique. Accuracy varies considerable

from element to element and from standard to standard. Percent deviance vs ppm diagrams were analyzed by visual inspection to determine realistic lower detection limits and the percent error at that concentration.

| <u>Element</u> | <u>Detection Limit ppm</u> | <u>Percent Error</u> |
|----------------|----------------------------|----------------------|
| Ba | 300 | 10 |
| Cu | 40 | 5 |
| Nb | 20 | 10 |
| Nd | 20 | 10 |
| Ni | 30 | 10 |
| Rb | 10 | 5 |
| Sr | 50 | 5 |
| V | 15 | 10 |
| Y | 10 | 10 |
| Zr | 50 | 10 |

Iron Oxidation State

Ferrous iron was determined by the method of Goldich S.S. 1984. This data was used to refine the loss on ignition (LOI) determinations. LOI was determined by measuring the weight loss of an oven dried sample during a 45 minute run in a 900°C muffle furnace. A correction for the mass gained by the oxidation of FeO is made by multiplying the weight % FeO by 0.111348 and adding this to the LOI value.

Mineral Proportions

Mineral modes were determined by 1000 count point counts. Coarse-grained rocks were analyzed by counting stained slaps using grid counting templates provided by Dr. Bruce Johnson of the U.S.G.S. Medium- and fine-grained rocks were counted in stained thin sections using standard mechanical stage techniques.

Argon Isotopic Analysis

Isotopic dating was accomplished using the facilities in the Department of Geological Sciences at the University of Maine in Orono. Following standard mineral separation techniques, conducted at CSM, samples with an estimated purity of at least 99.9% were weighed, encapsulated in Al foil and sealed in silica glass vials. They were then irradiated at the Phoenix Memorial Laboratory in the Ford Nuclear Reactor at the University of Michigan. Included in each silica vial as a flux monitor are samples of an international standard, MMhb-1, whose accepted age is 519.4 Ma (Alexander et al. 1978) and in-house (UMO) laboratory standards.

Argon is liberated from samples by radio frequency induction heating of a Mo crucible within a Pyrex extraction furnace. Extraction temperatures are estimated by optical pyrometry. The inert gas extraction and purification system utilizes standard purification methods including a Cu-CuO getter and SAES

cartridge getters (50 l/s and 10 l/s). Argon isotope compositions are determined using a Nuclide 6-60-SGS gas source, 15 cm radius, 60 degree sector Nier-type mass spectrometer with automated operations controlled by an IBM PC microcomputer.

Ages are calculated using the equations and correction factors given by Dalrymple et al. (1981). Decay constants for ^{40}K and the isotopic composition of K used in the age calculation are the values recommended by Steiger and Jager (1977). Atmospheric argon is analyzed several times a week to make accurate mass discrimination corrections. The ^{37}Ar is corrected for decay during the time interval between sample irradiation and isotopic analysis using a half-life of 35.1 days. Data is corrected for mass fractionation during analysis. The reported analytical uncertainty for individual analyses is a one sigma estimate determined by the equation of Dalrymple et al. (1981) using the uncertainties in time zero extrapolations and an uncertainty in J of 0.25%. Plateau ages represent an average age for consecutive increments which constitute a significant portion (50%) of the total ^{39}Ar in the sample and whose apparent ages cannot be considered different on the basis of the critical value test of Dalrymple and Lanpher (1969). The uncertainty estimates used in the critical value test for plateaus in individual samples exclude uncertainties in J-value and are considered at the 2 sigma level. Uncertainties reported for plateau ages are one standard deviation with n-1 weighting.

Appendix B

STATION TO SAMPLE NUMBER CORRELATION TABLE

| Map Number | Sample Number | Chem Group | Rock Name | Map Number | Sample Number | Chem Group | Rock Name | Map Number | Sample Number | Chem Group | Rock Name |
|------------|---------------|------------|-----------|------------|---------------|------------|-----------|------------|---------------|------------|-----------|
| 1 | 3G-108 | C | DI | 29 | MA-38 | M | TO | 60 | MA-68A | T | TO |
| 2 | 3G-109 | C | TO | 30 | 3G-129 | M | TO | 61 | GX-20 | K | MTO |
| 3 | 3G-110B | C | TO | 31 | MA-39A | T | TO | 62 | GX-21 | C | QD |
| 3 | 3G-110A | C | MTO | 31 | MA-39B | C | DI | 63 | GX-23 | K | GD |
| 4 | 3G-111 | K | GD | 31 | MA-39C | K | DI | 64 | GX-24 | K | GR |
| 5 | MA-20B | C | QD | 32 | MA-40 | K | GD | 65 | GX-25 | K | QD |
| 5 | MA-20 | K | GR | 33 | 3G-215A | K | GD | 66 | GX-26 | K | GR |
| 6 | MA-21 | K | TO | 34 | 3G-210 | K | MTO | 67 | GX-27 | K | GR |
| 7 | 3G-112 | K | GD | 35 | 3G-209A | C | MTO | 68 | GX-28 | K | GR |
| 7 | MA-22B | K | GR | 36 | 3G-208 | C | MTO | 69 | GX-29 | K | QD |
| 8 | 3G-113 | C | QD | 37 | BB-6A | K | QMD | 70 | GX-19 | K | GR |
| 9 | 3G-114 | C | QD | 38 | BB-5C | C | QD | 71 | GX-18 | K | GR |
| 10 | MA-25B | C | GB | 39 | 3G-206 | C | DI | 72 | GX-17 | K | QMD |
| 11 | MA-26 | C | MTO | 40 | BB-4A | C | TO | 73 | GX-13 | K | QMD |
| 11 | 3G-118 | C | MTO | 41 | 3G-205 | C | TO | 74 | GX-12 | K | QD |
| 12 | MA-27 | C | MTO | 42 | BB-3A | C | MTO | 75 | GX-10 | K | GR |
| 13 | MA-28 | C | MTO | 43 | 3G-204A | C | DI | 76 | GX-9A | C | QD |
| 14 | MA-29 | C | MTO | 44 | BB-2A | C | MTO | 76 | GX-9 | K | GD |
| 15 | MA-30 | K | QMD | 45 | 3G-203 | C | MTO | 77 | GX-8 | K | GR |
| 16 | 3G-121 | M | GD | 46 | 3G-202 | C | MTO | 78 | GX-6 | M | GD |
| 17 | MA-31 | K | QD | 47 | MA-61 | K | MTO | 79 | GX-5 | T | TO |
| 18 | MA-32 | C | MTO | 48 | 3G-218 | C | MTO | 80 | GX-4 | T | TO |
| 19 | 3G-123 | K | QD | 49 | MA-62A | C | TO | 81 | GX-3A | T | TO |
| 20 | 3G-124 | K | GD | 50 | 3G-219 | C | TO | 81 | GX-3B | C | DI |
| 20 | MA-33 | K | GR | 51 | MA-63 | C | TO | 82 | GX-1 | C | QD |
| 21 | MA-34A | K | MTO | 52 | 3G-220 | C | TO | 83 | MA-69A | T | TO |
| 22 | 3G-125 | K | GR | 53 | MA-64A | K | MTO | 84 | 3G-228 | K | GD |
| 23 | MA-35 | K | GR | 54 | MA-65A | C | QD | 85 | 3G-229 | T | TO |
| 24 | 3G-126 | C | QD | 55 | 3G-223 | C | TO | 86 | MA-70A | T | TO |
| 25 | MA-36D | M | GD | 56 | MA-66A | K | DI | 87 | MA-71B | T | TO |
| 25 | MA-36A | M | TO | 56 | MA-66B | M | GD | 88 | 3G-232 | T | TO |
| 26 | 3G-127 | C | QD | 57 | 3G-225 | K | QMD | 89 | 3G-233A | K | TO |
| 27 | MA-37 | M | GR | 58 | MA-67A | K | QD | 90 | 3G-234A | C | TO |
| 28 | 3G-128 | K | QD | 59 | 3G-226 | T | TO | | | | |

Appendix C

MAJOR ELEMENT DATA

trondhjemite rock series major element data in weight percent

| Sample | SiO2 | TiO2 | Al2O3 | Fe2O3 | FeO | MnO | MgO | CaO | Na2O | K2O | P2O5 | H2O+ | Total |
|---------|-------|------|-------|-------|------|------|------|------|------|------|------|------|--------|
| 3G-226 | 72.20 | 0.10 | 15.76 | 0.65 | 0.72 | 0.05 | 0.32 | 2.89 | 4.98 | 0.74 | 0.03 | 0.66 | 99.10 |
| 3G-229 | 69.33 | 0.16 | 16.89 | 0.73 | 0.87 | 0.05 | 0.50 | 3.50 | 5.14 | 0.96 | 0.05 | 0.52 | 98.70 |
| 3G-232 | 71.55 | 0.17 | 16.07 | 0.81 | 0.79 | 0.04 | 0.54 | 3.22 | 5.14 | 1.03 | 0.04 | 0.55 | 99.95 |
| 3G-233A | 70.50 | 0.17 | 16.11 | 0.92 | 0.90 | 0.04 | 0.53 | 3.55 | 4.94 | 0.92 | 0.03 | 0.37 | 98.98 |
| GX-3A | 73.40 | 0.07 | 15.55 | 0.35 | 0.44 | 0.02 | 0.03 | 1.66 | 6.25 | 1.41 | 0.01 | 0.41 | 99.60 |
| GX-4 | 74.81 | 0.07 | 14.51 | 0.36 | 0.49 | 0.03 | 0.08 | 1.43 | 5.72 | 1.47 | 0.02 | 0.42 | 99.41 |
| GX-5 | 74.72 | 0.09 | 15.22 | 0.45 | 0.50 | 0.02 | 0.15 | 2.30 | 5.34 | 1.03 | 0.00 | 0.50 | 100.32 |
| MA-39A | 70.70 | 0.18 | 17.30 | 0.55 | 1.16 | 0.03 | 0.67 | 4.56 | 4.59 | 0.72 | 0.04 | 0.45 | 100.95 |
| MA-68A | 72.10 | 0.12 | 16.46 | 0.73 | 0.77 | 0.05 | 0.32 | 3.42 | 5.29 | 0.65 | 0.03 | 0.50 | 100.44 |
| MA-69A | 73.76 | 0.07 | 15.84 | 0.66 | 0.47 | 0.02 | 0.10 | 1.87 | 6.39 | 1.33 | 0.01 | 0.30 | 100.82 |
| MA-70A | 68.33 | 0.19 | 17.79 | 0.81 | 0.98 | 0.06 | 0.46 | 3.69 | 6.16 | 0.75 | 0.04 | 0.39 | 99.65 |
| MA-71B | 73.18 | 0.07 | 15.54 | 0.44 | 0.51 | 0.04 | 0.08 | 1.96 | 5.65 | 1.44 | 0.00 | 0.60 | 99.51 |

mixed rock series major element data in weight percent

| Sample | SiO2 | TiO2 | Al2O3 | Fe2O3 | FeO | MnO | MgO | CaO | Na2O | K2O | P2O5 | H2O+ | Total |
|--------|-------|------|-------|-------|------|------|------|------|------|------|------|------|--------|
| 3G-121 | 72.37 | 0.34 | 14.35 | 1.50 | 1.18 | 0.04 | 0.73 | 2.32 | 4.39 | 2.19 | 0.05 | 0.56 | 100.02 |
| 3G-129 | 68.32 | 0.27 | 16.48 | 1.19 | 1.43 | 0.07 | 1.04 | 3.94 | 4.46 | 1.49 | 0.08 | 1.02 | 99.79 |
| 3G-228 | 73.18 | 0.06 | 15.36 | 0.27 | 0.30 | 0.01 | 0.00 | 1.16 | 5.76 | 2.38 | 0.02 | 0.58 | 99.08 |
| GX-6 | 68.86 | 0.30 | 15.42 | 1.10 | 1.96 | 0.07 | 1.94 | 3.89 | 4.11 | 1.96 | 0.06 | 1.18 | 100.85 |
| MA-36A | 78.30 | 0.06 | 12.85 | 0.62 | 0.42 | 0.43 | 0.06 | 1.31 | 3.71 | 2.05 | 0.00 | 0.56 | 100.37 |
| MA-36D | 69.99 | 0.11 | 17.09 | 0.57 | 0.81 | 0.22 | 0.32 | 2.20 | 5.68 | 2.41 | 0.00 | 0.57 | 99.97 |
| MA-37 | 71.89 | 0.17 | 16.19 | 0.97 | 0.90 | 0.05 | 0.41 | 3.25 | 4.39 | 1.39 | 0.04 | 0.59 | 100.24 |
| MA-38 | 69.93 | 0.19 | 17.78 | 0.87 | 0.82 | 0.07 | 0.35 | 3.07 | 4.73 | 1.94 | 0.05 | 0.62 | 100.42 |
| MA-66B | 69.04 | 0.31 | 16.39 | 0.75 | 1.26 | 0.02 | 1.03 | 3.76 | 4.17 | 1.97 | 0.04 | 1.44 | 100.18 |

calc-alkaline rock series major element data in weight percent

| Sample | SiO2 | TiO2 | Al2O3 | Fe2O3 | FeO | MnO | MgO | CaO | Na2O | K2O | P2O5 | H2O+ | Total |
|---------|-------|------|-------|-------|------|------|-------|-------|------|------|------|------|--------|
| 3G-111 | 68.12 | 0.45 | 15.39 | 2.13 | 2.20 | 0.10 | 1.81 | 3.72 | 3.51 | 2.27 | 0.07 | 0.76 | 100.53 |
| 3G-112 | 70.22 | 0.35 | 15.61 | 1.26 | 1.21 | 0.03 | 0.64 | 3.03 | 4.08 | 2.71 | 0.05 | 0.41 | 99.60 |
| 3G-123 | 51.78 | 1.29 | 17.31 | 3.98 | 5.19 | 0.16 | 5.95 | 8.75 | 3.53 | 1.21 | 0.21 | 1.70 | 101.06 |
| 3G-124 | 73.77 | 0.39 | 13.95 | 1.24 | 1.47 | 0.04 | 0.37 | 1.58 | 4.00 | 3.40 | 0.05 | 0.39 | 100.65 |
| 3G-125 | 75.17 | 0.25 | 13.28 | 0.80 | 0.66 | 0.04 | 0.16 | 1.15 | 3.89 | 3.99 | 0.01 | 0.30 | 99.70 |
| 3G-128 | 58.91 | 1.42 | 16.94 | 3.83 | 3.83 | 0.15 | 2.79 | 5.17 | 4.88 | 1.84 | 0.37 | 0.75 | 100.88 |
| 3G-210 | 54.52 | 0.75 | 17.87 | 3.65 | 5.30 | 0.18 | 3.96 | 7.44 | 3.09 | 1.33 | 0.17 | 1.25 | 99.51 |
| 3G-215A | 59.33 | 0.89 | 17.07 | 2.46 | 4.95 | 0.12 | 2.88 | 6.27 | 3.07 | 2.29 | 0.17 | 1.09 | 100.59 |
| 3G-225 | 55.92 | 0.88 | 18.06 | 3.24 | 4.35 | 0.14 | 4.05 | 7.29 | 3.77 | 1.68 | 0.21 | 1.00 | 100.59 |
| BB-6A | 56.17 | 1.24 | 16.88 | 3.33 | 4.67 | 0.13 | 4.25 | 6.95 | 3.91 | 2.02 | 0.31 | 0.71 | 100.57 |
| GX-10 | 73.46 | 0.27 | 13.33 | 1.27 | 1.76 | 0.05 | 0.38 | 2.42 | 3.25 | 3.08 | 0.02 | 0.56 | 99.85 |
| GX-12 | 58.97 | 0.79 | 16.99 | 2.76 | 4.72 | 0.13 | 3.52 | 6.75 | 3.43 | 1.36 | 0.14 | 1.10 | 100.66 |
| GX-13 | 63.74 | 0.91 | 15.59 | 2.55 | 2.67 | 0.10 | 1.95 | 3.86 | 4.04 | 2.50 | 0.22 | 0.98 | 99.11 |
| GX-17 | 59.94 | 1.05 | 17.42 | 3.59 | 3.06 | 0.12 | 2.66 | 5.45 | 3.81 | 1.96 | 0.29 | 1.12 | 100.47 |
| GX-18 | 75.84 | 0.25 | 12.83 | 0.73 | 0.58 | 0.04 | 0.00 | 0.59 | 3.56 | 4.88 | 0.01 | 0.50 | 99.81 |
| GX-19 | 76.27 | 0.26 | 12.94 | 1.45 | 0.00 | 0.03 | 0.00 | 0.34 | 3.18 | 5.02 | 0.01 | 0.48 | 99.98 |
| GX-20 | 58.02 | 0.95 | 17.97 | 3.28 | 4.03 | 0.11 | 3.38 | 6.24 | 3.66 | 1.92 | 0.20 | 0.93 | 100.69 |
| GX-23 | 66.73 | 0.55 | 15.40 | 1.66 | 2.61 | 0.07 | 1.59 | 3.53 | 3.39 | 3.43 | 0.08 | 0.83 | 99.87 |
| GX-24 | 66.71 | 0.90 | 15.03 | 2.55 | 3.39 | 0.14 | 1.03 | 3.07 | 4.30 | 2.84 | 0.20 | 0.74 | 100.90 |
| GX-25 | 54.38 | 1.24 | 16.09 | 2.84 | 6.80 | 0.16 | 4.80 | 7.98 | 3.09 | 1.28 | 0.25 | 1.49 | 100.40 |
| GX-26 | 76.98 | 0.08 | 12.23 | 0.38 | 0.30 | 0.03 | 0.00 | 0.51 | 3.88 | 4.51 | 0.00 | 0.26 | 99.16 |
| GX-27 | 71.59 | 0.28 | 14.15 | 0.95 | 1.19 | 0.05 | 0.66 | 2.22 | 3.51 | 3.70 | 0.00 | 0.69 | 98.99 |
| GX-28 | 76.56 | 0.14 | 12.34 | 0.60 | 0.44 | 0.02 | 0.00 | 0.77 | 2.97 | 4.83 | 0.00 | 0.31 | 98.98 |
| GX-8 | 68.79 | 0.41 | 14.53 | 1.55 | 1.57 | 0.10 | 1.11 | 2.84 | 3.42 | 3.49 | 0.06 | 1.02 | 98.89 |
| GX-9 | 67.12 | 0.51 | 15.73 | 1.81 | 3.66 | 0.08 | 0.85 | 3.85 | 3.42 | 2.77 | 0.08 | 1.01 | 100.89 |
| MA-20 | 77.52 | 0.11 | 12.14 | 0.54 | 0.29 | 0.01 | 0.00 | 0.71 | 2.61 | 5.50 | 0.00 | 0.22 | 99.65 |
| MA-21 | 67.69 | 0.51 | 15.42 | 2.08 | 2.62 | 0.10 | 1.82 | 4.03 | 3.64 | 2.24 | 0.08 | 0.62 | 100.85 |
| MA-22B | 76.27 | 0.28 | 12.72 | 1.01 | 0.95 | 0.03 | 0.21 | 1.11 | 3.31 | 4.22 | 0.02 | 0.30 | 100.43 |
| MA-30 | 59.58 | 1.06 | 16.61 | 2.99 | 3.99 | 0.14 | 3.47 | 5.70 | 4.26 | 1.63 | 0.25 | 1.07 | 100.75 |
| MA-31 | 55.94 | 0.80 | 16.62 | 4.10 | 4.48 | 0.14 | 4.91 | 8.54 | 2.83 | 1.19 | 0.07 | 1.55 | 101.17 |
| MA-33 | 77.99 | 0.12 | 12.36 | 0.68 | 0.47 | 0.01 | 0.00 | 0.53 | 2.93 | 5.25 | 0.00 | 0.28 | 100.62 |
| MA-34A | 60.94 | 1.45 | 14.86 | 3.07 | 6.46 | 0.20 | 1.91 | 4.84 | 3.61 | 1.95 | 0.55 | 1.50 | 101.34 |
| MA-35 | 73.47 | 0.38 | 13.52 | 1.32 | 1.37 | 0.02 | 0.71 | 1.87 | 2.78 | 4.14 | 0.06 | 0.56 | 100.20 |
| MA-39C | 49.95 | 1.02 | 11.69 | 2.99 | 6.34 | 0.17 | 11.59 | 10.28 | 1.81 | 1.02 | 0.52 | 1.98 | 99.36 |
| MA-40 | 62.38 | 0.57 | 16.41 | 2.41 | 3.14 | 0.11 | 2.80 | 5.38 | 3.70 | 2.06 | 0.17 | 0.84 | 99.97 |
| MA-64A | 61.73 | 0.62 | 16.93 | 2.69 | 3.48 | 0.10 | 2.77 | 5.76 | 3.04 | 2.06 | 0.09 | 1.38 | 100.65 |
| MA-66A | 49.47 | 0.69 | 13.41 | 2.84 | 5.89 | 0.13 | 10.96 | 10.00 | 1.96 | 1.13 | 0.11 | 2.51 | 99.10 |
| MA-67A | 55.75 | 0.98 | 17.80 | 3.44 | 4.66 | 0.13 | 4.59 | 7.24 | 3.66 | 1.85 | 0.20 | 0.93 | 101.23 |

calic rock series major element data in weight percent

| Sample | SiO ₂ | TiO ₂ | Al ₂ O ₃ | Fe ₂ O ₃ | FeO | MnO | MgO | CaO | Na ₂ O | K ₂ O | P ₂ O ₅ | H ₂ O+ | Total |
|---------|------------------|------------------|--------------------------------|--------------------------------|------|------|-------|-------|-------------------|------------------|-------------------------------|-------------------|--------|
| 3G-108 | 45.32 | 0.48 | 19.88 | 5.25 | 6.04 | 0.15 | 8.80 | 12.89 | 0.79 | 0.10 | 0.01 | 0.99 | 100.70 |
| 3G-109 | 65.66 | 0.54 | 16.20 | 2.57 | 2.94 | 0.12 | 2.28 | 4.80 | 3.85 | 1.22 | 0.10 | 0.83 | 101.11 |
| 3G-110A | 61.19 | 0.84 | 16.45 | 3.57 | 3.93 | 0.14 | 3.24 | 6.24 | 3.26 | 1.17 | 0.12 | 0.84 | 100.99 |
| 3G-110B | 74.82 | 0.35 | 12.75 | 1.47 | 1.54 | 0.04 | 0.79 | 3.02 | 3.34 | 1.21 | 0.04 | 0.45 | 99.82 |
| 3G-113 | 55.28 | 1.16 | 17.81 | 4.79 | 4.52 | 0.17 | 3.55 | 7.25 | 3.71 | 1.15 | 0.23 | 0.74 | 100.36 |
| 3G-114 | 59.77 | 1.24 | 16.29 | 3.80 | 4.32 | 0.18 | 2.77 | 5.71 | 4.65 | 1.03 | 0.31 | 0.90 | 100.97 |
| 3G-118 | 64.78 | 0.43 | 16.53 | 2.62 | 2.57 | 0.12 | 1.91 | 5.42 | 3.13 | 1.01 | 0.09 | 1.61 | 100.22 |
| 3G-126 | 63.52 | 0.46 | 17.60 | 2.61 | 2.47 | 0.13 | 1.96 | 5.97 | 3.77 | 0.92 | 0.13 | 0.67 | 100.21 |
| 3G-127 | 64.02 | 0.43 | 17.66 | 1.30 | 2.07 | 0.06 | 2.09 | 5.61 | 4.84 | 0.85 | 0.10 | 0.94 | 99.97 |
| 3G-202 | 59.95 | 0.50 | 16.88 | 3.30 | 3.49 | 0.15 | 3.02 | 6.58 | 3.11 | 0.79 | 0.10 | 1.56 | 99.43 |
| 3G-203 | 58.11 | 0.71 | 18.00 | 2.66 | 3.99 | 0.11 | 4.41 | 7.29 | 3.29 | 1.41 | 0.13 | 1.30 | 101.41 |
| 3G-204A | 58.65 | 0.88 | 17.28 | 3.14 | 3.62 | 0.10 | 3.60 | 6.50 | 3.95 | 1.31 | 0.16 | 1.49 | 100.68 |
| 3G-205 | 63.85 | 0.44 | 17.33 | 2.69 | 2.50 | 0.13 | 2.08 | 6.08 | 3.62 | 0.93 | 0.12 | 0.78 | 100.55 |
| 3G-206 | 47.46 | 0.76 | 18.65 | 4.80 | 5.33 | 0.18 | 7.55 | 11.14 | 2.87 | 0.24 | 0.28 | 1.53 | 100.79 |
| 3G-208 | 61.57 | 0.61 | 18.02 | 2.78 | 3.03 | 0.17 | 2.31 | 6.57 | 3.75 | 0.95 | 0.19 | 0.81 | 100.76 |
| 3G-209A | 63.82 | 0.50 | 16.22 | 2.59 | 3.13 | 0.13 | 2.67 | 5.67 | 2.97 | 1.29 | 0.07 | 0.94 | 100.00 |
| 3G-219 | 65.91 | 0.43 | 16.88 | 2.66 | 2.53 | 0.08 | 1.46 | 4.97 | 3.50 | 0.91 | 0.12 | 1.22 | 100.50 |
| 3G-220 | 70.39 | 0.29 | 15.40 | 1.30 | 1.63 | 0.08 | 0.92 | 3.96 | 4.06 | 1.05 | 0.07 | 1.43 | 100.47 |
| 3G-223 | 72.36 | 0.27 | 15.34 | 1.06 | 1.17 | 0.02 | 0.72 | 3.81 | 4.30 | 1.07 | 0.04 | 0.54 | 100.70 |
| 3G-234A | 66.27 | 0.35 | 16.96 | 1.20 | 2.88 | 0.08 | 1.92 | 5.34 | 3.10 | 1.24 | 0.07 | 1.08 | 100.49 |
| BB-2A | 56.91 | 0.94 | 17.04 | 2.64 | 4.56 | 0.11 | 4.47 | 6.99 | 3.25 | 1.47 | 0.17 | 1.44 | 99.99 |
| BB-3A | 62.50 | 0.51 | 17.51 | 3.28 | 2.88 | 0.15 | 2.48 | 6.46 | 3.23 | 1.16 | 0.13 | 0.90 | 101.19 |
| BB-4A | 70.42 | 0.30 | 15.74 | 1.19 | 1.59 | 0.05 | 0.89 | 4.12 | 3.67 | 0.98 | 0.08 | 0.59 | 99.62 |
| BB-5C | 54.77 | 0.79 | 17.69 | 2.92 | 4.76 | 0.19 | 5.03 | 8.68 | 3.73 | 0.89 | 0.25 | 0.99 | 100.69 |
| GX-1 | 54.01 | 0.97 | 20.12 | 3.46 | 4.07 | 0.11 | 3.82 | 7.89 | 4.12 | 0.93 | 0.32 | 1.08 | 100.90 |
| GX-21 | 59.33 | 0.90 | 17.11 | 3.45 | 3.32 | 0.10 | 3.53 | 6.30 | 4.04 | 1.27 | 0.21 | 1.15 | 100.71 |
| GX-29 | 52.73 | 1.07 | 17.45 | 2.72 | 5.47 | 0.15 | 6.82 | 10.36 | 2.28 | 0.70 | 0.08 | 1.25 | 101.08 |
| GX-3B | 59.93 | 0.65 | 17.15 | 2.14 | 3.88 | 0.10 | 4.37 | 6.40 | 3.41 | 1.41 | 0.16 | 1.25 | 100.85 |
| GX-9A | 51.83 | 0.50 | 14.96 | 2.28 | 5.82 | 0.18 | 8.39 | 10.90 | 2.04 | 0.66 | 0.04 | 2.38 | 99.98 |
| MA-20B | 48.96 | 1.48 | 20.75 | 5.44 | 4.82 | 0.21 | 3.92 | 9.27 | 3.76 | 0.16 | 0.46 | 0.99 | 100.22 |
| MA-25B | 49.25 | 0.13 | 16.10 | 0.90 | 7.39 | 0.19 | 10.91 | 13.04 | 0.88 | 0.17 | 0.01 | 1.79 | 100.76 |
| MA-26 | 65.47 | 0.39 | 16.62 | 2.48 | 2.50 | 0.12 | 1.68 | 5.34 | 3.45 | 1.39 | 0.10 | 0.94 | 100.48 |
| MA-27 | 56.00 | 0.70 | 17.30 | 3.55 | 4.50 | 0.15 | 3.26 | 6.48 | 3.02 | 1.16 | 0.12 | 1.95 | 98.19 |
| MA-28 | 60.83 | 0.65 | 17.13 | 3.18 | 3.86 | 0.14 | 3.06 | 6.74 | 2.95 | 0.92 | 0.12 | 1.34 | 100.92 |
| MA-29 | 59.84 | 0.77 | 17.26 | 2.77 | 4.77 | 0.14 | 3.47 | 6.72 | 2.53 | 1.49 | 0.11 | 1.34 | 101.21 |
| MA-32 | 61.71 | 0.51 | 17.70 | 3.04 | 3.36 | 0.11 | 2.66 | 6.68 | 3.52 | 0.90 | 0.12 | 0.80 | 101.11 |
| MA-39B | 49.54 | 1.52 | 17.36 | 3.59 | 6.09 | 0.17 | 6.04 | 10.18 | 3.56 | 0.51 | 0.86 | 1.17 | 100.59 |
| MA-61 | 58.37 | 1.22 | 16.65 | 3.88 | 4.89 | 0.18 | 2.98 | 6.23 | 4.00 | 1.16 | 0.33 | 1.13 | 101.02 |
| MA-62A | 67.76 | 0.33 | 15.90 | 1.92 | 1.74 | 0.10 | 1.38 | 4.20 | 3.77 | 1.35 | 0.08 | 0.68 | 99.21 |
| MA-63 | 61.78 | 0.47 | 17.60 | 2.88 | 2.18 | 0.12 | 2.16 | 6.19 | 3.50 | 0.83 | 0.14 | 1.57 | 99.42 |
| MA-65A | 57.37 | 0.77 | 17.58 | 3.34 | 4.48 | 0.15 | 3.51 | 7.26 | 2.62 | 1.24 | 0.12 | 1.65 | 100.11 |

Appendix D

TRACE ELEMENT DATA

trondhjemite rock series trace element data in ppm

| Sample | Ba | Cu | Nb | Nd | Ni | Rb | Sr | V | Y | Zr |
|---------|------|----|----|----|----|----|------|----|---|----|
| 3G-226 | 446 | 24 | 7 | 15 | 9 | 18 | 612 | 0 | 3 | 58 |
| 3G-229 | 325 | 12 | 7 | 16 | 10 | 30 | 742 | 0 | 5 | 63 |
| 3G-232 | 434 | 16 | 7 | 7 | 13 | 34 | 846 | 3 | 3 | 75 |
| 3G-233A | 439 | 14 | 8 | 6 | 12 | 27 | 871 | 2 | 5 | 80 |
| GX-3A | 1085 | 19 | 5 | 9 | 12 | 42 | 653 | 0 | 4 | 35 |
| GX-4 | 867 | 24 | 6 | 14 | 8 | 52 | 544 | 0 | 4 | 39 |
| GX-5 | 588 | 22 | 6 | 19 | 9 | 34 | 726 | 0 | 3 | 46 |
| MA-39A | 526 | 37 | 7 | 8 | 12 | 34 | 1009 | 4 | 4 | 73 |
| MA-68A | 339 | 32 | 7 | 14 | 9 | 19 | 673 | 0 | 5 | 52 |
| MA-69A | 836 | 23 | 5 | 10 | 11 | 51 | 696 | 0 | 3 | 37 |
| MA-70A | 305 | 34 | 7 | 16 | 13 | 22 | 772 | 14 | 7 | 67 |
| MA-71B | 805 | 20 | 7 | 5 | 9 | 44 | 634 | 0 | 5 | 77 |

mixed rock series trace element data in ppm

| Sample | Ba | Cu | Nb | Nd | Ni | Rb | Sr | V | Y | Zr |
|--------|------|----|----|----|----|----|-----|----|----|-----|
| 3G-121 | 565 | 16 | 11 | 25 | 10 | 75 | 247 | 11 | 15 | 131 |
| 3G-129 | 490 | 13 | 9 | 20 | 13 | 47 | 780 | 28 | 8 | 88 |
| 3G-228 | 715 | 20 | 6 | 11 | 8 | 54 | 436 | 0 | 6 | 32 |
| GX-6 | 624 | 21 | 9 | 16 | 21 | 66 | 581 | 60 | 14 | 63 |
| MA-36A | 662 | 19 | 9 | 30 | 10 | 40 | 387 | 0 | 17 | 43 |
| MA-36D | 1048 | 27 | 7 | 18 | 11 | 43 | 611 | 0 | 16 | 58 |
| MA-37 | 545 | 33 | 9 | 23 | 10 | 40 | 809 | 0 | 8 | 85 |
| MA-38 | 601 | 18 | 13 | 13 | 9 | 61 | 743 | 0 | 7 | 77 |
| MA-66B | 1158 | 17 | 9 | 14 | 13 | 52 | 595 | 16 | 4 | 86 |

T-3511

calcic rock series trace element data in ppm

| Sample | Ba | Cu | Nb | Nd | Ni | Rb | Sr | V | Y | Zr |
|---------|-----|-----|----|----|----|----|------|-----|----|-----|
| 3G-108 | 37 | 23 | 5 | 17 | 32 | 1 | 373 | 284 | 8 | 20 |
| 3G-109 | 308 | 24 | 5 | 23 | 16 | 35 | 346 | 83 | 19 | 87 |
| 3G-110A | 285 | 129 | 7 | 35 | 20 | 38 | 340 | 164 | 32 | 50 |
| 3G-110B | 416 | 23 | 6 | 14 | 13 | 39 | 257 | 32 | 9 | 159 |
| 3G-113 | 295 | 27 | 8 | 23 | 17 | 32 | 475 | 221 | 26 | 130 |
| 3G-114 | 291 | 30 | 7 | 34 | 19 | 20 | 382 | 126 | 44 | 186 |
| 3G-118 | 382 | 6 | 8 | 24 | 13 | 28 | 409 | 62 | 15 | 85 |
| 3G-126 | 393 | 20 | 9 | 25 | 15 | 23 | 540 | 63 | 21 | 92 |
| 3G-127 | 324 | 27 | 9 | 22 | 22 | 23 | 999 | 76 | 12 | 112 |
| 3G-202 | 319 | 17 | 6 | 19 | 15 | 17 | 417 | 129 | 18 | 80 |
| 3G-203 | 421 | 26 | 9 | 23 | 30 | 48 | 524 | 155 | 23 | 91 |
| 3G-204A | 418 | 52 | 9 | 32 | 29 | 41 | 508 | 138 | 32 | 273 |
| 3G-205 | 332 | 1 | 8 | 24 | 15 | 25 | 527 | 72 | 16 | 80 |
| 3G-206 | 142 | 42 | 6 | 10 | 54 | 4 | 975 | 263 | 13 | 14 |
| 3G-208 | 355 | 2 | 9 | 27 | 16 | 27 | 599 | 82 | 21 | 73 |
| 3G-209A | 420 | 7 | 9 | 18 | 14 | 46 | 418 | 97 | 16 | 92 |
| 3G-218 | 220 | 2 | 6 | 20 | 15 | 25 | 332 | 94 | 24 | 84 |
| 3G-219 | 177 | 10 | 8 | 25 | 15 | 20 | 595 | 58 | 13 | 85 |
| 3G-220 | 360 | 11 | 11 | 16 | 10 | 25 | 477 | 18 | 10 | 83 |
| 3G-223 | 366 | 55 | 8 | 29 | 17 | 43 | 431 | 175 | 15 | 111 |
| 3G-234A | 505 | 17 | 8 | 20 | 18 | 55 | 513 | 72 | 12 | 65 |
| BB-2A | 363 | 61 | 12 | 29 | 41 | 51 | 467 | 173 | 23 | 138 |
| BB-3A | 369 | 11 | 9 | 13 | 15 | 34 | 487 | 89 | 17 | 59 |
| BB-4A | 367 | 17 | 11 | 9 | 11 | 34 | 491 | 17 | 4 | 73 |
| BB-5C | 290 | 34 | 7 | 25 | 35 | 20 | 882 | 192 | 17 | 68 |
| GX-1 | 457 | 110 | 8 | 32 | 33 | 30 | 867 | 163 | 30 | 153 |
| GX-21 | 447 | 0 | 8 | 24 | 30 | 41 | 637 | 137 | 23 | 112 |
| GX-29 | 200 | 12 | 11 | 18 | 29 | 27 | 434 | 189 | 23 | 90 |
| GX-3B | 443 | 46 | 8 | 20 | 54 | 51 | 616 | 139 | 16 | 123 |
| GX-9A | 172 | 23 | 5 | 21 | 76 | 22 | 250 | 206 | 18 | 45 |
| MA-20B | 141 | 103 | 5 | 19 | 17 | 1 | 738 | 202 | 20 | 59 |
| MA-25B | 54 | 76 | 5 | 10 | 41 | 7 | 149 | 159 | 3 | 22 |
| MA-26 | 376 | 9 | 7 | 28 | 13 | 39 | 396 | 63 | 16 | 75 |
| MA-27 | 386 | 29 | 6 | 21 | 19 | 32 | 471 | 176 | 25 | 87 |
| MA-28 | 304 | 7 | 6 | 26 | 17 | 31 | 425 | 155 | 28 | 130 |
| MA-29 | 434 | 50 | 7 | 24 | 19 | 45 | 419 | 176 | 25 | 121 |
| MA-32 | 372 | 40 | 8 | 21 | 15 | 29 | 611 | 116 | 11 | 71 |
| MA-39B | 256 | 0 | 18 | 58 | 34 | 10 | 1256 | 311 | 24 | 153 |
| MA-61 | 302 | 40 | 10 | 27 | 17 | 28 | 418 | 162 | 36 | 124 |
| MA-62A | 515 | 17 | 7 | 16 | 13 | 36 | 399 | 32 | 14 | 82 |
| MA-63 | 391 | 10 | 8 | 15 | 15 | 23 | 628 | 77 | 12 | 74 |
| MA-65A | 441 | 43 | 6 | 26 | 19 | 79 | 339 | 80 | 34 | 188 |

T-3511

calc-alkaline rock series trace element data in ppm

| Sample | Ba | Cu | Nb | Nd | Ni | Rb | Sr | V | Y | Zr |
|---------|------|-----|----|----|-----|-----|-----|-----|----|-----|
| 3G-111 | 427 | 20 | 7 | 20 | 15 | 65 | 311 | 61 | 23 | 143 |
| 3G-112 | 549 | 37 | 9 | 13 | 12 | 56 | 313 | 18 | 10 | 155 |
| 3G-123 | 305 | 90 | 12 | 21 | 56 | 35 | 549 | 212 | 27 | 111 |
| 3G-124 | 1033 | 11 | 14 | 26 | 9 | 99 | 202 | 0 | 26 | 201 |
| 3G-125 | 739 | 14 | 11 | 21 | 11 | 142 | 149 | 2 | 14 | 124 |
| 3G-128 | 621 | 24 | 20 | 43 | 18 | 50 | 497 | 134 | 43 | 322 |
| 3G-210 | 460 | 42 | 7 | 24 | 19 | 45 | 502 | 182 | 27 | 82 |
| 3G-215A | 479 | 23 | 8 | 26 | 21 | 91 | 335 | 152 | 35 | 171 |
| 3G-225 | nd | nd | nd | nd | nd | nd | nd | nd | nd | nd |
| BB-6A | 739 | 120 | 11 | 38 | 35 | 61 | 616 | 247 | 27 | 231 |
| GX-10 | 951 | 10 | 9 | 25 | 13 | 74 | 176 | 12 | 28 | 119 |
| GX-12 | 323 | 36 | 8 | 23 | 20 | 45 | 399 | 160 | 24 | 112 |
| GX-13 | 674 | 64 | 18 | 30 | 23 | 72 | 399 | 65 | 27 | 246 |
| GX-17 | 481 | 66 | 9 | 52 | 17 | 55 | 675 | 122 | 27 | 219 |
| GX-18 | 694 | 23 | 10 | 42 | 11 | 151 | 112 | 1 | 30 | 189 |
| GX-19 | 732 | 16 | 10 | 36 | 10 | 166 | 114 | 0 | 29 | 194 |
| GX-20 | 434 | 66 | 10 | 25 | 19 | 81 | 436 | 153 | 32 | 150 |
| GX-23 | 609 | 6 | 10 | 27 | 15 | 140 | 270 | 60 | 23 | 183 |
| GX-24 | 630 | 4 | 12 | 33 | 15 | 90 | 302 | 23 | 47 | 300 |
| GX-25 | 375 | 53 | 9 | 24 | 31 | 34 | 468 | 223 | 30 | 137 |
| GX-26 | 29 | 42 | 12 | 21 | 5 | 313 | 16 | 0 | 21 | 70 |
| GX-27 | 638 | 17 | 11 | 25 | 9 | 162 | 231 | 3 | 18 | 128 |
| GX-28 | 740 | 14 | 9 | 32 | 5 | 169 | 110 | 0 | 15 | 92 |
| GX-8 | 502 | 45 | 10 | 25 | 14 | 99 | 365 | 23 | 14 | 157 |
| GX-9 | 1201 | 4 | 12 | 26 | 11 | 103 | 235 | 38 | 30 | 157 |
| MA-20 | 204 | 18 | 4 | 36 | 12 | 108 | 78 | 0 | 26 | 83 |
| MA-21 | 418 | 13 | 6 | 30 | 14 | 30 | 378 | 195 | 19 | 79 |
| MA-22B | 845 | 18 | 8 | 23 | 9 | 115 | 112 | 0 | 21 | 166 |
| MA-30 | 437 | 38 | 10 | 23 | 29 | 41 | 389 | 150 | 34 | 180 |
| MA-31 | 295 | 132 | 7 | 14 | 32 | 35 | 334 | 250 | 16 | 87 |
| MA-33 | 513 | 27 | 7 | 22 | 11 | 126 | 64 | 0 | 28 | 109 |
| MA-34A | 681 | 16 | 9 | 44 | 13 | 86 | 342 | 79 | 67 | 268 |
| MA-35 | 1076 | 28 | 10 | 26 | 11 | 102 | 235 | 36 | 20 | 184 |
| MA-39C | 474 | 0 | 17 | 39 | 164 | 28 | 425 | 224 | 22 | 118 |
| MA-40 | 513 | 11 | 9 | 28 | 24 | 70 | 616 | 119 | 18 | 130 |
| MA-64A | 613 | 5 | 7 | 32 | 16 | 62 | 361 | 132 | 34 | 63 |
| MA-66A | 215 | 234 | 7 | 18 | 134 | 33 | 458 | 188 | 10 | 57 |
| MA-67A | 461 | 84 | 10 | 30 | 30 | 70 | 616 | 204 | 19 | 96 |

Appendix E

MINERAL MODES

trondhjemite rock series mineral modes

| Sample | Name | Qtz | Plag | K-sp | Bio | Musc | Horn | Opx | Cpx | Gar | Opq |
|---------|------|-----|------|------|-----|------|------|-----|-----|-----|-----|
| 3G-226 | TO | 27 | 67 | 0 | 3 | 3 | 0 | 0 | 0 | 0 | 0 |
| 3G-229 | TO | 21 | 71 | 1 | 4 | 3 | 0 | 0 | 0 | 0 | 0 |
| 3G-232 | TO | 27 | 66 | 2 | 3 | 2 | 0 | 0 | 0 | 0 | 0 |
| 3G-233A | TO | 23 | 68 | 0 | 4 | 2 | 0 | 0 | 0 | 0 | 1 |
| GX-3A | TO | 27 | 63 | 4 | 3 | 1 | 0 | 0 | 0 | 0 | 1 |
| GX-4 | TO | 33 | 55 | 4 | 2 | 5 | 0 | 0 | 0 | 0 | 0 |
| GX-5 | TO | 52 | 41 | 1 | 2 | 4 | 0 | 0 | 0 | 0 | 0 |
| MA-39A | TO | 31 | 58 | 0 | 9 | 1 | 0 | 0 | 0 | 0 | 0 |
| MA-68A | TO | 26 | 65 | 0 | 4 | 5 | 0 | 0 | 0 | 0 | 1 |
| MA-69A | TO | 25 | 69 | 0 | 3 | 2 | 0 | 0 | 0 | 0 | 0 |
| MA-70A | TO | 24 | 66 | 0 | 8 | 1 | 0 | 0 | 0 | 0 | 0 |
| MA-71B | TO | 39 | 49 | 3 | 4 | 4 | 0 | 0 | 0 | 0 | 0 |

mixed rock series mineral modes

| Sample | Name | Qtz | Plag | K-sp | Bio | Musc | Horn | Opx | Cpx | Gar | Opq |
|--------|------|-----|------|------|-----|------|------|-----|-----|-----|-----|
| 3G-121 | GD | 28 | 57 | 10 | 4 | 0 | 0 | 0 | 0 | 0 | 1 |
| 3G-129 | TO | 32 | 57 | 2 | 7 | 0 | 0 | 0 | 0 | 0 | 1 |
| 3G-228 | GD | 21 | 61 | 15 | 1 | 1 | 0 | 0 | 0 | 0 | 0 |
| GX-6 | GD | 28 | 48 | 10 | 7 | 6 | 0 | 0 | 0 | 0 | 0 |
| MA-36A | TO | 39 | 49 | 1 | 0 | 10 | 0 | 0 | 0 | 1 | 0 |
| MA-36D | GD | 27 | 46 | 16 | 8 | 3 | 0 | 0 | 0 | 1 | 0 |
| MA-37 | GR | 38 | 30 | 24 | 5 | 2 | 0 | 0 | 0 | 0 | 0 |
| MA-38 | TO | 41 | 49 | 5 | 4 | 1 | 0 | 0 | 0 | 0 | 0 |
| MA-66B | GD | 26 | 59 | 9 | 6 | 0 | 0 | 0 | 0 | 0 | 0 |

calcic rock series mineral modes

| Sample | Name | Qtz | Plag | K-sp | Bio | Musc | Horn | Opx | Cpx | Gar | Opq |
|---------|------|-----|------|------|-----|------|------|-----|-----|-----|-----|
| 3G-108 | DI | 0 | 60 | 0 | 0 | 0 | 21 | 19 | 0 | 0 | 0 |
| 3G-109 | TO | 25 | 62 | 0 | 11 | 0 | 0 | 0 | 0 | 0 | 2 |
| 3G-110A | MTO | 20 | 59 | 0 | 9 | 0 | 11 | 0 | 0 | 0 | 1 |
| 3G-110B | TO | 36 | 54 | 3 | 5 | 0 | 0 | 0 | 0 | 0 | 1 |
| 3G-113 | QD | 10 | 57 | 0 | 12 | 0 | 16 | 0 | 0 | 0 | 4 |
| 3G-114 | QD | 15 | 60 | 4 | 4 | 0 | 14 | 0 | 0 | 0 | 3 |
| 3G-118 | MTO | 31 | 48 | 1 | 0 | 0 | 19 | 0 | 0 | 0 | 1 |
| 3G-126 | QD | 16 | 65 | 0 | 9 | 0 | 9 | 0 | 0 | 0 | 2 |
| 3G-127 | QD | 14 | 58 | 1 | 9 | 0 | 16 | 0 | 0 | 0 | 0 |
| 3G-202 | MTO | 18 | 51 | 0 | 2 | 0 | 24 | 0 | 0 | 0 | 4 |
| 3G-203 | MTO | 18 | 53 | 0 | 11 | 0 | 16 | 0 | 0 | 0 | 2 |
| 3G-204A | DI | 3 | 76 | 1 | 3 | 0 | 14 | 0 | 0 | 0 | 1 |
| 3G-205 | TO | 29 | 51 | 0 | 11 | 0 | 6 | 0 | 0 | 0 | 1 |
| 3G-206 | DI | 0 | 50 | 0 | 0 | 0 | 46 | 0 | 0 | 0 | 4 |
| 3G-208 | MTO | 18 | 58 | 0 | 11 | 0 | 12 | 0 | 0 | 0 | 1 |
| 3G-209A | MTO | 23 | 43 | 0 | 17 | 0 | 9 | 0 | 6 | 0 | 1 |
| 3G-218 | MTO | 23 | 52 | 0 | 4 | 0 | 16 | 0 | 0 | 0 | 4 |
| 3G-219 | TO | 30 | 51 | 0 | 16 | 0 | 0 | 0 | 0 | 0 | 2 |
| 3G-220 | TO | 22 | 68 | 2 | 7 | 0 | 0 | 0 | 0 | 0 | 1 |
| 3G-223 | TO | 32 | 59 | 1 | 9 | 0 | 0 | 0 | 0 | 0 | 0 |
| 3G-234A | TO | 19 | 64 | 0 | 11 | 0 | 4 | 0 | 0 | 0 | 1 |
| BB-2A | MTO | 13 | 48 | 0 | 10 | 0 | 28 | 0 | 0 | 0 | 1 |
| BB-3A | MTO | 24 | 52 | 0 | 9 | 0 | 12 | 0 | 0 | 0 | 1 |
| BB-4A | TO | 36 | 49 | 4 | 10 | 0 | 0 | 0 | 0 | 0 | 1 |
| BB-5C | QD | 9 | 51 | 0 | 6 | 0 | 31 | 0 | 0 | 0 | 2 |
| GX-1 | QD | 5 | 62 | 0 | 13 | 0 | 16 | 0 | 0 | 0 | 3 |
| GX-21 | QD | 13 | 58 | 3 | 7 | 0 | 16 | 0 | 0 | 0 | 2 |
| GX-29 | QD | 9 | 48 | 1 | 8 | 0 | 13 | 0 | 20 | 0 | 1 |
| GX-3B | DI | 14 | 54 | 0 | 14 | 0 | 15 | 0 | 0 | 0 | 1 |
| GX-9A | QD | 5 | 38 | 0 | 0 | 0 | 57 | 0 | 0 | 0 | 1 |
| MA-20B | QD | 1 | 77 | 0 | 2 | 0 | 10 | 2 | 1 | 0 | 6 |
| MA-25B | GB | 0 | 54 | 0 | 0 | 0 | 19 | 17 | 9 | 0 | 0 |
| MA-26 | MTO | 23 | 57 | 0 | 6 | 0 | 11 | 0 | 0 | 0 | 1 |
| MA-27 | MTO | 19 | 59 | 0 | 7 | 0 | 13 | 0 | 0 | 0 | 1 |
| MA-28 | MTO | 25 | 54 | 0 | 10 | 0 | 9 | 0 | 0 | 0 | 1 |
| MA-29 | MTO | 29 | 40 | 0 | 23 | 0 | 6 | 1 | 0 | 0 | 0 |
| MA-32 | MTO | 22 | 54 | 0 | 12 | 0 | 9 | 0 | 0 | 0 | 2 |
| MA-39B | DI | 3 | 56 | 0 | 2 | 0 | 37 | 0 | 0 | 0 | 2 |
| MA-61 | MTO | 15 | 53 | 2 | 6 | 0 | 20 | 0 | 0 | 0 | 3 |
| MA-62A | TO | 32 | 52 | 3 | 11 | 0 | 0 | 0 | 0 | 0 | 2 |
| MA-63 | TO | 23 | 60 | 0 | 6 | 0 | 6 | 0 | 0 | 0 | 1 |
| MA-65A | QD | 14 | 60 | 0 | 5 | 0 | 17 | 0 | 0 | 0 | 2 |

calc-alkaline rock series mineral modes

| Sample | Name | Qtz | Plag | K-sp | Bio | Musc | Horn | Opx | Cpx | Gar | Opq |
|---------|------|-----|------|------|-----|------|------|-----|-----|-----|-----|
| 3G-111 | GD | 29 | 41 | 14 | 11 | 0 | 4 | 0 | 0 | 0 | 1 |
| 3G-112 | GD | 0 | 0 | 0 | 0 | 0 | 0 | 0 | 0 | 0 | 0 |
| 3G-123 | QD | 4 | 55 | 1 | 0 | 0 | 34 | 4 | 0 | 0 | 2 |
| 3G-124 | GD | 30 | 41 | 20 | 8 | 0 | 0 | 0 | 0 | 0 | 2 |
| 3G-125 | GR | 33 | 27 | 36 | 3 | 0 | 0 | 0 | 0 | 0 | 0 |
| 3G-128 | QD | 11 | 56 | 6 | 9 | 0 | 12 | 2 | 0 | 0 | 3 |
| 3G-210 | MTO | 17 | 43 | 0 | 17 | 0 | 15 | 0 | 0 | 0 | 6 |
| 3G-215A | GD | 14 | 45 | 9 | 13 | 0 | 8 | 0 | 10 | 0 | 2 |
| 3G-225 | QMD | 11 | 59 | 7 | 8 | 0 | 12 | 0 | 2 | 0 | 0 |
| BB-6A | QMD | 9 | 46 | 5 | 16 | 0 | 10 | 4 | 5 | 0 | 2 |
| GX-10 | GR | 33 | 26 | 30 | 7 | 0 | 2 | 0 | 0 | 0 | 2 |
| GX-12 | QD | 15 | 58 | 3 | 7 | 0 | 13 | 1 | 0 | 0 | 2 |
| GX-13 | QMD | 12 | 53 | 21 | 4 | 0 | 2 | 0 | 1 | 0 | 2 |
| GX-17 | QMD | 15 | 58 | 13 | 8 | 0 | 2 | 1 | 0 | 0 | 2 |
| GX-18 | GR | 38 | 20 | 38 | 2 | 0 | 0 | 0 | 0 | 0 | 2 |
| GX-19 | GR | 37 | 21 | 38 | 2 | 0 | 0 | 0 | 0 | 0 | 2 |
| GX-20 | MTO | 15 | 54 | 3 | 15 | 0 | 9 | 0 | 0 | 0 | 2 |
| GX-23 | GD | 27 | 39 | 21 | 5 | 0 | 7 | 0 | 0 | 0 | 1 |
| GX-24 | GR | 18 | 42 | 26 | 4 | 1 | 6 | 0 | 0 | 0 | 2 |
| GX-25 | QD | 6 | 57 | 5 | 5 | 0 | 12 | 8 | 0 | 0 | 3 |
| GX-26 | GR | 37 | 26 | 34 | 2 | 0 | 0 | 0 | 0 | 0 | 0 |
| GX-27 | GR | 35 | 27 | 31 | 5 | 0 | 1 | 0 | 0 | 0 | 1 |
| GX-28 | GR | 35 | 21 | 40 | 2 | 0 | 0 | 0 | 0 | 0 | 1 |
| GX-8 | GR | 27 | 36 | 29 | 2 | 0 | 2 | 0 | 0 | 0 | 1 |
| GX-9 | GD | 37 | 40 | 12 | 6 | 0 | 4 | 0 | 0 | 0 | 0 |
| MA-20 | GR | 37 | 22 | 41 | 0 | 0 | 0 | 0 | 0 | 0 | 0 |
| MA-21 | TO | 27 | 53 | 6 | 6 | 0 | 6 | 0 | 0 | 0 | 2 |
| MA-22B | GR | 35 | 28 | 29 | 8 | 0 | 0 | 0 | 0 | 0 | 0 |
| MA-30 | QMD | 11 | 55 | 9 | 7 | 0 | 13 | 2 | 0 | 0 | 2 |
| MA-31 | QD | 9 | 57 | 5 | 1 | 0 | 24 | 2 | 0 | 0 | 2 |
| MA-33 | GR | 32 | 25 | 41 | 2 | 0 | 0 | 0 | 0 | 0 | 1 |
| MA-34A | MTO | 23 | 44 | 6 | 9 | 0 | 17 | 0 | 0 | 0 | 2 |
| MA-35 | GR | 33 | 31 | 29 | 6 | 0 | 0 | 0 | 0 | 0 | 0 |
| MA-39C | DI | 0 | 22 | 2 | 4 | 0 | 73 | 0 | 0 | 0 | 0 |
| MA-40 | GD | 27 | 41 | 11 | 5 | 0 | 12 | 0 | 0 | 0 | 0 |
| MA-64A | MTO | 17 | 57 | 1 | 13 | 8 | 0 | 0 | 0 | 0 | 2 |
| MA-66A | DI | 1 | 32 | 3 | 0 | 0 | 65 | 0 | 0 | 0 | 0 |
| MA-67A | QD | 12 | 59 | 3 | 10 | 0 | 13 | 3 | 0 | 0 | 1 |

Appendix F

Ar/Ar ISOTOPIC DATA

| Temp x°C | 40Ar 39Ar | 37Ar 39Ar | 36Ar 39Ar | Moles 39Ar | 40Ar %Total | %Ar40 Rad | K/Ca | Age (Ma) |
|-------------|--------------|--------------|--------------|---------------|----------------|--------------|---------|----------------|
| 88-2A-B | | | | | | | | |
| J = .005785 | | | | | | | | |
| 800 | 62.49 | 38.5754 | 0.1545 | 0.5 | 0.0 | 31.9 | 0.0123 | 202.4 +/-100.5 |
| 905 | 8.32 | 0.0279 | 0.0073 | 353.6 | 13.6 | 73.6 | 17.5624 | 62.8 +/- 0.7 |
| 960 | 7.59 | 0.0190 | 0.0032 | 389.3 | 15.0 | 87.1 | 25.7891 | 67.7 +/- 0.9 |
| 1000 | 7.28 | 0.0224 | 0.0018 | 727.3 | 28.0 | 92.2 | 21.8746 | 68.7 +/- 0.7 |
| 1025 | 7.08 | 0.0298 | 0.0011 | 428.8 | 16.5 | 94.9 | 16.4426 | 68.8 +/- 0.7 |
| FUSE | 7.21 | 0.0375 | 0.0015 | 695.2 | 26.8 | 93.4 | 13.0663 | 68.9 +/- 0.7 |
| TOTAL | | | | 2594.7 | 100.0 | | | 67.9 |
| PLATEAU AGE | | | | | | | | 68.8 +/- 0.5 |

| E-40/39 | E-37/39 | E-36/39 | TEMP |
|---------|---------|---------|------|
| 5.77 | 5.84 | 8.75 | 800 |
| .06 | 1.37 | .77 | 905 |
| .06 | 3.19 | 3.44 | 960 |
| .05 | .92 | 2.4 | 1000 |
| .05 | .85 | 3.25 | 1025 |
| .06 | .77 | 1.51 | FUSE |

| Temp x°C | 40Ar 39Ar | 37Ar 39Ar | 36Ar 39Ar | Moles 39Ar | 40Ar %Total | %Ar40 Rad | K/Ca | Age (Ma) |
|-------------|--------------|--------------|--------------|---------------|----------------|--------------|--------|--------------|
| BB-2A-H | | | | J = .00571 | | | | |
| 975 | 31.27 | 1.3687 | 0.0775 | 40.9 | 13.5 | 27.0 | 0.3576 | 85.0 +/- 2.0 |
| 1000 | 18.11 | 5.7868 | 0.0383 | 29.9 | 9.9 | 39.9 | 0.0843 | 73.3 +/- 1.5 |
| 1025 | 11.21 | 9.1410 | 0.0169 | 65.7 | 21.8 | 61.7 | 0.0532 | 70.4 +/- 1.3 |
| 1040 | 10.09 | 8.4458 | 0.0129 | 49.2 | 16.3 | 68.6 | 0.0576 | 70.4 +/- 1.1 |
| 1050 | 10.11 | 8.2803 | 0.0119 | 24.3 | 8.1 | 71.5 | 0.0588 | 73.4 +/- 1.9 |
| 1065 | 10.31 | 8.8907 | 0.0124 | 16.8 | 5.5 | 71.1 | 0.0547 | 74.5 +/- 4.0 |
| 1075 | 9.97 | 10.8791 | 0.0135 | 12.3 | 4.1 | 68.5 | 0.0447 | 69.5 +/- 2.2 |
| 1085 | 13.97 | 13.3811 | 0.0253 | 11.9 | 3.9 | 54.0 | 0.0362 | 76.8 +/- 4.6 |
| 1100 | 15.03 | 13.6889 | 0.0289 | 24.3 | 8.0 | 50.3 | 0.0354 | 77.1 +/- 3.6 |
| 1125 | 17.08 | 13.9246 | 0.0334 | 15.7 | 5.2 | 48.6 | 0.0348 | 84.4 +/- 3.6 |
| 1145 | 20.08 | 13.9498 | 0.0405 | 7.5 | 2.5 | 45.9 | 0.0348 | 93.4 +/- 9.7 |
| FUSE | 28.28 | 14.1011 | 0.0671 | 3.5 | 1.2 | 33.8 | 0.0344 | 96.9 +/- 9.9 |
| TOTAL | | | | 301.9 | 100.0 | | | 75.5 |
| PLATEAU AGE | | | | | | | | 71.9 +/- 3.8 |

| E-40/39 | E-37/39 | E-36/39 | TEMP |
|--------------|--------------|---------|------|
| .07 | .12 | .4 | 975 |
| .05 | .08 | .58 | 1000 |
| .07 | 9.000001E-02 | 1.16 | 1025 |
| .08 | 9.000001E-02 | 1.18 | 1040 |
| .13 | .13 | 2.43 | 1050 |
| .07 | 9.000001E-02 | 5.38 | 1065 |
| .13 | .13 | 2.62 | 1075 |
| 9.000001E-02 | .15 | 3.06 | 1085 |
| .07 | 9.000001E-02 | 2.08 | 1100 |
| 9.000001E-02 | 9.000001E-02 | 1.8 | 1125 |
| .1 | .11 | 4.12 | 1145 |
| .21 | .22 | 2.54 | FUSE |

| Temp | 40Ar | 37Ar | 36Ar | Moles | 40Ar | %Ar40 | K/Ca | Age (Ma) |
|------|------|------|------|-------|--------|-------|------|----------|
| xC | 39Ar | 39Ar | 39Ar | 39Ar | %Total | Rad | | |

6X-9-H

J = .002983

| | | | | | | | | |
|------|--------|--------|--------|------|------|------|--------|---------------|
| 850 | 109.30 | 1.9760 | 0.1476 | 15.9 | 3.2 | 60.2 | 0.2476 | 323.8 +/- 4.8 |
| 900 | 34.95 | 3.8999 | 0.0419 | 31.2 | 6.2 | 65.4 | 0.1253 | 119.3 +/- 2.5 |
| 950 | 29.40 | 4.3920 | 0.0193 | 66.3 | 13.2 | 81.7 | 0.1112 | 125.2 +/- 1.4 |
| 975 | 28.95 | 4.4700 | 0.0174 | 54.9 | 11.0 | 83.3 | 0.1093 | 125.8 +/- 1.6 |
| 1000 | 28.12 | 4.5360 | 0.0136 | 80.4 | 16.1 | 86.9 | 0.1077 | 127.4 +/- 1.3 |
| 1025 | 26.77 | 4.5920 | 0.0108 | 82.2 | 16.4 | 89.3 | 0.1063 | 124.7 +/- 1.3 |
| 1075 | 26.76 | 4.6580 | 0.0098 | 82.2 | 16.4 | 90.5 | 0.1048 | 126.2 +/- 1.8 |
| FUSE | 28.78 | 4.8890 | 0.0086 | 87.3 | 17.4 | 92.4 | 0.0999 | 138.2 +/- 1.4 |

TOTAL 500.4 100.0 133.9

PLATEAU AGE 125.9 +/- 2.6

| E-40/39 | E-37/39 | E-36/39 | TEMP |
|---------|---------|---------|------|
| .24 | .78 | .75 | 850 |
| .16 | .47 | 1.69 | 900 |
| .08 | .11 | 1.3 | 950 |
| .11 | .18 | 1.97 | 975 |
| .07 | .05 | .44 | 1000 |
| .07 | .07 | 1.67 | 1025 |
| .08 | .104 | 4.32 | 1075 |
| .07 | .17 | 1.9 | FUSE |

| Temp | 40Ar | 37Ar | 36Ar | Moles | 40Ar | %Ar40 | K/Ca | Age (Ma) |
|----------|------|--------|--------|---------------------|--------|-------|---------|--------------|
| xC | 39Ar | 39Ar | 39Ar | 39Ar | %Total | Rad | | |
| BX-19-WR | | | | $\lambda = .003016$ | | | | |
| 550 | 4.75 | 0.0406 | 0.0046 | 189.4 | 19.7 | 70.7 | 12.0835 | 18.2 +/- 0.9 |
| 700 | 3.90 | 0.0266 | 0.0031 | 218.5 | 22.7 | 75.7 | 18.4138 | 16.0 +/- 1.2 |
| 800 | 3.54 | 0.0211 | 0.0017 | 164.3 | 17.1 | 85.0 | 23.2224 | 16.3 +/- 1.2 |
| 850 | 3.53 | 0.0253 | 0.0027 | 94.5 | 9.8 | 76.1 | 19.3749 | 14.6 +/- 1.6 |
| 950 | 3.83 | 0.0248 | 0.0043 | 80.8 | 8.4 | 65.7 | 19.7736 | 13.6 +/- 1.2 |
| 1025 | 4.01 | 0.0645 | 0.0049 | 69.5 | 7.2 | 62.9 | 7.5942 | 13.7 +/- 2.2 |
| FUSE | 5.58 | 0.0963 | 0.0086 | 144.1 | 15.0 | 53.7 | 5.0879 | 16.2 +/- 1.5 |

TOTAL 961.2 100.0 16.0

PLATEAU AGE 15.1 +/- 2.6

| E-40/39 | E-37/39 | E-36/39 | TEMP |
|---------|---------|---------|------|
| .13 | 4.71 | 6.15 | 550 |
| .06 | 2.94 | 12.34 | 700 |
| .05 | 17.79 | 21.43 | 800 |
| .29 | 54.06 | 18.19 | 850 |
| .1 | 4.61 | 8.57 | 950 |
| .17 | 24.91 | 13.86 | 1025 |
| .05 | 4.32 | 5.31 | FUSE |

| Temp | 40Ar | 37Ar | 36Ar | Moles | 40Ar | %Ar40 | K/Ca | Age (Ma) |
|------|------|------|------|-------|--------|-------|------|----------|
| C | 39Ar | 39Ar | 39Ar | 39Ar | %Total | Rad | | |

6X-20-H

J = .002913

| | | | | | | | | |
|------|-------|--------|--------|------|------|------|--------|---------------|
| 875 | 57.79 | 0.8091 | 0.1450 | 49.3 | 10.0 | 25.9 | 0.6052 | 77.1 +/- 3.9 |
| 925 | 37.45 | 3.0138 | 0.0754 | 37.4 | 7.6 | 41.0 | 0.1622 | 79.2 +/- 2.2 |
| 950 | 31.24 | 5.8708 | 0.0474 | 37.4 | 7.6 | 56.6 | 0.0831 | 91.0 +/- 2.9 |
| 975 | 27.69 | 7.5473 | 0.0283 | 57.7 | 11.7 | 71.9 | 0.0646 | 102.2 +/- 2.4 |
| 1000 | 26.71 | 7.8510 | 0.0242 | 66.0 | 13.4 | 75.5 | 0.0620 | 103.6 +/- 1.2 |
| 1025 | 26.03 | 7.9699 | 0.0213 | 68.7 | 13.9 | 78.1 | 0.0611 | 104.4 +/- 1.5 |
| 1100 | 24.49 | 8.0085 | 0.0168 | 77.3 | 15.7 | 82.2 | 0.0608 | 103.4 +/- 1.2 |
| FUSE | 23.47 | 8.1867 | 0.0127 | 99.3 | 20.1 | 86.7 | 0.0595 | 104.5 +/- 1.3 |

| | | | | | | | | |
|-------|--|--|--|-------|-------|--|--|------|
| TOTAL | | | | 493.2 | 100.0 | | | 98.2 |
|-------|--|--|--|-------|-------|--|--|------|

| | | | | | | | | |
|-------------|--|--|--|--|--|--|--|---------------|
| PLATEAU AGE | | | | | | | | 104.0 +/- 1.6 |
|-------------|--|--|--|--|--|--|--|---------------|

| E-40/39 | E-37/39 | E-36/39 | TEMP |
|--------------|--------------|---------|------|
| 9.000001E-02 | .43 | .88 | 875 |
| .08 | .26 | .9 | 925 |
| .11 | .13 | 1.95 | 950 |
| .07 | .24 | 2.64 | 975 |
| .05 | .08 | .89 | 1000 |
| .05 | 9.000001E-02 | 1.65 | 1025 |
| 9.000001E-02 | .07 | 1.39 | 1100 |
| 9.000001E-02 | .18 | 2.13 | FUSE |

*

| Temp | 40Ar | 37Ar | 36Ar | Moles | 40Ar | %Ar40 | K/Ca | Age (Ma) |
|-------------|------|--------|--------|-------------|--------|-------|---------|--------------|
| xC | 39Ar | 39Ar | 39Ar | 39Ar | %Total | Rad | | |
| <hr/> | | | | | | | | |
| GX-27-B | | | | J = .005803 | | | | |
| 905 | 3.31 | 0.0065 | 0.0040 | 368.1 | 15.5 | 63.2 | 75.3842 | 21.8 +/- 0.5 |
| 967 | 2.76 | 0.0173 | 0.0022 | 289.4 | 12.2 | 75.1 | 28.3233 | 21.5 +/- 0.4 |
| 1005 | 2.50 | 0.0268 | 0.0014 | 496.7 | 20.9 | 82.0 | 18.2832 | 21.4 +/- 0.6 |
| 1040 | 2.27 | 0.0233 | 0.0007 | 604.2 | 25.5 | 89.2 | 21.0297 | 21.1 +/- 0.2 |
| FUSE | 2.54 | 0.0170 | 0.0015 | 613.2 | 25.9 | 81.1 | 28.8232 | 21.4 +/- 0.6 |
| TOTAL | | | | 2371.7 | 100.0 | | | 21.4 |
| PLATEAU AGE | | | | | | | | 21.3 +/- 0.5 |

| E-40/39 | E-37/39 | E-36/39 | TEMP |
|---------|---------|---------|------|
| .03 | 8.32 | 1.75 | 905 |
| .03 | 1.23 | 2.23 | 967 |
| .04 | 1.72 | 7.14 | 1005 |
| .05 | .76 | 2.34 | 1040 |
| .06 | 2.11 | 6.27 | FUSE |

| Temp | 40Ar | 37Ar | 36Ar | Moles | 40Ar | %Ar40 | K/Ca | Age (Ma) |
|------|------|------|------|-------|--------|-------|------|----------|
| xC | 39Ar | 39Ar | 39Ar | 39Ar | %Total | Rad | | |

MA-21-B

J = .005688

| | | | | | | | | |
|------|------|--------|--------|--------|------|------|----------|--------------|
| 825 | 8.92 | 0.0158 | 0.0096 | 176.3 | 6.5 | 67.8 | 31.0123 | 61.0 +/- 1.1 |
| 890 | 5.96 | 0.0065 | 0.0031 | 618.9 | 22.9 | 84.0 | 75.3842 | 50.7 +/- 0.6 |
| 940 | 5.24 | 0.0058 | 0.0008 | 250.4 | 9.2 | 94.7 | 84.4824 | 50.2 +/- 0.5 |
| 975 | 5.29 | 0.0077 | 0.0012 | 232.7 | 8.6 | 92.6 | 63.6360 | 49.6 +/- 0.6 |
| 1000 | 5.06 | 0.0078 | 0.0003 | 290.7 | 10.7 | 97.5 | 62.8201 | 49.9 +/- 0.5 |
| FUSE | 5.11 | 0.0047 | 0.0008 | 1139.3 | 42.1 | 94.6 | 104.2550 | 48.9 +/- 0.5 |

| | | | | | | | | |
|-------|--|--|--|--------|-------|--|--|------|
| TOTAL | | | | 2708.3 | 100.0 | | | 50.4 |
|-------|--|--|--|--------|-------|--|--|------|

| | | | | | | | | |
|-------------|--|--|--|--|--|--|--|--------------|
| PLATEAU AGE | | | | | | | | 49.5 +/- 1.2 |
|-------------|--|--|--|--|--|--|--|--------------|

| E-40/39 | E-37/39 | E-36/39 | TEMP |
|---------|---------|---------|------|
|---------|---------|---------|------|

| | | | |
|-----|------|------|------|
| .06 | 2.61 | 1.65 | 825 |
| .06 | 1.63 | 1.96 | 890 |
| .05 | 5.44 | 4.01 | 940 |
| .05 | 4.09 | 3.75 | 975 |
| .04 | 1.86 | 7.15 | 1000 |
| .07 | 1.33 | 2.16 | FUSE |

| Temp | 40Ar | 37Ar | 36Ar | Moles | 40Ar | %Ar40 | K/Ca | Age (Ma) |
|------|------|------|------|-------|--------|-------|------|----------|
| xC | 39Ar | 39Ar | 39Ar | 39Ar | %Total | Rad | | |

MA-21-H

J = .005848

| | | | | | | | | |
|------|-------|---------|--------|------|------|------|--------|--------------|
| 925 | 22.57 | 0.6117 | 0.0477 | 22.9 | 5.7 | 37.6 | 0.8007 | 87.4 +/- 2.4 |
| 960 | 13.77 | 0.9754 | 0.0291 | 14.0 | 3.5 | 37.9 | 0.5020 | 54.2 +/- 5.2 |
| 985 | 13.20 | 3.9074 | 0.0289 | 11.2 | 2.8 | 37.4 | 0.1250 | 51.5 +/- 2.6 |
| 1010 | 10.10 | 9.8827 | 0.0206 | 29.5 | 7.4 | 47.3 | 0.0492 | 50.1 +/- 2.4 |
| 1025 | 8.55 | 11.0197 | 0.0158 | 41.5 | 10.4 | 55.4 | 0.0441 | 49.7 +/- 1.9 |
| 1040 | 7.95 | 11.1450 | 0.0145 | 51.8 | 12.9 | 57.0 | 0.0436 | 47.6 +/- 0.9 |
| 1065 | 11.76 | 11.2461 | 0.0263 | 51.2 | 12.8 | 41.3 | 0.0432 | 51.0 +/- 1.5 |
| 1080 | 9.48 | 11.2760 | 0.0196 | 99.9 | 25.0 | 48.2 | 0.0431 | 48.0 +/- 1.0 |
| 1100 | 9.72 | 11.2685 | 0.0202 | 40.3 | 10.1 | 47.6 | 0.0431 | 48.6 +/- 2.0 |
| 1125 | 10.83 | 11.4018 | 0.0229 | 19.3 | 4.8 | 45.7 | 0.0426 | 52.0 +/- 2.1 |
| FUSE | 14.77 | 10.2573 | 0.0268 | 18.7 | 4.7 | 51.8 | 0.0474 | 79.5 +/- 2.7 |

| | | | | | | | | |
|-------|--|--|--|-------|-------|--|--|------|
| TOTAL | | | | 400.3 | 100.0 | | | 52.9 |
|-------|--|--|--|-------|-------|--|--|------|

| | | | | | | | | |
|-------------|--|--|--|--|--|--|--|--------------|
| PLATEAU AGE | | | | | | | | 49.2 +/- 2.9 |
|-------------|--|--|--|--|--|--|--|--------------|

| E-40/39 | E-37/39 | E-36/39 | TEMP |
|---------|---------|---------|------|
|---------|---------|---------|------|

| | | | |
|--------------|-----|------|------|
| .05 | .12 | .79 | 925 |
| 9.000001E-02 | .14 | 2.96 | 960 |
| .14 | .15 | 1.44 | 985 |
| 9.000001E-02 | .1 | 1.89 | 1010 |
| .06 | .07 | 1.87 | 1025 |
| .11 | .14 | .9 | 1040 |
| .07 | .07 | .91 | 1065 |
| .12 | .12 | .73 | 1080 |
| .05 | .08 | 1.55 | 1100 |
| .04 | .05 | 1.5 | 1125 |
| .07 | .07 | 1.61 | FUSE |

| Temp | 40Ar | 37Ar | 36Ar | Moles | 40Ar | %Ar40 | K/Ca | Age (Ma) |
|------|------|------|------|-------|--------|-------|------|----------|
| xC | 39Ar | 39Ar | 39Ar | 39Ar | %Total | Rad | | |

MA-37-B

J = .005839

| | | | | | | | | |
|------|------|--------|--------|-------|------|------|---------|--------------|
| 825 | 8.70 | 0.0413 | 0.0104 | 214.6 | 7.6 | 64.3 | 11.8640 | 57.9 +/- 0.9 |
| 880 | 6.90 | 0.0092 | 0.0019 | 581.6 | 20.6 | 91.3 | 53.2605 | 65.2 +/- 0.9 |
| 925 | 6.66 | 0.0124 | 0.0008 | 398.4 | 14.1 | 95.9 | 39.5158 | 66.1 +/- 0.7 |
| 960 | 6.73 | 0.0405 | 0.0006 | 230.6 | 8.2 | 96.8 | 12.0984 | 67.4 +/- 0.8 |
| 1000 | 6.85 | 0.0185 | 0.0015 | 332.8 | 11.8 | 93.0 | 26.4861 | 65.8 +/- 1.0 |
| 1040 | 6.68 | 0.0106 | 0.0008 | 579.6 | 20.5 | 95.9 | 46.2261 | 66.3 +/- 0.7 |
| FUSE | 6.91 | 0.0284 | 0.0014 | 486.0 | 17.2 | 93.5 | 17.2532 | 66.8 +/- 0.7 |

| | | | | | | | | |
|-------|--|--|--|--------|-------|--|--|------|
| TOTAL | | | | 2823.6 | 100.0 | | | 65.5 |
|-------|--|--|--|--------|-------|--|--|------|

| | | | | | | | | |
|-------------|--|--|--|--|--|--|--|--------------|
| PLATEAU AGE | | | | | | | | 66.5 +/- 1.6 |
|-------------|--|--|--|--|--|--|--|--------------|

| E-40/39 | E-37/39 | E-36/39 | TEMP |
|---------|---------|---------|------|
| .12 | .39 | 1.07 | 825 |
| .08 | 1.11 | 5.2 | 880 |
| .06 | .83 | 5.05 | 925 |
| .07 | .79 | 13.89 | 960 |
| .05 | 1.31 | 7.72 | 1000 |
| .04 | 1 | 2.4 | 1040 |
| .1 | .54 | 2.11 | FUSE |

| Temp | 40Ar | 37Ar | 36Ar | Moles | 40Ar | %Ar40 | K/Ca | Age (Ma) |
|------|------|------|------|-------|--------|-------|------|----------|
| xC | 39Ar | 39Ar | 39Ar | 39Ar | %Total | Rad | | |

MA-39C-H

J = .00582

| | | | | | | | | |
|------|-------|---------|--------|------|------|------|--------|---------------|
| 925 | 23.90 | 0.3144 | 0.0384 | 77.1 | 16.3 | 52.5 | 1.5582 | 127.1 +/- 1.5 |
| 975 | 16.27 | 3.5940 | 0.0240 | 55.3 | 11.7 | 58.0 | 0.1360 | 96.7 +/- 1.3 |
| 1000 | 14.73 | 11.8899 | 0.0193 | 80.8 | 17.1 | 67.6 | 0.0408 | 102.5 +/- 1.1 |
| 1025 | 13.77 | 13.4457 | 0.0173 | 97.9 | 20.8 | 70.5 | 0.0361 | 100.1 +/- 1.1 |
| 1040 | 13.77 | 11.4332 | 0.0179 | 52.3 | 11.1 | 68.0 | 0.0425 | 96.6 +/- 1.4 |
| 1050 | 14.87 | 11.7638 | 0.0218 | 27.0 | 5.7 | 62.8 | 0.0413 | 96.4 +/- 5.3 |
| 1065 | 17.85 | 13.6610 | 0.0325 | 18.7 | 4.0 | 52.2 | 0.0355 | 96.3 +/- 2.9 |
| 1085 | 18.08 | 15.2129 | 0.0310 | 20.9 | 4.4 | 55.9 | 0.0318 | 104.3 +/- 2.2 |
| 1110 | 19.09 | 14.9324 | 0.0331 | 18.9 | 4.0 | 54.9 | 0.0324 | 108.1 +/- 3.2 |
| FUSE | 21.18 | 14.2141 | 0.0392 | 22.5 | 4.8 | 50.6 | 0.0341 | 110.2 +/- 7.3 |

| | | | | | | | | |
|-------|--|--|--|-------|-------|--|--|-------|
| TOTAL | | | | 471.3 | 100.0 | | | 104.8 |
|-------|--|--|--|-------|-------|--|--|-------|

| | | | | | | | | |
|-------------|--|--|--|--|--|--|--|--------------|
| PLATEAU AGE | | | | | | | | 98.4 +/- 6.0 |
|-------------|--|--|--|--|--|--|--|--------------|

| E-40/39 | E-37/39 | E-36/39 | TEMP |
|---------|---------|---------|------|
|---------|---------|---------|------|

| | | | |
|--------------|--------------|------|------|
| .11 | .32 | .35 | 925 |
| .06 | .06 | .66 | 975 |
| .05 | 9.000001E-02 | .48 | 1000 |
| .05 | .08 | .51 | 1025 |
| .07 | 9.000001E-02 | .91 | 1040 |
| .2 | .11 | 4.01 | 1050 |
| .14 | .14 | 1.41 | 1065 |
| .12 | .14 | 1.02 | 1085 |
| 9.000001E-02 | 9.000001E-02 | 1.58 | 1110 |
| 9.000001E-02 | 9.000001E-02 | 3.16 | FUSE |

| Temp | 40Ar | 37Ar | 36Ar | Moles | 40Ar | %Ar40 | K/Ca | Age (Ma) |
|------|------|------|------|-------|--------|-------|------|----------|
| xC | 39Ar | 39Ar | 39Ar | 39Ar | %Total | Rad | | |

MA-66A-H

J = .005697

| | | | | | | | | |
|-------------|--------|---------|--------|-------|-------|------|--------|----------------|
| 855 | 202.61 | 4.7778 | 0.5958 | 3.9 | 2.7 | 13.3 | 0.1022 | 258.1 +/- 40.7 |
| 925 | 100.35 | 6.6133 | 0.2951 | 3.9 | 2.6 | 13.6 | 0.0737 | 135.7 +/- 21.6 |
| 975 | 42.15 | 24.3484 | 0.1154 | 15.9 | 10.8 | 23.7 | 0.0198 | 101.6 +/- 3.9 |
| 990 | 20.41 | 22.6194 | 0.0484 | 50.0 | 34.2 | 38.7 | 0.0213 | 80.8 +/- 1.1 |
| 1010 | 22.81 | 22.0973 | 0.0552 | 22.8 | 15.6 | 36.2 | 0.0218 | 84.3 +/- 3.7 |
| 1025 | 32.08 | 21.8146 | 0.0877 | 7.4 | 5.1 | 24.6 | 0.0221 | 80.7 +/- 5.5 |
| 1040 | 28.96 | 18.8765 | 0.0781 | 5.7 | 3.9 | 25.5 | 0.0256 | 75.3 +/- 7.9 |
| 1065 | 21.15 | 20.7629 | 0.0504 | 10.7 | 7.3 | 37.4 | 0.0232 | 80.7 +/- 3.1 |
| FUSE | 20.40 | 21.6298 | 0.0478 | 26.0 | 17.7 | 39.2 | 0.0223 | 81.6 +/- 1.6 |
| TOTAL | | | | 146.3 | 100.0 | | | 89.8 |
| PLATEAU AGE | | | | | | | | 81.9 +/- 4.5 |

| E-40/39 | E-37/39 | E-36/39 | TEMP |
|--------------|---------|---------|------|
| .8 | .9 | .91 | 855 |
| .52 | .58 | 1.15 | 925 |
| .11 | .11 | .56 | 975 |
| .05 | .06 | .25 | 990 |
| .08 | .08 | 1.11 | 1010 |
| .35 | .35 | .98 | 1025 |
| .18 | .18 | 1.71 | 1040 |
| .14 | .15 | .99 | 1065 |
| 9.000001E-02 | .11 | .48 | FUSE |

| Temp x°C | 40Ar 39Ar | 37Ar 39Ar | 36Ar 39Ar | Moles 39Ar | 40Ar %Total | %Ar40 Rad | K/Ca | Age (Ma) |
|-------------|--------------|--------------|--------------|---------------|----------------|--------------|----------|--------------|
| MA-70A-B | | | | | | | | |
| J = .003046 | | | | | | | | |
| 750 | 31.54 | 0.0555 | 0.0646 | 28.5 | 3.9 | 39.4 | 8.8285 | 67.0 +/- 6.2 |
| 750 | 15.17 | 0.0025 | 0.0074 | 204.9 | 28.1 | 85.3 | 196.9450 | 69.7 +/- 2.1 |
| 830 | 14.78 | 0.0013 | 0.0053 | 132.9 | 18.2 | 89.2 | 366.2179 | 71.0 +/- 1.9 |
| 890 | 16.21 | 0.0031 | 0.0066 | 65.7 | 9.0 | 87.7 | 159.9213 | 76.5 +/- 2.1 |
| 950 | 15.17 | 0.0040 | 0.0053 | 69.3 | 9.5 | 89.4 | 123.7058 | 73.1 +/- 3.2 |
| 1025 | 14.34 | 0.0128 | 0.0037 | 127.8 | 17.5 | 92.2 | 38.2212 | 71.2 +/- 3.2 |
| FUSE | 14.56 | 0.0199 | 0.0043 | 100.8 | 13.8 | 91.0 | 24.6723 | 71.3 +/- 2.7 |
| TOTAL | | | | 729.9 | 100.0 | | | 71.3 |
| PLATEAU AGE | | | | | | | | 72.6 +/- 5.0 |

| E-40/39 | E-37/39 | E-36/39 | TEMP |
|---------|---------|---------|------|
| 1.44 | 10.1 | 1.91 | 750 |
| .48 | 13.9 | 7.95 | 750 |
| 1.08 | 54.9 | 2.83 | 830 |
| 1.06 | 78 | 3.2 | 890 |
| 1.9 | 55.4 | 3.26 | 950 |
| 2.07 | 25.8 | 2.5 | 1025 |
| 1.05 | 60.3 | 15.2 | FUSE |

| Temp | 40Ar | 37Ar | 36Ar | Moles | 40Ar | %Ar40 | K/Ca | Age (Ma) |
|------|------|------|------|-------|--------|-------|------|----------|
| xC | 39Ar | 39Ar | 39Ar | 39Ar | %Total | Rad | | |

MA-71B-B

J = .005803

| | | | | | | | | |
|------|------|--------|--------|--------|------|------|-----------|--------------|
| 855 | 8.49 | 0.0036 | 0.0060 | 332.5 | 11.9 | 78.7 | 136.1107 | 68.6 +/- 0.8 |
| 940 | 7.82 | 0.0018 | 0.0032 | 387.7 | 13.9 | 87.4 | 272.2218 | 70.2 +/- 0.8 |
| 1000 | 7.63 | 0.0023 | 0.0024 | 1158.2 | 41.5 | 90.2 | 213.0431 | 70.7 +/- 0.7 |
| 1025 | 7.45 | 0.0019 | 0.0018 | 593.4 | 21.2 | 92.3 | 257.8944 | 70.7 +/- 0.7 |
| 1040 | 7.39 | 0.0001 | 0.0015 | 205.8 | 7.4 | 93.5 | 4900.0000 | 70.9 +/- 0.8 |
| FUSE | 8.26 | 0.0152 | 0.0046 | 115.4 | 4.1 | 83.1 | 32.2365 | 70.5 +/- 1.1 |

| | | | | | | | | |
|-------|--|--|--|--------|-------|--|--|------|
| TOTAL | | | | 2793.0 | 100.0 | | | 70.4 |
|-------|--|--|--|--------|-------|--|--|------|

| | | | | | | | | |
|-------------|--|--|--|--|--|--|--|--------------|
| PLATEAU AGE | | | | | | | | 70.5 +/- 0.9 |
|-------------|--|--|--|--|--|--|--|--------------|

| E-40/39 | E-37/39 | E-36/39 | TEMP |
|---------|---------|---------|------|
|---------|---------|---------|------|

| | | | |
|-----|---------|------|------|
| .06 | 16.49 | 1.01 | 855 |
| .04 | 29.15 | 2.07 | 940 |
| .05 | 7.97 | 1.26 | 1000 |
| .05 | 27.45 | 2.22 | 1025 |
| .06 | 2216.69 | 4.74 | 1040 |
| .04 | 13.54 | 2.91 | FUSE |

| Temp | 40Ar | 37Ar | 36Ar | Moles | 40Ar | %Ar40 | K/Ca | Age (Ma) |
|------|------|------|------|-------|--------|-------|------|----------|
| xC | 39Ar | 39Ar | 39Ar | 39Ar | %Total | Rad | | |

MA-71B-M

J = .005828

| | | | | | | | | |
|------|-------|--------|--------|--------|------|------|------------|--------------|
| 855 | 15.17 | 0.0047 | 0.0229 | 126.9 | 4.9 | 55.1 | 104.2550 | 85.8 +/- 2.4 |
| 940 | 9.31 | 0.0008 | 0.0074 | 1081.7 | 41.7 | 76.1 | 612.4996 | 73.0 +/- 0.7 |
| 1000 | 9.26 | 0.0001 | 0.0073 | 499.5 | 19.2 | 76.3 | 74900.0000 | 72.7 +/- 0.9 |
| 1025 | 8.78 | 0.0009 | 0.0057 | 420.7 | 16.2 | 80.4 | 544.4440 | 72.7 +/- 0.8 |
| 1040 | 8.19 | 0.0001 | 0.0035 | 301.1 | 11.6 | 86.9 | 74900.0000 | 73.3 +/- 0.9 |
| FUSE | 8.65 | 0.0002 | 0.0046 | 166.4 | 6.4 | 83.8 | 72450.0000 | 74.7 +/- 1.4 |

| | | | | | | | | |
|-------|--|--|--|--------|-------|--|--|------|
| TOTAL | | | | 2596.3 | 100.0 | | | 73.7 |
|-------|--|--|--|--------|-------|--|--|------|

| | | | | | | | | |
|-------------|--|--|--|--|--|--|--|--------------|
| PLATEAU AGE | | | | | | | | 72.8 +/- 0.7 |
|-------------|--|--|--|--|--|--|--|--------------|

| E-40/39 | E-37/39 | E-36/39 | TEMP |
|---------|---------|---------|------|
|---------|---------|---------|------|

| | | | |
|--------------|--------|------|------|
| .1 | 22.76 | 1.63 | 855 |
| .08 | 26.01 | .37 | 940 |
| .06 | 120.43 | 1.07 | 1000 |
| 9.000001E-02 | 71.94 | .69 | 1025 |
| .11 | 35.88 | 2.84 | 1040 |
| .11 | 426.4 | 4.48 | FUSE |

| Temp | 40Ar | 37Ar | 36Ar | Moles | 40Ar | %Ar40 | K/Ca | Age (Ma) |
|------|------|------|------|-------|--------|-------|------|----------|
| xC | 39Ar | 39Ar | 39Ar | 39Ar | %Total | Rad | | |

3G-210-B

J = .005862

| | | | | | | | | |
|------|------|--------|--------|-------|------|------|----------|--------------|
| 800 | 9.67 | 0.0533 | 0.0090 | 239.6 | 8.6 | 72.2 | 9.1929 | 72.4 +/- 0.9 |
| 905 | 8.29 | 0.0101 | 0.0027 | 519.1 | 18.7 | 89.9 | 48.5145 | 77.2 +/- 0.8 |
| 960 | 7.92 | 0.0048 | 0.0010 | 642.0 | 23.1 | 95.8 | 102.0830 | 78.5 +/- 1.0 |
| 1000 | 7.73 | 0.0106 | 0.0009 | 635.7 | 22.9 | 96.1 | 46.2261 | 76.9 +/- 0.9 |
| 1050 | 7.72 | 0.0081 | 0.0007 | 474.7 | 17.1 | 96.8 | 60.4935 | 77.3 +/- 0.9 |
| FUSE | 8.27 | 0.0375 | 0.0025 | 270.7 | 9.7 | 90.6 | 13.0663 | 77.6 +/- 1.1 |

| | | | | | | | | |
|-------|--|--|--|--------|-------|--|--|------|
| TOTAL | | | | 2781.7 | 100.0 | | | 77.1 |
|-------|--|--|--|--------|-------|--|--|------|

| | | | | | | | | |
|-------------|--|--|--|--|--|--|--|--------------|
| PLATEAU AGE | | | | | | | | 77.3 +/- 1.1 |
|-------------|--|--|--|--|--|--|--|--------------|

| E-40/39 | E-37/39 | E-36/39 | TEMP |
|---------|----------|---------|------|
| .05 | .5 | .97 | 800 |
| .06 | 2.67 | 1.61 | 905 |
| .11 | 9.28 | 11.42 | 960 |
| .08 | 2.52 | 7.32 | 1000 |
| .12 | 9.060001 | 8.51 | 1050 |
| .04 | 2.39 | 5.06 | FUSE |

Appendix G

GPP PROGRAM MODIFICATIONS

GPP a geochemical program written by D.J. Geist, B.H. Baker, and A.R. McBirney at the University of Oregon has been a useful tool in organizing and evaluating the major- and trace-element data. The program has several flaws and weaknesses, some of which I have corrected.

Operationally GPP is intended to run on a two floppy disk IBM PC and the program had to be modified to allow operation on a hard drive equipped computer. The alteration consisted of removing the drive designation from the link calls between the thirteen application nodules. This allows GPP to be run from any drive and maintains the original system of data storage. Running GPP off a hard drive greatly increases the speed of the program because of the many independent modules involved.

Raw trace-element X-ray data must be corrected for mass absorption of induced X-rays by the major-elements in the sample. A calculation and data file correction procedure was added to GPP in the form of a new module (MABSCO.BAS) linked to the main GPP data handling menu. Because GPP does not include a plotter driver, MABSCO.BAS also converts GPP data files to the format used by another geochemistry program, IGPET written by M.J. Carr. IGPET has rather limited data base and data handling capabilities but its figure

composition routines and HP plotter driver produce good quality diagrams. By using GPP and IGPET together with the translation program a more flexible and capable data analysis tool was created. The following printout is a hard copy of the MABSCO.BAS module added to GPP which incorporates both the trace-element corrections and the GPP to IGPET conversion routines. Several people helped in the design and coding of MABSCO.BAS, Eric Nelson assisted in GPP file reading procedures, Steve Weaver provided the mass absorption algorithms and suffered through much of the debugging process.

```

10 CLS:
20 PRINT " *****MABSCO.BAS*****"
30 PRINT " This program calculates mass absorption coefficients "
40 PRINT " for trace element corrections due to interferences"
50 PRINT " from the major elements in the sample.
60 PRINT
70 PRINT " You will need to identify an input GPP data file."
80 PRINT " The program can create a Mabsco corrected GPP file"
90 PRINT " as well as tranfering data to IGPET."
95 PRINT
100 PRINT " File extensions are not needed because the program"
110 PRINT " will create the file extensions for each file it"
120 PRINT " produces, and assumes the source GPP file"
123 PRINT " has a .dat extension"
125 PRINT
127 PRINT
128 INPUT " THE DATA FILE IS ON DISK? _:";SD$
129 INPUT " THE NEW FILES WILL BE PUT OÑ DISK? _:";DD$
130 INPUT " THE GPP DATA FILE IS NAMED _";GPDATA$
140 PRINT
150 INPUT " Do you want the MABSCO conversion? Y or N";M$
160 PRINT
170 INPUT " Do you want to convert data from a GPP file to IGPET?";C$
180 DIM EL$(26), SAMP$(125), E(125,26), F(16), MS1(125), A(125), G(16),
    MS2(125), MS2.5(125), H(16), NEWDAT(125,26), DISC$(125)
185 GPPDATA$ = SD$+GPDATA$+".DAT":' SOURCE GPP FILE
190 GPMAB$ = DD$ + GPDATA$ +"M.DAT":' CREATED MABSCO
CORRECTED DATA(GPP FILE)
200 IGPETF$ = DD$ + GPDATA$ + ".FMT":' TOTAL CHEM IGPET
FORMAT FILE
210 IGPETD$ = DD$ + GPDATA$ + ".ROC":' TOTAL CHEM IGPET
DATA FILE
220 IGPETM$ = DD$ + GPDATA$ + "C.ROC":' MAJOR ELEM IGPET
DATA FILE
230 IGPETMF$ = DD$ + GPDATA$ + "C.FMT":' MAJOR ELEM IGPET
FORMAT FILE
240 OPEN "I",#1,GPPDATA$
245 PRINT
250 PRINT " READING GPP DATA FILE"
260 PRINT
280 INPUT #1, F$, D$, SAMP$, ELEMS
290 FOR I=1 TO ELEMS
300 INPUT #1, EL$(I)
310 NEXT I
320 FOR I=1 TO SAMP$
330 INPUT #1, SAMP$(I), DISC$(I)
340 NEXT I
350 FOR I=1 TO SAMP$

```

```

360 FOR J=1 TO ELEMS
370 INPUT #1, E(I,J)
380 NEXT J
390 NEXT I
400 IF M$ = "N" THEN 1560:    CALCULATES MABSCO REGION 1
405 PRINT "  CALCULATING MASS ABSORBTION COEFFICIENTS"
410 F(1) = .0961:'    Si
420 F(2) = .3648:'    Ti
430 F(3) = .0877:'    Al
440 F(4) = .6563:'    Fe2O3
450 F(5) = .7256:'    FeO
460 F(6) = .6502:'    Mn
470 F(7) = .0788:'    Mg
480 F(8) = .3314:'    Ca
490 F(9) = .0716:'    Na
500 F(10)= .3301:'    K
510 F(13)= .1285:'    P
520 FOR I=1 TO SAMPS
530 FOR J=1 TO 10
540 A(I) = A(I) + F(J) * E(I,J)
550 NEXT J
560 A(I) = A(I) + F(13) * E(I,13)
570 MS1(I) = A(I)/10
580 NEXT I
590 A(I) = 0
600 G(1) = .6682:'    Si    CALCULATES MABSCO REGION 2 610 G(2) =
    2.5356:'    Ti
620 G(3) = .6097:'    Al
630 G(4) = .6262:'    FE2O3
640 G(5) = .6692:'    FEO
650 G(6) = .602:'    Mn
660 G(7) = .548:'    Mg
670 G(8) = 2.3035:'    Ca
680 G(9) = .4981:'    Na
690 G(10) = 2.2938:'    K
700 G(13) = .8941:'    P
710 FOR I=1 TO SAMPS
720 FOR J=1 TO 10
730 A(I) = A(I) + G(J) * E(I,J)
740 NEXT J
750 A(I) = A(I) + G(13) * E(I,13)
760 MS2(I) = A(I)/80
765 NEXT I
770 A(I) = 0
780 H(1) = 1.5978:'    Si    CALCULATES MABSCO REGION 2.5
790 H(2) = .8797:'    Ti
800 H(3) = 1.458:'    Al
810 H(4) = 1.2698:'    FE2O3

```

```

820 H(5) = 1.356:'   FEO
830 H(6) = 1.2489:'  Mn
840 H(7) = 1.2962:'  Mg
850 H(8) = 4.5967:'  Ca
860 H(9) = 1.0967:'  Na
870 H(10) = 4.5598:' K
880 H(13) = 1.6966:' P
890 FOR I=1 TO SAMPS
900 FOR J=1 TO 10
910 A(I) = A(I) + H(J) * E(I,J)
920 NEXT J
930 A(I) = A(I) + H(13) * E(I,13)
940 MS2.5(I) = A(I)/200
950 NEXT I
960 CLS:PRINT:PRINT:PRINT
970 INPUT "DISPLAY THE MABSCO VALUES? Y or N";P$
980 IF P$ = "N" THEN 1190
990 CLS
1000 PRINT GPMAB$:PRINT
1010 PRINT " The listed MABSCO values are repectively 1/10, 1/80, 1/200"
1020 PRINT " OF THEIR TRUE VALUES FOR EASE OF HANDLING."
1030 PRINT
1040 PRINT "MABSCO1: CU, NB, NI, RB, SR, Y, ZR,"
1050 PRINT "MABSCO2: ND, SM"
1060 PRINT "MABSCO2.5: BA, TI, V"
1070 PRINT
1080 PRINT " #      SAMPLE #      MABSCO1      MABSCO2
      MABSCO2.5":LPRINT
1090 I=1
1100 FOR J=I TO SAMPS
1110 FOR I=J TO 9+I
1120 PRINT "  I;TAB(10);SAMP$(I);TAB(21);MS1(I);TAB(33);MS2(I);
      TAB(45);MS2.5(I)
1130 IF I=SAMPS THEN 1150
1140 NEXT I
1150 INPUT "CONTINUE";P$
1160 IF P$="N" THEN 1190
1170 J=I
1180 NEXT J
1190 CLS:PRINT:PRINT:PRINT
1200 PRINT
1210 PRINT
1220 PRINT " PLEASE WAIT, CORRECTING TRACE ELEMENT VALUES AND
      WRITING GPP FILE"

1225 PRINT
1230 FOR I=1 TO SAMPS:'   CORRECTS TRACE ELEMENT VALUES
1240 NEWDAT(I,15)=E(I,15)*MS2.5(I):'   Ba
1250 NEWDAT(I,16)=E(I,16)*MS1(I):'   Cu

```

```

1260 NEWDAT(I,17)=E(I,17)*MS1(I):'      Nb
1270 NEWDAT(I,18)=E(I,18)*MS2(I):'      Nd
1280 NEWDAT(I,19)=E(I,19)*MS1(I):'      Ni
1290 NEWDAT(I,20)=E(I,20)*MS1(I):'      Rb
1300 NEWDAT(I,21)=E(I,21)*MS2(I):'      Sm
1310 NEWDAT(I,22)=E(I,22)*MS1(I):'      Sr
1320 NEWDAT(I,23)=E(I,23)*MS2.5(I):'    V
1330 NEWDAT(I,24)=E(I,24)*MS1(I):'      Y
1340 NEWDAT(I,25)=E(I,25)*MS1(I):'      Zr
1350 NEWDAT(I,26)=E(I,26)*MS2.5(I):'    Ti
1360 NEXT I
1365 OPEN "O",#6,GPMAB$
1370 PRINT #6, GPMAB$:'      CREATES THE GPP-MABSCO DATA FILE
1380 PRINT #6, D$
1390 PRINT #6, SAMPS
1400 PRINT #6, ELEMS
1410 FOR I = 1 TO ELEMS
1420 PRINT #6, EL$(I)
1430 NEXT I
1440 FOR I=1 TO SAMPS
1450 PRINT #6, SAMP$(I)
1460 PRINT #6, DISC$(I)
1470 NEXT I
1480 FOR I=1 TO SAMPS
1490 FOR J=1 TO 14
1500 PRINT #6, E(I,J)
1510 NEXT J
1520 FOR J=15 TO ELEMS
1530 PRINT #6, NEWDAT(I,J)
1540 NEXT J
1550 NEXT I
1555 CLOSE #1, #6
1560 IF C$ = "N" THEN 1750
1565 PRINT " WRITING IGPET DATA AND FORMAT FILES"
1568 PRINT
1570 OPEN "O",#2, IGPETF$:'      CREATING IGPET TOTAL
                                DATA FORMAT FILE
1580 PRINT #2, "25"
1590 PRINT #2, "SiO2,TiO2,Al2O3,Fe2O3,FeO,MnO,MgO,CaO,Na2O,K2O,P2O5,
H2O+,H2O-,Ba,Cu,Nb,Nd,Ni,Rb,Sm,Sr,V,Y,Zr,Ti":CLOSE
1595 CLOSE #2
1600 OPEN "O",#5, IGPETMF$:'      CREATING IGPET MAJOR ELEMENT
                                FORMAT FILE
1610 PRINT #5, "13"
1620 PRINT #5, "SiO2,TiO2,AL2O3,Fe2O3,FeO,MnO,MgO,CaO,Na2O,K2O,P2O5,
H2O-":CLOSE
1625 CLOSE #5
1627 OPEN "O",#3,IGPETD$:'      CREATING TOTAL IGPET DATA FILE

```

```
1630 Z = 1
1640 WRITE #3, GPDATA$+".FMT"
1650 FOR I=1 TO SAMPS
1660 WRITE #3, Z,Z,Z,Z,SAMP$(I)
1670 WRITE #3,E(I,1),E(I,2),E(I,3),E(I,4),E(I,5),E(I,6),E(I,7),
      E(I,8),E(I,9),E(I,10),E(I,13),E(I,11),E(I,12)
1675 IF M$="N" THEN 1686
1680 WRITE #3,NEWDAT(I,15),NEWDAT(I,16),NEWDAT(I,17),
      NEWDAT(I,18),NEWDAT(I,19),NEWDAT(I,20),
      NEWDAT(I,21),NEWDAT(I,22),NEWDAT(I,23),
      NEWDAT(I,24),NEWDAT(I,25),NEWDAT(I,26)
1683 IF M$="Y" THEN 1690
1686 WRITE #3,E(I,15),E(I,16),E(I,17),E(I,18),E(I,19),E(I,20),
      E(I,21),E(I,22),E(I,23),E(I,24),E(I,25),E(I,26)
1690 NEXT I
1695 CLOSE #3
1697 OPEN "O",#4,IGPETM$:'          CREATING MAJOR ELEMENT
                                   IGPET DATA FILE

1700 WRITE #4, GPDATA$+"C.FMT"
1710 FOR I=1 TO SAMPS
1720 WRITE #4, Z,Z,Z,Z,SAMP$(I)
1730 WRITE #4,E(I,1),E(I,2),E(I,3),E(I,4),E(I,5),E(I,6),E(I,7),
      E(I,8),E(I,9),E(I,10),E(I,13),E(I,11),E(I,12)
1740 NEXT I
1750 PRINT " THATS ALL FOLKS!!!! YOUR FILES ARE READY"
1760 END
```

Appendix H

PUBLISHED ABSTRACTS

Bruce et al. 1986a

Geochronology and Petrology of the Patagonia batholith:

Implications for Magma Genesis and Arc Evolution

Current accounts of the Patagonia batholith fail to describe the lithologic variability which ranges from norite and hornblende gabbro through typical biotite-hornblende tonalite to leuco granite. Magmatic evolution is diachronous and follows a regular mafic to felsic trend. The only observed exceptions are syn- and post-plutonic mafic dikes. Early, temporally-restricted, peraluminous magmas show crustal contamination.

The three magmatic episodes defined by Halpern (1973), are supported by 22 new $^{40}\text{Ar}/^{39}\text{Ar}$ ages. The period of greatest magmatic activity coincides with other tectonic events. The time of intrusion of Late Jurassic to Early Cretaceous magmas correlates with the opening of the back-arc basin and ophiolite formation. The main plutonic interval, (Late Cretaceous) matches the "early Andean" orogenic event documented by Herve et al. (1981), for Cordillera Darwin in the southernmost Chilean Andes. The time of intrusion of younger plutons does not correlate with any specific tectonic event, but appears to coincide with a period of significant uplift and erosion.

Magmatic epidote from several areas suggest emplacement depths greater than 25 km. These samples represent early magmatism and suggest that even the oldest dated plutons intruded a thick crust. How the arc was thickened prior to the main plutonic phase is unclear. Epizonal granites that cut these mesozonal plutons bracket the time of uplift and provide an average uplift rate of 0.4 mm/a for the interval 77 to 22 Ma. This uplift coincides with development of the foreland fold and thrust belt that lies to the east.

Bruce et al. (1986b)

Age-Lithology Relationships in the Patagonian batholith:

A Model for Arc-Crustal Growth

Two well-studied areas in the Patagonian batholith have different overlapping age distributions: 144-83 Ma at 48°S and 98-22 Ma at 53°S, Chile. Each area contains the same progression of mafic to felsic lithologies. The oldest rocks are norites and gabbros; these are followed by diorites, tonalites, and finally granites. Sr and Nd data strongly suggest that, following early arc development, magmas of all types have been continuously produced. The geographic distribution of ages and lithologies suggest a general model of arc-crustal evolution resulting from magmatic input and subsequent differential uplift.

Assumptions used in the model are as follows. (1) Mafic, intermediate, and felsic magmas are continuously produced. (2) The level that magmas rise to in the crust is principally controlled by their chemistry; acknowledging exception, felsic magmas will crystallize at shallower depth than will mafic magmas. (3) Arc-orogenic belts are constantly uplifting as isostatic adjustments to erosion and magmatic input occur. Thus, older mafic plutons are uplifted to the level in the crust where younger felsic plutons are emplaced. Deeper levels in the crust contain progressively younger plutons. Subsequent differential uplift juxtaposes areas with unique age distributions. Areas with young maximum ages have uplifted the most. Areas with large age spans had slow uplift rates during their magmatic interval.

Mafic, intermediate, and felsic magmas are continuously produced throughout arc evolution. The combinations of age and lithology exposed today are a result of differential uplift.

Bruce et al. (1987a)

Magmatic Rock Series of the Patagonian batholith:

Evidence for Multiple Magma Types

Geochemistry and modal data distinguish three plutonic rock series from the Golfo Xaultegua region, 53° S, Chile: calc-alkaline (CA), calcic (C), and high-aluminum trond-hjemite (HAT) series. These series were derived from significantly different parental magmas. The CA and C series extend from 46 to 76% SiO₂. At low SiO₂ contents CA rocks are distinguished from C rocks by the presence of potassium feldspar. CA series rocks have notably higher LIL element

contents. The LIL difference cannot be completely accounted for by variations in potassium feldspar and biotite. At the same SiO_2 content, hornblendes from CA series rocks, contain 2 to 5 times more calculated K_2O than from C series rocks, indicating a higher $a\text{K}_2\text{O}$ in their parental liquid. This, plus the higher potassium feldspar content, suggests that CA series rocks crystallized from LIL enriched magmas. Rb/Sr and Sm/Nd data suggest that little crustal contamination occurred, and that the LIL enrichment therefore occurred in the mantle. Both high and low LIL liquids theoretically can be generated within the mantle wedge. The rock series intruded over a 75 Ma period, indicating that the enrichment mechanism was an ongoing mantle process.

The HAT series rocks have low K_2O , CaO and TiO_2 , and have high Na_2O , Sr and Al_2O_3 . They contain muscovite and occasionally garnet in addition to quartz, plagioclase and biotite. Their chemical signature, mineralogy and low (i)Sr values (0.70443-0.70469), indicate that the HAT series could be derived from partial melting of mafic C series rocks. Compared to the C rock series, low CaO, and high Sr, Na_2O , and Al_2O_3 suggest that plagioclase was nearly or completely consumed during melting. The HAT series intruded shortly after the peak of the Andean orogeny, which is marked by a major magmatic episode and a period of crustal thickening. Such processes would facilitate the melting of older plutons. Melt products of older CA rock series could produce high SiO_2 members of the CA series.

Bruce et al. 1987b

Pluton Emplacement and Magmatic Arc Construction:

A Model from the Patagonian batholith

Field relations, geochronology, and Sr isotope data from the Patagonian batholith are integrated into an arc construction model that relates crustal growth at convergent margins to pluton emplacement and differential uplift. The Patagonian batholith in the southern Chilean Andes represents the eroded roots of a subduction-related magmatic arc developed along the Andean convergent margin between late Jurassic and Tertiary time. Crystallization ages range from 157-15 Ma and record semi-continuous magmatic activity during this period. In three areas studied in detail (generally 10,00 sq. km) a progression of mafic to felsic rocks is consistently observed: excluding dikes and contaminated peraluminous rocks, mafic plutons (norite, gabbro, hornblende diorite) intrude first and were followed by progressively more felsic plutons (quartz diorite, tonalite, granodiorite, and granite). This progression is confirmed by Ar/Ar, Rb/Sr, and U-Pb geochronology in three study areas. Different areas have distinct ranges in age. Such relationships can be interpreted to represent diachronous magmatism along the arc. However, a pattern of decreasing initial $^{87}\text{Sr}/^{86}\text{Sr}$ with time for samples from three widely distributed areas suggests that

a long-term crustal evolution occurred throughout the magmatic arc, and that magmas of all the observed types (mafic to felsic) were generated and emplaced through the recorded history of the batholith. As an alternative to diachronous magmatism, we present a model of arc-crustal growth that relates the age-lithology relationship to pluton emplacement depth and uplift history.

The model assumes semi-continuous uplift of middle to upper crustal levels in the thermally-weakened arc, resulting from protracted intrusion of low-density magmas at these levels. Within an uplifting crustal block, deeper plutons will take longer to reach the surface than shallow plutons. Thus, as exposed today in a coherent block, older plutons must have been intruded at deeper levels than younger plutons. Furthermore, because the batholith shows a consistent age-lithology relationship (old mafic to young felsic progression), it can be concluded that the mafic plutons were intruded at a deeper level than felsic plutons. The model thus suggests that older (mafic) plutons were uplifted to the intrusion depth of younger (felsic) plutons.

The apparent age of a batholith, or of individual areas within a batholith, is to a large degree controlled by the uplift history of the arc. The model has several corollaries. 1) During the period of recorded magmatism in the area, time-integrated uplift rate is inversely proportional to the range in ages. Thus, an area with a wide range in ages experienced a relatively slow uplift rate during the recorded magmatic period. 2) Total uplift since the earliest recorded magmatism is inversely proportional to the age of the oldest pluton. Thus an area with older plutonism will have undergone less uplift compared to an area with relatively younger plutonism. These corollaries hold only when comparing areas with comparable lithologic variation.

Similar age-lithology relationships have been reported from batholiths in Peru, California (Sierra Nevada), Idaho, and SE Alaska, suggesting that our model may be applicable in other magmatic arcs. However, the age-lithology patterns produced by the proposed processes could be obscured by other geologic events (e.g., structural or metamorphic overprints). Also, data must be available from a large area and covering a large time span for the time-integrated effects of the processes to be observed in the age-lithology patterns.

Bruce et al. (1987c)

Changing Contributions of the Crust and Mantle during Andean Arc Construction

Generation of magmas that form continent-hosted magmatic arcs is influenced by preexisting geology, subduction kinematics, and crustal thickness in the arc. Sr and Nd isotope data from two Andean batholiths define two trends of evolving arc plutonism related to changing contributions from the crust and mantle. These trends are most affected by crustal thickness. Preexisting geology and subduction kinematics appear to influence the rate of change rather than its direction.

Sr_i values decrease and Nd_i values increase in southern Chile, reflecting a decreasing crustal contribution with time. This is due to the combined effects of progressive dehydration of the basement, development of an intrusive plumbing system, and bulk dilution of the basement. Plutons were emplaced into a thin (estimated 10-20 km) Late Paleozoic accretionary prism. The base of this thin crust was not hot enough to promote regional melting, therefore crustal melting was restricted to areas adjacent to plutons. Arc magmatism did not thicken the crust sufficiently to cause regional melting. The trend of decreasing crustal component with time is opposite that seen in Peru, where plutons intruded thicker continental crust.

Sr_i values increase with decreasing age in Peru, reflecting an increasing crustal contribution with time. Although the effects of dehydration, plumbing, and dilution inhibited crustal involvement, the thick Peruvian crust (currently 50-70 km) promoted lower crustal melting. Continued arc magmatism directly added heat and increased crustal thickness, causing further crustal melting, and decreasing the relative contribution of mantle melts to arc plutonism.